UNICAMP

UPPSALA
UNIVERSITET

MILENA DE ALBUQUERQUE MOREIRA

SYNTHESIS OF THIN PIEZOELECTRIC ALN FILMS IN VIEW OF SENSORS AND TELECOM APPLICATIONS

SÍNTESE DE FILMES FINOS DE ALN PIEZOELÉTRICO PARA APLICAÇÕES EM SENSORES E DISPOSITIVOS DE ALTA FREQUÊNCIA

CAMPINAS
2014

UNICAMP

UPPSALA
UNIVERSITET

UNIVERSIDADE ESTADUAL DE CAMPINAS
FACULDADE DE ENGENHARIA ELÉTRICA E DE COMPUTAÇÃO
DEPARTAMENTO DE SEMICONDUTORES, INSTRUMENTOS E FOTÔNICA

MILENA DE ALBUQUERQUE MOREIRA

SYNTHESIS OF THIN PIEZOELECTRIC ALN FILMS IN VIEW OF SENSORS AND TELECOM APPLICATIONS

SÍNTESE DE FILMES FINOS DE ALN PIEZOELÉTRICO PARA APLICAÇÕES EM SENSORES E DISPOSITIVOS DE ALTA FREQUÊNCIA

Doctorate thesis presented to the Electrical Engineering Post graduation Program of the School of Electrical Engineering of the University of Campinas to obtain the Ph.D. grade in Electrical Engineering, in field of Electronic, Microelectronic and Optoelectronic.

Tese apresentada ao Programa de Pós-graduação em Engenharia Elétrica da Faculdade de Engenharia Elétrica e de Computação da Universidade de Campinas como parte dos requisitos exigidos para a obtenção do título de Doutora em Engenharia Elétrica na área de Eletrônica, Microeletrônica e Optoeletrônica.

Orientador: Prof. Dr. Ioshiaki Doi

ESTE EXEMPLAR CORRESPONDE À VERSÃO FINAL DA TESE
DEFENDIDA PELA ALUNA MILENA DE ALBUQUERQUE MOREIRA
E ORIENTADA PELO PROF. DR. IOSHIAKI DOI

Assinatura do Orientador

____

CAMPINAS
2014

Ficha catalográfica
Universidade Estadual de Campinas
Biblioteca da Área de Engenharia e Arquitetura
Luciana Pietrosanto Milla - CRB 8/8129

M813s
Moreira, Milena de Albuquerque, 1977-
Synthesis of thin piezoelectric AlN films in view of sensors and telecom applications / Milena de Albuquerque Moreira. – Campinas, SP : [s.n.], 2014.

Orientador: Ioshiaki Doi.
Tese (doutorado) – Universidade Estadual de Campinas, Faculdade de Engenharia Elétrica e de Computação.

1. Nitreto de alumínio. 2. Materiais piezoelétricos. 3. Filmes finos. I. Doi, Ioshiaki,1944-. II. Universidade Estadual de Campinas. Faculdade de Engenharia Elétrica e de Computação. III. Título.

Informações para Biblioteca Digital

Título em outro idioma: Síntese de filmes finos de AlN piezoelétrico para aplicações em sensores e dispositivos de alta frequência
Palavras-chave em inglês:
Aluminum nitride
Piezoelectric materials
Thin films
Área de concentração: Eletrônica, Microeletrônica e Optoeletrônica
Titulação: Doutora em Engenharia Elétrica
Banca examinadora:
Ioshiaki Doi [Orientador]
Ilia Katardjiev
Katia Franklin Albertin Torres
Edmundo da Silva Braga
Leandro Tiago Manera
Data de defesa: 24-09-2014
Programa de Pós-Graduação: Engenharia Elétrica

COMISSÃO JULGADORA - TESE DE DOUTORADO

Candidata: Milena de Albuquerque Moreira

Data da Defesa: 24 de setembro de 2014

Título da Tese: "Synthesis of Thin Piezoelectric Aln Films in View of Sensors and Telecom Applications (Síntese de Filmes Finos de AlN Piezoelétrico para Aplicações em Sensores e Dispositivos de Alta Frequência)"

Prof. Dr. Ioshiaki Doi (Presidente): Ioshiaki Doi

Prof. Dr. Ilia Katardjiev: Ilia Katardjiev

Profa. Dra. Katia Franklin Albertin Torres:

Prof. Dr. Edmundo da Silva Braga: EBraga

Prof. Dr. Leandro Tiago Manera:

ABSTRACT

The requirements of the consumer market on high frequency devices have been more and more demanding over the last decades. Thus, a continuing enhancement of the devices' performance is required in order to meet these demands. In a macro view, changing the design of the device can result in an improvement of its performance. In a micro view, the physical properties of the device materials have a strong influence on its final performance. In the case of high frequency devices based on piezoelectric materials, a natural way to improve their performance is through the improvement of the properties of the piezoelectric layer. The piezoelectric material studied in this work is AlN, which is an outstanding material among other piezoelectric materials due to its unique combination of material properties.

This thesis presents results from experimental studies on the synthesis of AlN thin films in view of telecom, microelectronic and sensor applications. The main objective of the thesis is to custom design the functional properties of AlN to best suit these for the specific application in mind. This is achieved through careful control of the crystallographic structure and texture as well as film composition.

The piezoelectric properties of AlN films were enhanced by doping with Sc. Films with different Sc concentrations were fabricated and analyzed, and the coupling coefficient (k_t^2) was enhanced a factor of two by adding 15 % of Sc to the AlN films. The enhancement of k_t^2 is of interest since it can contribute to a more relaxed design of high frequency devices. Further, in order to obtain better deposition control of c-axis tilted AlN films, a new experimental setup were proposed. When this novel setup was used, films with well-defined thicknesses and tilt uniformity were achieved. Films with such characteristics are very favorable to use in sensors based on electroacoustic devices operating in viscous media. Studies were also performed in order to obtain c-axis oriented AlN films deposited directly on Si substrates at reduced temperatures. The deposition technique used was HiPIMS, and the results indicated significant improvements in the film texture when comparing to the conventional Pulsed DC deposition process.

Keywords: Aluminum nitride. Reactive sputtering. C-axis oriented films. Tilted films. Electroacoustic devices. Piezoelectric materials. Aluminum scandium nitride. HiPIMS, High-k dielectric.

RESUMO

Os requisitos do mercado consumidor de dispositivos de alta frequência têm sido cada vez mais exigentes nas últimas décadas. Assim, é necessária uma melhoria contínua no desempenho dos dispositivos a fim de atender a estes requisitos. Numa visão macro, alterações no desenho dos dispositivos podem resultar em melhoria de desempenho. Em uma visão micro, as propriedades físicas dos materiais que compõem os dispositivos têm uma forte influência no desempenho final dos mesmos. No caso de dispositivos de alta frequência baseados em materiais piezoelétricos, uma forma natural de melhorar o seu desempenho é através da melhoria das propriedades da camada piezoelétrica. O material piezoelétrico estudado neste trabalho é o Nitreto de Alumínio (AlN), o qual destaca-se entre outros materiais piezoelétricos devido à sua combinação única de propriedades.

Esta tese apresenta o resultado de estudos experimentais na síntese de filmes finos de AlN tendo em vista aplicações em altas frequências, microeletrônica e sensores. O principal objetivo desta tese é a melhoria nas propriedades funcionais do AlN para melhor atender aos requisitos das aplicações em questão. Isto é obtido através do controle cuidadoso da estrutura, textura cristalográfica e composição do filme.

As propriedades piezoelétricas dos filmes de AlN foram melhoradas através da dopagem dos filmes com Sc. Amostras com diferentes concentrações de Sc foram fabricadas e analisadas, e o valor do coeficiente de acoplamento eletromagnético (k_t^2) foi duplicado ao adicionar 15 % de Sc aos filmes de AlN. O aumento no valor de k_t^2 é desejável uma vez que pode diminuir as restrições no projeto de dispositivos de alta frequência. Neste trabalho é proposta também uma nova configuração experimental com o objetivo de obter um melhor controle na deposição de filmes de AlN inclinados no eixo-c. Filmes com uniformidade em espessura e inclinação foram obtidos ao utilizar-se a referida configuração experimental. Filmes com tais características são aplicáveis em sensores baseados em dispositivos eletroacústicos operando em meio líquido/viscoso. Foram também realizados estudos com o objetivo de obter filmes de AlN orientados no eixo-c e depositados diretamente sobre substratos de Si e a temperaturas reduzidas. A técnica de deposição utilizada foi HiPIMS e os resultados indicam melhorias significativas na textura dos filmes quando comparados com o processo de deposição convencional por corrente-direta pulsada.

Palavras-chave: Nitreto de alumínio. Pulverização catódica reativa. Filmes orientados no eixo-c. Filmes inclinados. Dispositivos eletroacústicos. Materiais piezoelétricos. Nitreto de alumínio escândio. HiPIMS. Alto-k dielétrico.

SAMMANFATTNING

Kraven i konsumentledet på högfrekvenskomponenter har ökat de senaste decennierna. Därför krävs en konstant förbättrad prestanda i dessa komponenter för att möta dessa krav. Ett angreppssätt på makronivå kan vara förändrad komponentdesign. På mikronivå kan förändringar i de fysikaliska egenskaperna i komponenters material ge betydande förbättringar i prestanda. Vad gäller högfrekvenskomponenter baserade på piezoelektriska material så är ett naturligt sätt att öka prestandan genom att förbättra egenskaperna i det piezoelektriska lagret. I mitt arbete har jag studerat AlN, vilket är ett utmärkt piezoelektriskt material beroende på dess goda kombination av fysikaliska egenskaper.

Dena avhandling presenterar resultat från experimentella studier av syntes av tunna filmer med avseende på tillämpningar inom telekommunikation, mikroelektronik och sensorer. Huvudspåret i avhandlingen är att skräddarsy de materiella egenskaperna hos AlN baserat på respektive tillämpnings specifika behov. Detta uppnås genom noggrann styrning av kristallografisk struktur och textur, likväl som tunnfilmens materiella sammansättning.

De piezoelektriska egenskaperna hos AlN-baserad tunnfilm förbättrades genom att dopa filmen med Sc. Tunnfilm med olika koncentration av Sc skapades och analyserades. Kopplingsfaktorn (k_t^2) förbättrades med en faktor två genom att dopa AlN-tunnfilm med femton procent Sc. Förbättringen av kopplingsfaktorn är intressant eftersom det bidrar till att designen av komponenter inte längre lider av lika stora begränsningar avseende effektförbrukning, ytmässig storlek med mera. För att uppnå bättre kontroll av den vertikala kristallografiska axeln i lutad AlN-baserad tunnfilm så experimenterades det med en ny typ av avsättningsprocess. När denna nya process användes så uppnåddes tunnfilm med både jämn tjocklek och jämn kristallografisk lutning. Tunnfilm med dessa egenskaper används med fördel i elektroakustiska sensorer som skall användas i viskös miljö.

Vidare så genomfördes studier för att uppnå AlN-baserad tunnfilm med vertikal kristallografisk axel där avsättning skedde direkt på kiselbaserade substrat vid lägre temperatur än normalt. Avsättningsprocessen som användes här var baserad på HiPIMS. Resultaten tyder på avsevärda förbättringar i tunnfilmens struktur, i en jämförelse med en ordinarie avsättningsprocess baserad på Pulsed DC.

Nyckelord: Aluminiumnitrid. Reaktiv sputtring. Linjering längs c-axeln. Film med vinklad struktur. Elektroakustiska anordningar. Piezoelektriska material. Aluminium-Scandium-nitrid. HiPIMS. Hög dielektricitetskonstant.

CONTENTS

1 INTRODUCTION ... 1

2 THEORETICAL BACKGROUND ... 7

2.1 C-AXIS ORIENTED ALN ... 7

2.2 TILTED ALN ... 9

2.3 DOPED ALN ... 12

2.4 ELECTROACOUSTIC DEVICES ... 14

2.5 HIGH-K ALN ... 16

2.6 HIGH POWER IMPULSE MAGNETRON SPUTTERING (HIPIMS) ... 17

3 RESULTS AND DISCUSSIONS ... 21

3.1 SYNTHESIS AND CHARACTERIZATION OF ALSCN FILMS ... 21

3.2 ELECTROACOUSTIC PROPERTIES OF ALSCN FILMS ... 25

3.3 HIPIMS AND ALN FILMS ... 30

4 SUMMARY OF INCLUDED PAPERS ... 37

4.1 PAPER I: THIN ALN FILMS DEPOSITED BY REACTIVE HIPIMS AND PULSED DC SPUTTERING: A COMPARATIVE STUDY ... 37

4.2 PAPER II: EFFICIENT RF VOLTAGE TRANSFORMER WITH BANDPASS FILTER CHARACTERISTICS ... 38

4.3 PAPER III: PREPARATION AND CHARACTERIZATION OF HIGH-K ALUMINIUM NITRIDE (ALN) THIN FILM FOR SENSOR AND INTEGRATED CIRCUITS APPLICATIONS ... 41

4.4 PAPER IV: ALUMINUM SCANDIUM NITRIDE THIN-FILM BULK ACOUSTIC RESONATORS FOR WIDE BAND APPLICATIONS ... 43

4.5 PAPER V: SYNTHESIS OF C-TILTED ALN FILMS WITH A GOOD TILT AND THICKNESS UNIFORMITY ... 45

4.6 PAPER VI: ELECTRICAL CHARACTERIZATION AND MORPHOLOGICAL PROPERTIES OF ALN FILMS PREPARED BY DC REACTIVE MAGNETRON SPUTTERING ... 48

5 CONCLUDING REMARKS ... 51

REFERENCES ... 53

APPENDIX ... 59

APPENDIX A – LIST OF INCLUDED PAPERS ... 61

APPENDIX B - AUTHOR’S CONTRIBUTION IN THE INCLUDED PAPERS 63
APPENDIX C - CONFERENCE CONTRIBUTIONS 65
APPENDIX D – PAPER I 67
APPENDIX E – PAPER II 73
APPENDIX F – PAPER III 77
APPENDIX G – PAPER IV 83
APPENDIX H – PAPER V 89
APPENDIX I – PAPER VI 95

ACKNOWLEDGMENTS

It is not unusual that research and PhD studies go through a long and not necessarily straightforward way. So many things can happen… So many things can go wrong. You never know. The only way to figure it out is… GO! And I couldn’t have made it to this point if I was alone. So, I would like to express my eternal gratitude to all of you!

PS: I hope I hadn’t forgotten anyone. But if this happened, just let me know and we can schedule an “I’m sorry” coffee.

(in no specific order)

Ioshiaki Doi, my supervisor in Brazil, for your wise and careful advice. I could always count on you!

Ilia Katardjiev, my supervisor in Sweden, for taking me on as a guest PhD student and letting me continue working in the Thin Films Group after the first year.

J. A. Diniz, always open to hear how things are going, plans for the future... Thank you for your valuable advice and suggestions!

Jair Fernandes, sharing research projects with you was a pleasure.

Johan Bjurström, co-worker and co-supervisor for a while, I learned a lot with you when we worked together.

Jörgen Ohlsson, thank you for standing by my side when necessary. I really appreciated it! And thank you for helping me through the final steps of the PhD studies.

Tomas Nyberg, we worked together for a short period, but your contributions were essential to the improvement of this work.

Tomas Kubart, thank you for the common project and for bringing me to the HiPIMS world.

Örjan Vallin, constantly ready to help (and to understand my “dålig svenska”). And thank you for supporting me when I crashed the MRD-I.

Marianne Asplund, you were an angel for me at FTE. Always taking care of me, checking if everything was alright. Very kind!

Regina and Mara, for the mind refreshing coffee breaks and very nice talks.

To the CCS and MSL staff, for all the help with the clean room work.

Pedro Salomé, you were so patient hearing all my bla-bla-bla! Thank you for your friendship, relaxing fikas and valuable advice.

Sara, Shabnam, Linli, Wiliana, Janaína, Valeria, Johan A., Saman-san, Kiran, Katja, Markus, Juan, Jose, Jessica and Oscar, than you for boosting my days with talks, laughing and nice fika time. Your friendship is invaluable!

Ulf Sahlin, min älskling, thank you for you unwearying support. Always encouraging me, you hold my hand, you make me stronger. Tack, sötnos!

Last but certainly not least, my family. Minha família querida, eu nem sei o que dizer... eu nem sei como agradecer. Palavras não conseguem expressar o sentimento e o significado do quanto eu sou grata a vocês! Constantemente me apoiando, constantemente me incentivando, mesmo que minhas decisões nos afastem fisicamente. De todo coração, com toda força de minha alma, meu muito obrigada! Eu amo vocês!

Milena de Albuquerque Moreira

LIST OF FIGURES

Figure 1.1 - C-axis oriented AlN film deposited by Pulsed DC on top of a Mo layer. 3

Figure 1.2 - One dimensional representation of particle displacement in a medium (a) without any wave motion, and (b) with longitudinal wave propagation. 3

Figure 1.3 - One dimensional representation of particle displacement in a medium (a) without any wave motion, and (b) with shear thickness wave propagation. 5

Figure 1.4 - C-axis tilted AlN film deposited by Pulsed DC on Si substrate. 5

Figure 2.1 - Schematic of the dipoles distribution along a piezoelectric net:(a) grains aligned in various directions, and (b) grains aligned along the same direction. 8

Figure 2.2 - Simplified schematic of different deposition setups for tilted films: (a) off-axis deposition, (b) tilted substrate, (c) tilted and off-centered, and (d) two-stage deposition process. 10

Figure 2.3 - Schematic of the nucleation layer with random crystal planes. 11

Figure 2.4 - Schematic of deposition methods to sputter doped AlN thin films: (a) concentric ring-shaped targets, (b) dopant inserts into the Al target, (c) alloyed Al target, and (d) co-sputter with two different targets. 13

Figure 2.5 - Comparative plot of the deposition rate of AlN films deposited under similar conditions by HiPIMS and Pulsed DC. 19

Figure 3.1 - ERDA analysis of $Al_{(1-x)}Sc_xN$ films. 22

Figure 3.2 - Influence of deposition temperature on the texture of AlScN (FWHM plot). 23

Figure 3.3 - Simplified schematic the substrates and stacked layers used to grow $Al_{(1-x)}Sc_xN$ films: (a) Si, (b) Si/AlN interlayer and (c) Si/AlN interlayer/Mo. 25

Figure 3.4 - θ-2θ scans of $Al_{(1-x)}Sc_xN$ films of the FBAR devices (x = 0, 0.03, 0.09 and 0.15). . 26

Figure 3.5 - Electromechanical coupling (k_t^2) and quality factor (Q-factor) as a function of the Sc concentration in $Al_{(1-x)}Sc_xN$ films. 28

Figure 3.6 - Figure of merit (FOM) calculated for FBAR devices based on $Al_{(1-x)}Sc_xN$ and Sc concentration of 0, 3, 9 and 15%. 28

Figure 3.7 - Temperature coefficient of frequency (TCF) for FBAR devices based on $Al_{(1-x)}Sc_xN$ and Sc concentrations of 0, 3, 9 and 15%. 29

Figure 3.8 - Dielectric permittivity, ε_r, and dielectric losses, tan δ, as a function of the Sc concentration in $Al_{(1-x)}Sc_xN$ films. 30

Figure 3.9 - θ-2θ scans of AlN films deposited by HiPIMS at room temperature and different gas flows ratio (Ar/N_2) on top of (a) Si substrates and (b) textured Mo substrates. 32

Figure 3.10 - θ-2θ scans of AlN films deposited by HiPIMS at fixed gas flow ratio (Ar/N_2 35/35 sccm) and different deposition temperatures on top of (a) Si substrates and (b) textured Mo substrates. 33

Figure 3.11 - θ-2θ scans of AlN films deposited by Pulsed DC and HiPIMS on Si substrates: (a) at room temperature and different gas compositions for the Pulsed DC films; (b) at 400 ºC and Ar/N_2 35/35 sccm as gas flow composition. 34

Figure 3.12 - θ-2θ scans of AlN films deposited by Pulsed DC and HiPIMS on textured Mo layers: (a) at room temperature and different gas compositions for the Pulsed DC films; (b) at 400 ºC and Ar/N_2 35/35 sccm as gas flow composition. 35

Figure 3.13 - FWHM of AlN films deposited by Pulsed DC and HiPIMS on Si and textured Mo substrates, at room temperature and 400 ºC. 36

Figure 4.1 - Cross section schematic of the transfilter. 39

Figure 4.2 - Top view of the fabricated transfilter. 40

Figure 4.3 - Schematic of a truly passive and addressable RTS by the use of transfilters (PBVT: see footnote). 40

Figure 4.4 - Schematic cross-section of a MISFET device and an inset of its intrinsic MIS capacitor. 42

Figure 4.5 - Cross-section view of the resonator structure. 44

Figure 4.6 - One dimensional representation of particle displacement in a medium (a) without any wave motion, and (b) with shear thickness wave propagation. 46

Figure 4.7 - Array of tilted magnetrons. 47

Figure 4.8 - XRD pole plot figures of tilted AlN films deposited by use of (a) a conventional magnetron with circular symmetry and (b) an array of tilted magnetrons. 48

Figure 4.9 - Schematic of the MIS capacitors fabricated. 49

LIST OF TABLES

Table 3.1 - Brief summary of the hardware setup and deposition conditions of $Al_{(1-x)}Sc_xN$ films. 23
Table 3.2 - FWHM (degrees) of $Al_{0.91}Sc_{0.09}N$ (002) and Mo (110) films. 25
Table 4.1 - Summary of the deposition conditions of HiPIMS and conventional Pulsed DC... 37
Table 4.2 - Electrical parameters (measured and calculated) of the AlN/SiO_2 stacked layer. .. 42
Table 4.3 - Electrical parameters of MISFET and EISFET devices. 43
Table 4.4 - Deposition conditions of the $Al_{(1-x)}Sc_xN$ layers.. 43
Table 4.5 - Measured and extracted $Al_{(1-x)}Sc_xN$ parameters. 45

LIST OF SYMBOLS AND ABBREVIATIONS

A	Capacitor area
AC	Alternating current
ADS	Advanced Design System
$Al_{(1-x)}Sc_xN$	Aluminum Scandium Nitride
Al_2O_3	Aluminum oxide (or alumina or sapphire)
AlN	Aluminum nitride
Ar	Argon
B	Boron
BAW	Bulk acoustic wave
C	Capacitance
C_{33}	Stiffness
C_{fb}	Flat-band capacitance
C_{max}	Maximum capacitance
C_{min}	Minimum capacitance
Cr	Chromium
C-V	Current-voltage
CVD	Chemical vapour deposition
d	Diameter of the gas particles
DC	Direct current
e_{33}	Piezoelectric constant
ECR	Electron cyclotron resonance
EISFET	Electrolyte insulator semiconductor field effect transistor
EOT	Equivalent oxide thickness
ERDA	Elastic recoil detection analysis
FBAR	Film bulk acoustic resonator
FOM	Figure of merit
f_p	Parallel resonance frequency
f_s	Series resonance frequency
FWHM	Full width at half maximum
Gm	Transconductance

HCM	Hollow cathode magnetron
HfO_2	Hafnium dioxide
HiPIMS	High power impulse magnetron sputtering
IC	Integrated circuit
ICP	Inductively coupled plasma
I_{DS}	Drain-source current
IDT	Interdigital transducer
I_{off}	Current-off
IPVD	Ionized physical vapor deposition
ISFET	Ion sensitive field effect transistor
k	Dielectric constant
k_B	Boltzmann constant
k_{eff}^2	Effective electromechanical coupling
k_t^2	Electromechanical coupling coefficient or Intrinsic electromechanical coupling
MBE	Molecular beam epitaxy
MBVD	Modified Butterworth-Van Dyke
MEMS	Microelectromechanical systems
MFP	Mean free path
MIM	Metal-insulator-metal
MIS	Metal-insulator-semiconductor
MISFET	Metal insulator semiconductor field effect transistor
Mo	Molybdenum
N	Nitrogen
N_A	Substrate acceptor concentration
NB	Nowotny-Benes model
N_t	Charge trap density
P	Pressure
PBVT	Piezoelectric bandpass voltage transformer
PVD	Physical vapor deposition
PZT	Lead zirconate titanate
Q_B	Unloaded quality factor
Q-factor	(or only Q) Quality factor
Q_p	Quality factor at parallel resonance frequency

R_0	Shunt resistance
RF	Radio frequency
RFID	Radio-frequency identification
R_s	Series parasitic resistance
RTS	Radio triggered switch
Sc	Scandium
ScN	Scandium nitride
SiO_2	Silicon dioxide
S_t	Subthreshold swing
t	Thickness of the capacitor insulator
T	Temperature
Ta	Tantalum
tan δ	Dielectric losses
TCF	Temperature coefficient of frequency
Ti	Titanium
TiO_2	Titanium dioxide
V_{fb}	Flat-band voltage
V_{GS}	Gate-source voltage
VLSI	Very large scale integration
V_{th}	Threshold voltage
WLA	Wireless local area network
XRD	X-ray diffraction
Y	Yttrium
ZnO	Zinc oxide
ZrO_2	Zirconium dioxide
ε_0	Absolute dielectric permittivity
ε_{33}	Dielectric constant
ε_r	Relative dielectric permittivity
ϕ_{ms}	Work function metal-semiconductor

"*What we know is a drop,*

what we don't know is an ocean"

(Isaac Newton)

1 INTRODUCTION

The requirements of the consumer market of high frequency devices, such as resonators and filters, have been more and more demanding over the last decades. Thus, a continuing enhancement of the devices' performance is required in order to meet these demands. In a macro view, changes in the design of the device can result in an improvement of its performance. In a micro view, the physical properties of the device materials also have a strong influence on its final performance. In the case of high frequency devices based on piezoelectric materials, a natural way to improve their performance is through the improvement of the properties of the piezoelectric layer.

This thesis summary presents the results from experimental studies on the synthesis of Aluminum Nitride (AlN) thin films in view of telecom, microelectronic and sensor applications. Thus, the main objective of this thesis is to custom design the functional properties of AlN to best suit these for the specific application in mind. This is achieved through careful control of the crystallographic structure and texture as well as film composition. Foremost, why is AlN the material of choice for this work?

AlN is a well-known and established compound among other piezoelectric materials. It is an III-V compound semiconductor with hexagonal wurtzite structure and unique electronic properties such as [1-5]:

- Wide bandgap (6.2 eV),
- High thermal conductivity (2 $W.(cm.K)^{-1}$, comparable to pure Al),
- High electrical resistivity (1 x 10^{16} Ω.cm), and
- High resistance to breakdown voltage (5 x 10^5 V/cm).

Moreover, AlN is also an interesting material due to its piezoelectric and electroacoustic properties, for instance [2-4, 6, 7]:

- High quality factor (around 3000 at 2 GHz for bulk acoustic wave devices (BAW)),
- Moderate coupling coefficient (6.5% for BAW),
- Moderate piezoelectric constant (e_{33}, 1.55 C/m^2),
- High acoustic velocity (11300 m/s for BAW), and
- Low propagation losses.

Besides its intrinsic characteristics, AlN thin films are chemically stable and compatible with the IC-fabrication technology. The combination of all these properties makes AlN one of the most used piezoelectric materials for the fabrication of electroacoustic devices, e.g. thin film BAW bandpass filters.

Molecular beam epitaxy (MBE) [8, 9], chemical vapour deposition (CVD) [10-12] and sputtering [1-4, 13-15] are some of the techniques commonly used to grow AlN films. The choice of the deposition technique is defined by the specific application. Noteworthy, MBE and CVD require high deposition temperatures, making them incompatible with the fabrication of electroacoustic devices. In this sense, sputter-deposition of AlN films is a suitable choice for the fabrication of these devices since it requires relatively low deposition temperatures.

Some advantages of the reactive sputtering technique compared to other deposition techniques are high deposition rates, excellent texture control and film uniformity. AlN thin films can be deposited by means of several variants of the sputtering technique such as:

- High power impulse magnetron (HiPIMS) [16, 17],
- Direct current (DC) magnetron [1, 3, 16],
- Pulsed DC magnetron [4, 17], and
- Radio frequency (RF) magnetron [14, 18].

The sputtering methods used in this work are DC, Pulsed DC and HiPIMS[1].

The properties of the piezoelectric layer define the performance of the electroacoustic device, since these properties impact directly on the electroacoustic properties (insertion loss, coupling coefficient, quality factor, bandwidth, dielectric constant, etc.). Therefore, a careful control of the process deposition conditions is a requirement for the growth of highly textured (c-axis oriented) AlN films (Figure 1.1).

One way to evaluate the texture of c-axis oriented AlN film is by the analysis of the rocking curve of its (002) X-ray diffraction (XRD) peak. The better the orientation of the film, the smaller the full width at half maximum (FWHM) of the (002) peak, thus indicating better alignment of the c-axis of the individual grains with the surface normal.

The electromechanical coupling, which is a measure of the conversion efficiency between electric and mechanical energy, is highest for longitudinal deformation along the c-axis of

[1] Also known as HPPMS (high power pulsed magnetron sputtering).

wurtzite AlN. Noting that modern telecom applications require large bandwidths and that the bandwidth is proportional to the electromechanical coupling, it transpires that films with excellent c-texture are needed for such applications. Consequently, most commercial telecom devices make use of longitudinal bulk waves propagating along the c-axis. Electrical excitation is effected by an electric field also parallel to the c-axis (along the film thickness) for which reason such devices are said to make use of thickness excited longitudinal bulk waves. The term longitudinal denotes the direction of the particle displacement which is parallel to the wave vector as illustrated in Figure 1.2.

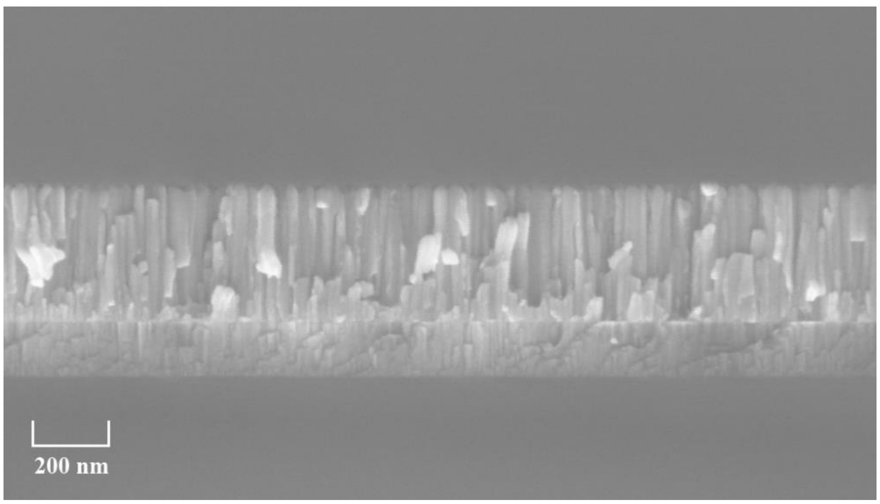

Figure 1.1 - C-axis oriented AlN film deposited by Pulsed DC on top of a Mo layer.

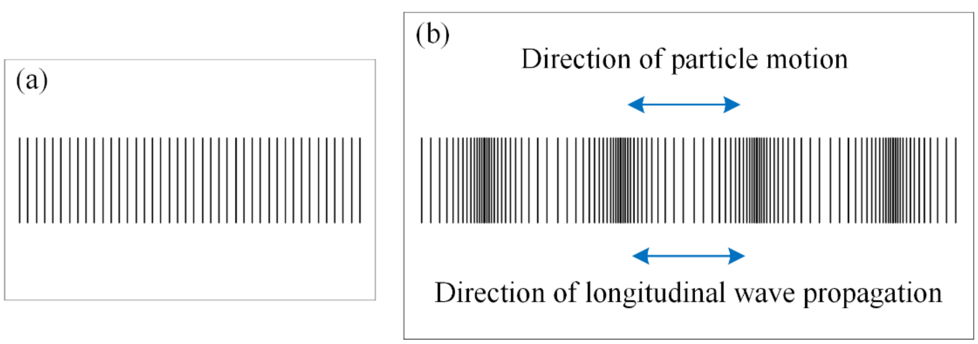

Figure 1.2 - One dimensional representation of particle displacement in a medium (a) without any wave motion, and (b) with longitudinal wave propagation.

As indicated above, the primary use of the electroacoustic technology is its application in the telecom field (oscillators, filters, delay lines, and so on). However, there has been a growing use of thin film electroacoustic devices in sensing applications. This is due to their higher sensitivity, resolution as well as reliability when comparing with other type of sensors [19]. In the past few years thin film electroacoustic based sensors have been reported, for instance, pressure sensors [19, 20], gravimetric sensors [20], temperature sensors [19], gas flow sensors [21, 22] and biosensors [22-25].

Notwithstanding, the use of the thin film electroacoustic technology for sensors is not straightforward, particularly for sensors operating in liquid/viscous media, e.g. chemical and biochemical sensors. This is due to the fact that longitudinal and surface waves exhibit a considerable acoustic leakage into liquid/viscous media, ergo resulting in a loss of sensor resolution. To this end, shear wave resonators are employed since shear waves do not propagate in liquids and hence exhibit considerably lower acoustic losses in such media. Unfortunately, the piezoelectric constants of AlN are such that electrical excitation of shear waves is only effected by an electric field having a non-zero angle with the c-axis. More specifically, when this angle is $\theta = 90^o$ (i.e. a-textured films) the mode is pure shear (Figure 1.3). In the case where θ is smaller than 90^o the mode excited is quasi-shear, that is, it has one shear and one longitudinal components. The latter declines rapidly with θ and hence at angles larger, say, than 20^o the longitudinal excitation is negligible and hence the acoustic leakage associated with the longitudinal component is also negligible. Ideally, one would like to use the pure shear mode, but the technological difficulties associated with growing unipolar a-textured films render this approach impractical. For this reason, focus has shifted towards the synthesis of textured AlN films with a tilted c-axis (Figure 1.4) which in turn allows thickness excitation of quasi-shear waves. This thesis studies both the nucleation and growth mechanisms that allow the synthesis of thin AlN films with a tilted c-axis in view of shear wave electroacoustic sensors.

The above two examples illustrate how desired functional (electroacoustic and dielectric) properties are achieved through control of both the crystallographic structure and texture of the films. Another area of study in this thesis is enhancing the functional properties of AlN through compositional changes. To this end, recent studies demonstrate improvement of various electroacoustic and piezoelectric properties of AlN films by doping these films with metalloids, such as B [26-28], and transition metals, like Ti [29], Sc [30, 31], Y [32], Cr [33, 34] and Ta [35].

Thus, in this thesis we demonstrate for the first time the potential of highly c-textured thin AlScN films for wideband telecom applications. This, along with other works in the thesis, represent a third area of studies where the enhanced functional properties of the films thus synthesized are demonstrated experimentally through the fabrication of specific devices and components, which are subsequently characterized electrically, and thus complete the cycle of the research.

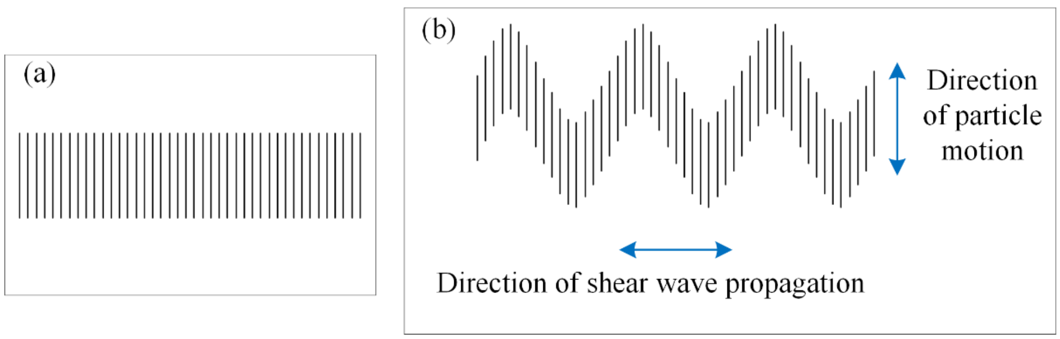

Figure 1.3 - One dimensional representation of particle displacement in a medium (a) without any wave motion, and (b) with shear thickness wave propagation.

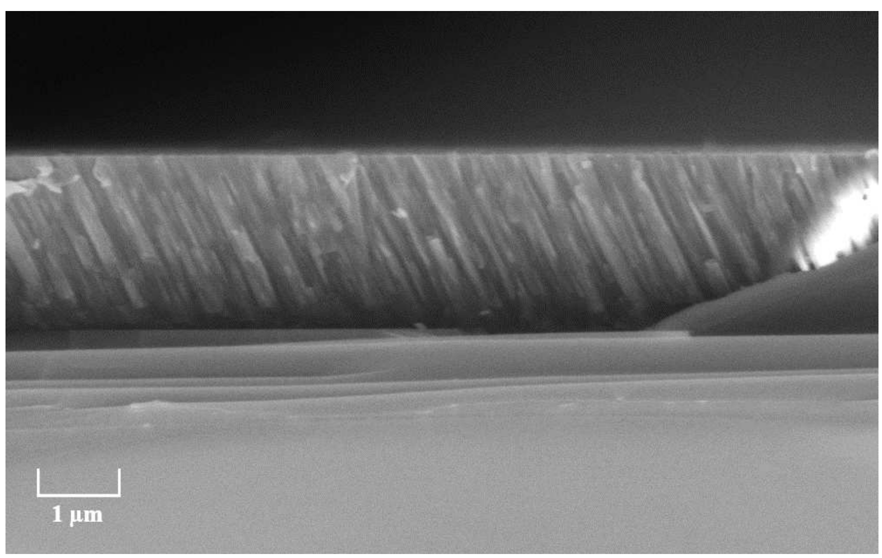

Figure 1.4 - C-axis tilted AlN film deposited by Pulsed DC on Si substrate.

In the following chapters, a brief background about the underlying concepts will be presented followed by a description of the experimental procedures adopted. Subsequently, the main results of the research will be presented and discussed, along with a summary of the included papers. Finally, the conclusions from the work are presented.

2 THEORETICAL BACKGROUND

As previously mentioned, the goal of this work is the improvement of AlN properties in view of sensors and telecom applications. To this end, many different aspects of synthesis and characterization of AlN films were studied. For instance:

- Enhancement of the piezoelectric properties of c-axis oriented AlN films by doping,
- Alternative approach to deposition of c-axis tilted AlN films,
- High-k AlN films,
- Fabrication of electroacoustic devices, and
- Improvement in the nucleation layer by the use of ion assisted sputter deposition (HiPIMS).

Since this work includes various aspects related to AlN thin films, the purpose of this chapter is to bring up the discussion by presenting a brief overview of the different topics discussed in this summary. Furthermore, a literature review and the state-of-art of related research are presented to some extent.

2.1 C-AXIS ORIENTED ALN

The electromechanical coupling coefficient k_t^2 is a numerical value that represents the efficiency of piezoelectric materials to convert electrical into acoustic energy (and vice versa) for a given acoustic mode. Therefore, the higher the k_t^2, the higher the electrical-acoustic energy conversion. The piezoelectric response of wurtzite AlN is the integral effect of the individual dipole contributions of all the grains comprising the film. Thus, a highly c-axis oriented film yields a high k_t^2 coefficient since the grains will be aligned along the same direction, collaborating then to the same sign to the piezoelectric response (Figure 2.1) [36].

Sputtered AlN films can grow in a crystalline or an amorphous phases, and furthermore the crystalline films can grow in textured and non-textured ways [3]. One further peculiarity of wurtzite AlN is that it is a polar material. In this context it is equally important that c-textured films are in addition unidirectional in order to be piezoelectric. The Al atoms sputtered from the

Al target will react with the N atoms and ions present in the plasma, creating AlN clusters[2]. Thus, a good control of the deposition parameters is crucial in order to obtain highly c-axis textured films.

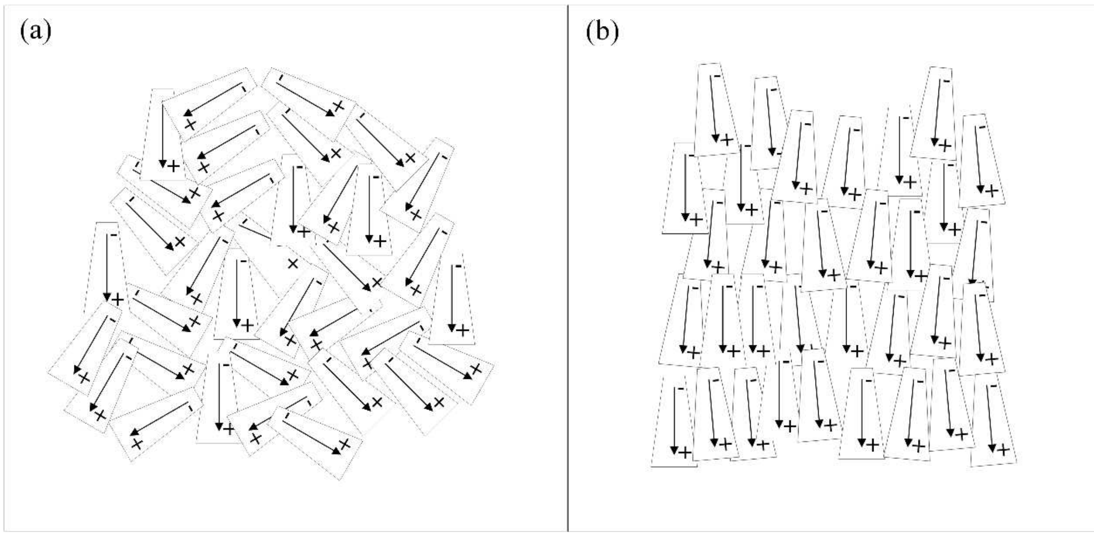

Figure 2.1 - Schematic of the dipoles distribution along a piezoelectric net:(a) grains aligned in various directions, and (b) grains aligned along the same direction.

In the case of sputtered films, some of the most important deposition parameters to consider are: substrate temperature, processing pressure, Ar/N_2 flow rate, discharge power and target-to-substrate distance. It is essential to provide the adatoms[3] with the right amount of energy [6, 36]. To this end, the optimal balance between these deposition parameters must be achieved[4]. Obviously, this balance varies for different experimental setups.

The mean free path[5] (MFP) of a sputtered atom is given by

$$MFP = \frac{k_B T}{\sqrt{2}\pi d^2 p} \tag{1}$$

where k_B is the Boltzmann constant (~1.38×10^{-23} J/K), T is the temperature (in Kelvin), d is the diameter of the gas particles (in meters) and p is the pressure (in Pascals). As indicated by the above equation, the MFP is influenced by both pressure and temperature. To further illustrate the

---

[2] A cluster has an intermediate size between a single crystal and a bulk solid material.
[3] Adatom is a non-absorbed atom lying on the crystal surface and that can migrate over it.
[4] Other important parameters to consider are film thickness, substrate bias and deposition rate [6].
[5] Mean free path is the average distance that an atom can move without colliding at another atom.

influence of pressure, the MFP of the sputtered Al atoms at a pressure of 20 mTorr is around 1 cm (at room temperature); on the other hand, the MFP is equivalent to 10 cm at a pressure of 2 mTorr [37].

At low gas pressures, the number of collisions and scattering by the gas molecules is also low (larger MFP), which means that the atoms sputtered from the target will retain a significant fraction of their initial kinetic energy when arriving at the substrate surface. This in turn favors the growth of wurtzite structure of AlN [3] since this relatively high kinetic energy enhances the adatom mobility, ergo making them diffuse over the surface [38] and eventually finding a low energy lattice site. Noteworthy, the adatom mobility can also be enhanced by increased substrate temperature.

The growth of c-axis textured films is dependent not only on the deposition conditions. The substrate material and its crystallographic structure also play an important role in the film growth. Thus, AlN films deposited on top of highly textured metal films having a hexagonal surface symmetry show higher c-axis texture due to crystallographic similarity [39]. Besides, the roughness of the bottom material should be considered since it can influence the adatom mobility of sputtered AlN. Comparing films prepared under the same deposition conditions but on materials with different roughness/smoothness, the adatom mobility is much higher on smooth surfaces. Thus, in order to provide the same adatom mobility on rough surfaces, it is necessary to improve the kinetic energy of the sputtered particles (by means of increasing the deposition temperature, for example). Another important aspect of surface roughness is that nucleation of AlN grains with the c-plane parallel to the surface is thermodynamically the most energetically favorable. Hence, the FWHM of the rocking curve is proportional to the surface roughness, or in other words high roughness results in a poor c-texture. This fact can also be used for the growth of AlN films with a tilted c-axis as discussed next.

2.2 TILTED ALN

For some specific applications, such as biosensors based on the electroacoustic technology and operating in liquid/viscous media, AlN films with a tilted c-axis are more suitable than the c-axis oriented ones [22-25, 40]. Resonators using the shear wave mode are most suited for such applications due to the decrease of acoustic losses when comparing with the longitudinal wave mode ones. The reason for this is that shear waves do not propagate in liquids and hence acoustic leakage typical for longitudinal waves is totally eliminated when employing shear waves. Unfortunately, shear waves cannot be excited in c-textured AlN films with an electric field along the film thickness while lateral field excitation exhibits extremely low couplings. Therefore, for thickness excitation of shear waves, films with a tilted c-axis are required.

There are a variety of methods available to deposit tilted AlN films. Some of them are (see Figure 2.2):

i. Off-axis (or off-normal) deposition [41, 42],
ii. Tilted substrate deposition [43, 44],
iii. Tilted and off-centered target deposition [45, 46], and
iv. Two-stage deposition process [40].

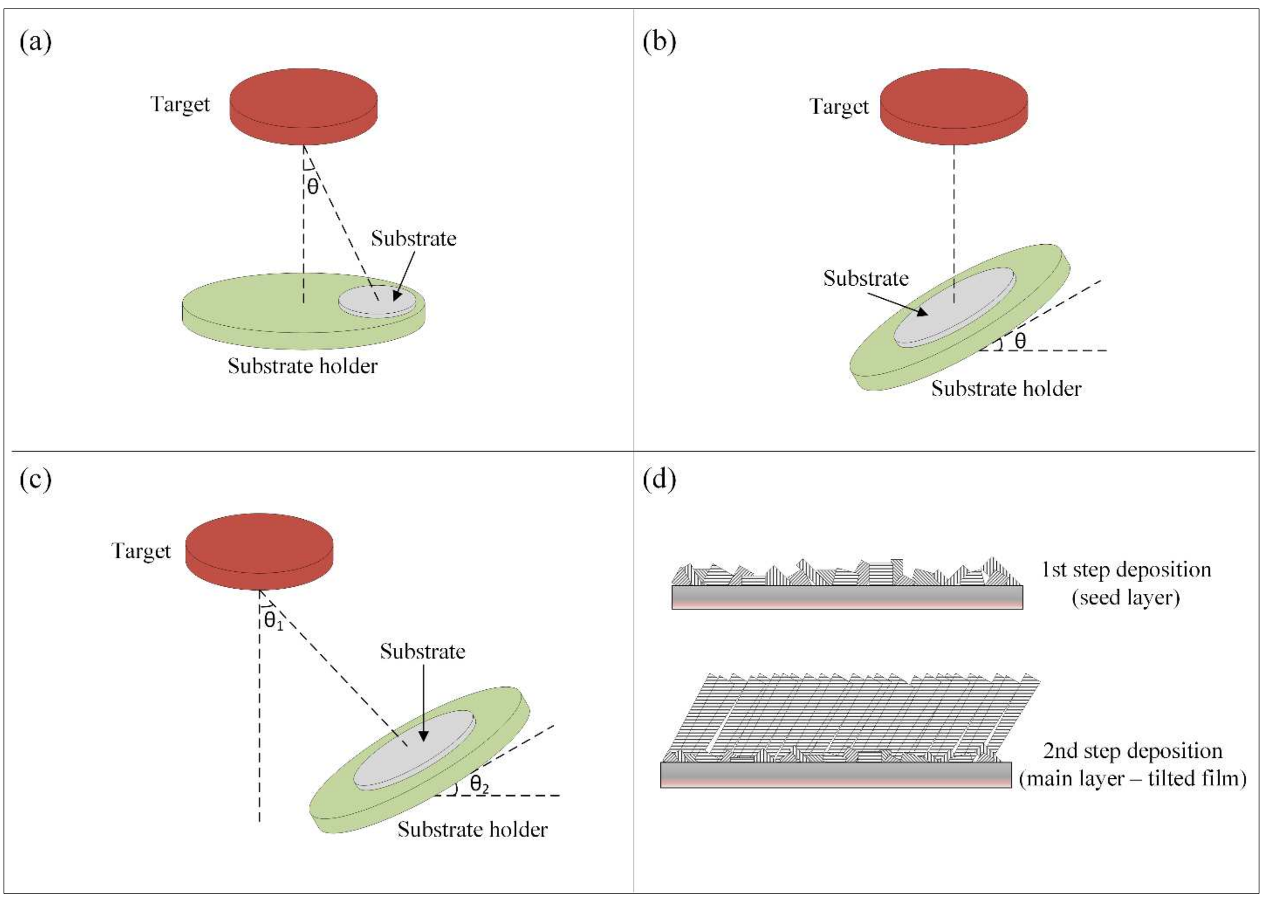

Figure 2.2 - Simplified schematic of different deposition setups for tilted films: (a) off-axis deposition, (b) tilted substrate, (c) tilted and off-centered, and (d) two-stage deposition process.

The three first methods require modifications in the standard setup of sputtering systems, whereas the latter one does not require any additional hardware changes. The general concept of these methods will be briefly discussed in here.

As in any sputter-deposition process, the deposition conditions strongly influence the growth of tilted films. It is well established that the adatom mobility plays an important role in obtaining highly textured films during sputter deposition [42, 44, 46-48]. Hence, in order to create conditions favorable for the nucleation of non c-oriented grains, adatom mobility needs to be suppressed. This is the reason the Uppsala deposition process consists of the following two steps, as presented in Paper V. An initial thin and “non-textured” seed layer is grown (Figure 2.3) by operating at relatively high process pressure and keeping the substrate at room temperature. All this results in a complete thermalization of the sputtered atoms, and hence in operating the deposition process in the diffusion limited regime. The resulting seed layer exhibits different textures, most notably (103) and (002). Once the seed layer has been deposited, growth of the film proceeds at low process pressures and elevated substrate temperature, both of which favor good crystal growth. The succeeding film growth however has no chance to proceed differently but to follow the crystallographic texture of the seed layer. In addition, the low pressure deposition in combination with a small target-to-substrate distance also yield a directional deposition flux. This results in competitive column growth, i.e., cones having the c-axis along the direction of the deposition flux grow fastest. In turn, this results in a film with c-tilt lying in the plane of the deposition flux at any given point on the substrate.

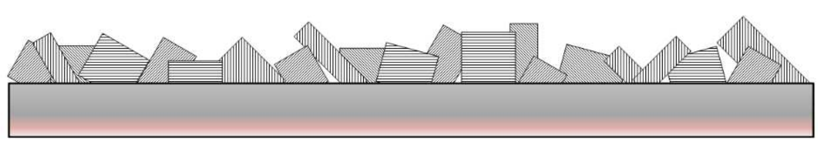

Figure 2.3 - Schematic of the nucleation layer with random crystal planes.

In the three first methods mentioned previously (i-iii), the tilted columns have a preferential growth due to the alignment with the tilted flux. This is very similar to what occurs during glancing angle deposition of sculptured thin films [49]. In the method (iv), the seed layer has a (103) dominant population rather than a totally random film [40]. Even though there is no intentional tilt of the flux, the magnetron disposition at the target generates a race track, which in turn provides the tilted flux direction towards the substrate (see Figure 2.2d).

2.3 DOPED ALN

The constantly increasing requirements for stringent specifications of the telecom market requires continuous improvement in the performance of high frequency devices. To this end, basically two steps can be considered: (i) improvements in device design, and (ii) enhancement of the properties of the constituent materials. Both steps aim at advances in the devices performance by achieving lower losses, higher resolution, higher bandwidth, lower production costs, lower capacitance parasitic, and so on.

One of the goals of this work is to improve the piezoelectric properties of AlN films. It is well-known that AlN possesses various properties suitable for high frequency devices (chemical stability, compatibility with IC-technology process, high quality factor, etc.). Owing to this, AlN is a promising material for use in high frequency devices (resonators, filters and oscillators, for instance). Although, the relatively low piezoelectric response does restrict its use in some applications, such as filters that require larger bandwidths.

It has been recently reported that a doping of AlN films with certain chemical elements can be beneficial to the improvement of its piezoelectric properties [26-35, 50-52]. However, this process is not straightforward. It is necessary to synthesize the new material (doped AlN) in order to find the optimized doping concentration and deposition conditions (and evidently this optimization varies for different dopant materials). This means that, even if the best deposition conditions are well-known for a certain equipment to achieve highly textured AlN films, the same conditions cannot be directly applied for the new material (AlXN[6]). For instance, gas flows, deposition temperature and target(s) power(s) must be optimized.

Nowadays there are four main methods to sputter AlXN thin films (Figure 2.4):

i. Concentric ring-shaped targets [29],
ii. Dopant inserts in the Al target [33, 34],
iii. Alloyed Al target [51], and
iv. Co-sputter by use of two different targets [52].

[6] AlXN is written in here as a simplified way to refer to doped AlN films. “X” can be any dopant.

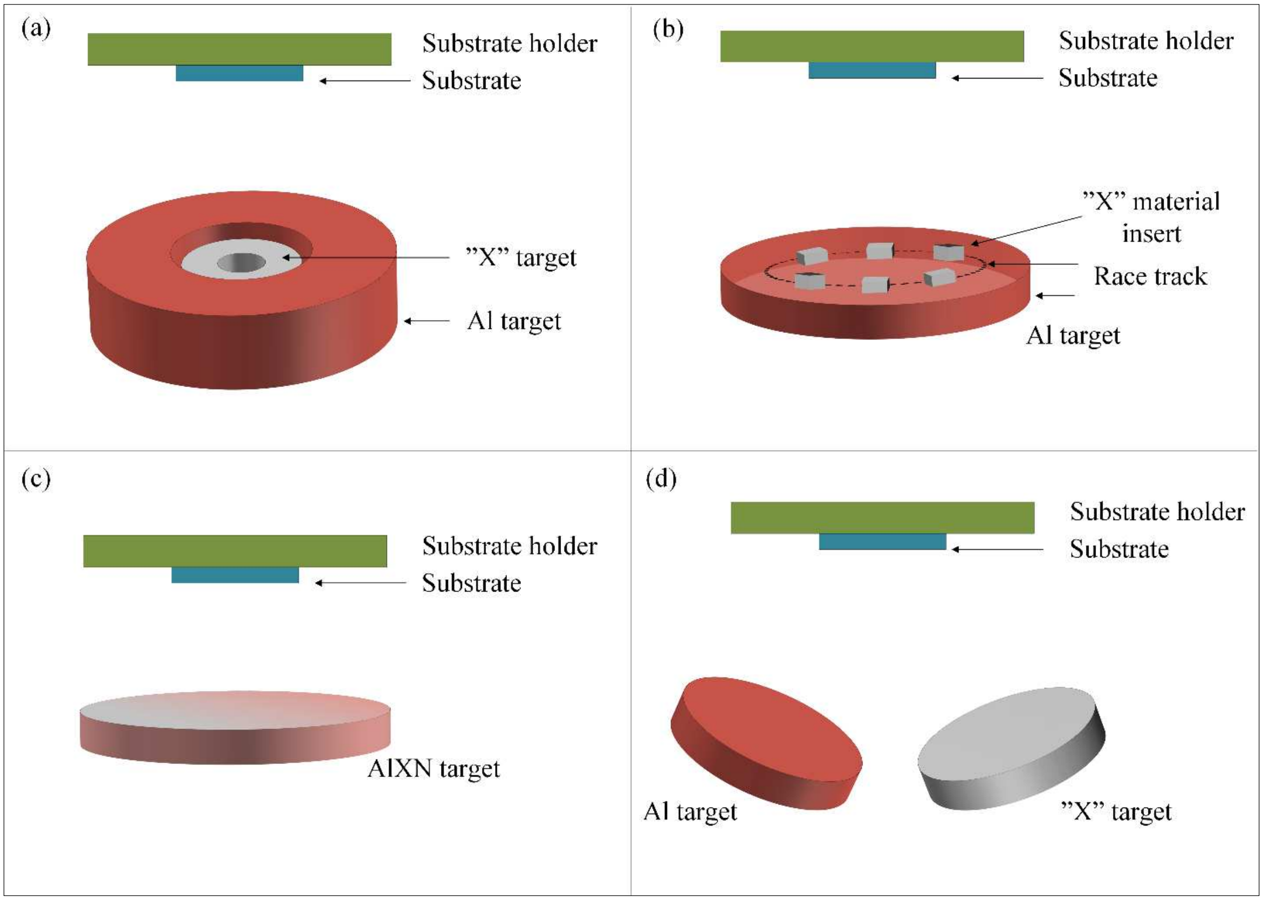

Figure 2.4 - Schematic of deposition methods to sputter doped AlN thin films: (a) concentric ring-shaped targets, (b) dopant inserts into the Al target, (c) alloyed Al target, and (d) co-sputter with two different targets.

The disadvantage of the three first methods (i-iii) is that the constituents ratio Al/X is fixed at all depositions. This disadvantage does not exist for the method (iv), where the ratio Al/X can be modified by changing the sputter power of each target (Al and X material).

Specifically for electroacoustic devices based on AlN thin films, a dopant that has attracted a lot of attention nowadays is Sc. Ab-initio calculations and experimental results suggest the enhancement of the piezoelectric properties of AlN by doping it with a certain amount of Sc [7, 53]. This work experimentally investigated the synthesis of highly c-textured aluminum scandium nitride[7] ($Al_xSc_{(1-x)}N$) thin films as well as evaluated their piezoelectric properties (Paper IV). The deposition method chosen is co-sputtering (Figure 2.4d).

[7] It is usual to find in the literature the nomenclature scandium aluminum nitride ($Sc_{(1-x)}Al_xN$) for the same material.

Scandium nitride (ScN) is a III-V nitride with rock-salt structure (non-polar[8]), and AlN is III-V nitride with wurtzite structure (polar[9]). There is a transition region between wurtzite and rock-salt structures by doping AlN films with Sc. Some authors support that this intermediate phase state is responsible for the improvement in the piezoelectric response of the film [30].

The electromechanical coupling (k_t^2) is directly related to the properties of the piezoelectric films. The equation that defines k_t^2 can be written as

$$k_t^2 = \frac{{e_{33}}^2}{\left(C_{33}+\frac{{e_{33}}^2}{\varepsilon_{33}}\right)\varepsilon_{33}} \tag{2}$$

where e_{33}, C_{33} and ε_{33} are the piezoelectric constant, stiffness and dielectric constant, respectively. It can be seen from the previous equation that an increase in the piezoelectric constant and a decrease in the stiffness of the material contribute to the improvement of k_t^2. Both goals can be achieved by doping AlN films with Sc, which has been proved theoretically [7, 53] and experimentally [30, 31, 51, 52].

Noteworthy, an increase of 500% in the piezoelectric response of AlN films doped with Sc was experimentally demonstrated [30]. Unfortunately, other properties such as the acoustic losses and sound velocity somewhat deteriorate (which can be expected by the decrease of the stiffness coefficient). With respect to filter design an important figure of merit is the product k_t^2 x Q. Thus, in this case a tradeoff between k_t^2 and Q is sought so that the product between these is higher than that of pure AlN.

2.4 ELECTROACOUSTIC DEVICES

Electroacoustic devices can be designed in various ways in order to explore different propagation modes. Some of these modes are [54]:

- Longitudinal BAW,
- Shear BAW,
- Surface acoustic wave,

[8] In a non-polar structure there is an equal distribution of charges in the molecule.
[9] In a polar structure there is a non-similar distribution of charges, i.e., there is a positive charge in one end of the molecule and a negative charge in the other end.

- Shear-horizontal acoustic plate mode,
- Surface transverse wave,
- Love wave, and
- Flexural plate wave.

The structures of different types of electroacoustic devices differ in terms of the active layer material (piezoelectric materials) and the particle displacement relative to the wave propagation direction.

A range of these acoustic modes are already exploited in the telecom market, where they have been used as filters and oscillators, for instance. However, as mentioned before (Chapter 1), there has been a growing interest in their application in the sensing field. In this case, the piezoelectricity is used in an indirect[10] way [50]: sensing is achieved through perturbation of the acoustic wave that propagates through the piezoelectric layer. This perturbation may be the result of a biochemical reaction or a temperature change, or strain due to external force, etc. Typically, this perturbation results in a frequency shift and/or change in the propagation losses, which subsequently are calibrated by the readout electronics to provide the sensing information (temperature, pressure, viscosity, mass, etc.). Noteworthy, the overall performance of the resonator of the electroacoustic sensor will affect the design of the final readout circuit insofar as quality factor[11] and electromechanical coupling define sensitivity and resolution of the sensor [50].

The design of the electroacoustic sensors is driven by their final application. For instance, the choice of the acoustic propagation mode and the active layer material will determine whether the sensor can be used in gaseous or in-liquid media. As an example, one can mention the use of tilted AlN films (instead of c-axis oriented) in the shear wave mode (instead of the longitudinal one) is the most suitable for in-liquid media applications [23, 40-42, 44].

In this work, electroacoustic devices were used as a tool to study the effects in the electroacoustic properties of AlN films by doping these films with different Sc concentrations (Paper IVIV). FBAR (film bulk acoustic resonator) was the electroacoustic device fabricated.

[10] In the direct use, the piezoelectric concept is straightforward: the sensing parameters causes a mechanical deformation in the piezoelectric layer, and consequently an electrical signal will be generated.

[11] The quality factor of an oscillating system is defined as the ratio between the energy stored and the energy dissipated by the system during the one oscillation cycle [54].

2.5 HIGH-K ALN

It is well known that the dimensions of the devices based on the transistor technology are continuously scaling down. For this reason, the thickness of the gate dielectric must follow the re-scaling of the transistors in order to keep the same capacitance between gate and the channel regions. To illustrate the relationship between gate thickness and capacitance, the gate dielectric can be modeled in a simplified way as a parallel plate capacitor, to which the capacitance C is given by

$$C = \frac{k\, \varepsilon_0\, A}{t} \tag{3}$$

where k is the dielectric constant of the gate material, ε_0 is the absolute dielectric permittivity, A is the capacitor area and t is the thickness of the capacitor insulator (in this case, the gate layer).

The most used gate dielectric in the Si based VLSI (very large scale integration) technology is SiO_2, which already reached its physical thickness limit in the scaling down process. For gate thickness scales below 2 nm the leakage current[12] is strongly pronounced due to the tunneling current effect, driving the device to a worsened performance because of the increased power consumption and lowered reliability[13]. An alternative is to increase the dielectric constant coefficient k, thus having a degree of freedom to work with thicker gate layers while keeping a high capacitance. To this end, materials with higher dielectric constants to replace the SiO_2 gate have drawn attention in the last few years. Some of these materials are Al_2O_3, HfO_2, ZrO_2, TiO_2 and AlN [55, 56].

However, there are some technological problems to handle when using oxides as gate dielectric material, such as the appearance of SiO_2 or silicates in the interface layer between the gate oxide and Si substrate. These interfacial layers have a lower-k coefficient, leading to a decrease in the overall capacitance density [55]. In this sense, nitrides and oxi-nitrides have been calling more attention as an alternative to replace SiO_2 as the gate dielectric layer. Thus, AlN films stand as a suitable material since the nitride film suppress the rise of interfacial layers between high-k dielectric and Si substrate (mostly due to the high amount of oxidized elements

---

[12] Also called as off-current, it is defined as the small amount of current that continues to flow between source and drain after the gate voltage is turned off.

[13] The reliability of a device describes its capacity in working for certain period of time under stated conditions.

with oxide gate films). An experimental work to evaluate the possibility to use AlN as gate dielectric is presented in Paper III.

2.6 HIGH POWER IMPULSE MAGNETRON SPUTTERING (HIPIMS)

Magnetron sputtering have been used in a wide range of research and industrial applications over the last decades. However, the continuous and increasing demand for new materials and improved properties leads to the need for development of new deposition techniques in order to achieve better control of the deposition process. To this end, techniques to increase the degree of ionization of sputtered species have been studied and developed [57], and the HiPIMS is one of those. Considering that HiPIMS is an emerging technique and not fully explored yet, a short and brief description of this sputtering process will be presented in here.

The PVD (physical vapor deposition) methods characterized by a flux of ions higher than the flux of neutrals of the deposited species are called IPVD (ionized physical vapor deposition) [58, 59]. There are different methods among the IPVD technique, such as [59, 60]:

- Cathodic arc deposition,
- HCM (hollow cathode magnetron), and
- HiPIMS.

Alternative ways to enhance the ionization fraction in conventional magnetron sputtering is to use a supplementary ICP (inductively coupled plasma) or ECR (electron cyclotron resonance).

The common characteristic of the aforementioned methods is the possibility of a good control of energy and direction of the sputtered material. Notwithstanding, comparing with other IPVD methods, an advantage of HiPIMS is its simplicity since any sputtering machine based on magnetrons can be turned into a HiPIMS system by only replacing the power supply.

The basic concept of HiPIMS is the delivery of a high degree of ionization to the system by means of a high density plasma. To this end, the power supply should deliver pulses in the order of $kW.cm^{-2}$ (the power supplies used in conventional magnetron sputtering systems provide pulses in the range of a few tens $W.cm^{-2}$) [59, 61]. Comparing the values of plasma densities for both techniques, conventional magnetron sputtering delivers electron densities in the range 10^{14} – 10^{16} m^{-3}, while this values for HiPIMS are commonly in the range 10^{18} – 10^{20} m^{-3} [57, 59].

High density plasma is achieved by means of high power pulses delivered to the magnetron at low frequency and low duty cycle[14]. In other words, the HiPIMS pulse can be compared to an impulse: pulse with very high amplitude and long time gap between the pulses [61]. Noteworthy, due to the high electrical power delivered to the target surface, a low duty cycle is mandatory in order to avoid target overheating.

As in any sputtering technique, the properties of the films deposited by HIPIMS can be adjusted by tuning the deposition parameters. Pressure, temperature, substrate, target power, etc., influence the characteristics of the films. However, it is important to highlight here the enhancement that the increased ionization gives to the films properties. Improvements in roughness, density, adhesion and hardness are observed when comparing HiPIMS and conventional magnetron sputtering techniques [61].

One drawback of the HiPIMS technique is the reduction of the deposition rate (compared with Pulsed DC depositions under similar conditions[15], see Figure 2.5). Some authors explain this behavior by the phenomenon of back attraction of the sputtered and highly ionized species back to the target [16, 59, 61]. Alternative setup arrangements have been studied in order to increase the deposition rate [57].

There are just a few studies reported in the literature presenting AlN films deposited by HiPIMS. The work presented in Paper I intends to contribute in an overall analysis of AlN films sputtered by HiPIMS. Moreover, Paper I presents and discuss the results of highly c-axis textured AlN films deposited by this technique.

[14] Duty cycle is the fraction of time in which the signal (pulse) is active (on) within one period.
[15] Refer to Paper I for further information regarding the deposition parameters of both processes.

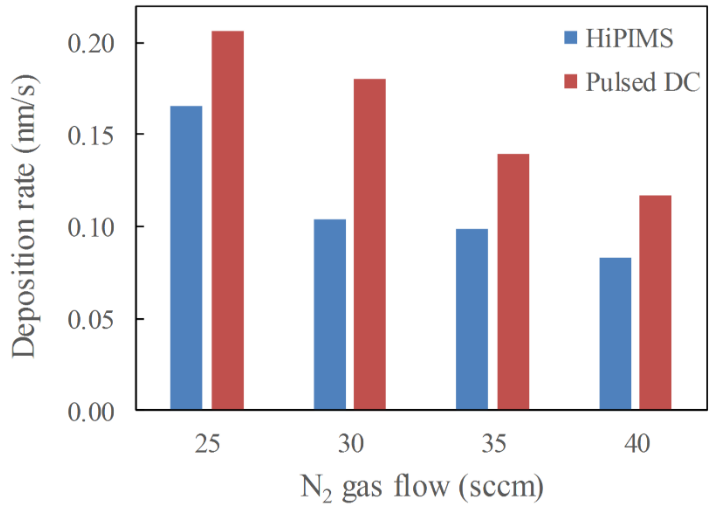

Figure 2.5 - Comparative plot of the deposition rate of AlN films deposited under similar conditions by HiPIMS and Pulsed DC.

3 RESULTS AND DISCUSSIONS

This chapter highlights and discusses more deeply some of the main achievements of this work regarding the synthesis and characterization of thin piezoelectric films as this represents the main thrust of this thesis. It does not mean though that the topics that are not included in here are less significant. Notwithstanding the results and discussions in the papers, some of the results presented in this chapter have not been published yet. Therefore, the discussion based on these non-published results intends to complement the published work as well as, in an overall analysis, contribute to the field of piezoelectric materials for high frequency applications.

An extended summary of all results in this thesis are presented in Chapter 4.

3.1 SYNTHESIS AND CHARACTERIZATION OF ALSCN FILMS

As previously mentioned, the $Al_{(1-x)}Sc_xN$ films investigated in this work were deposited by the Pulsed DC co-sputtering method (refer to Figure 2.4d). The total amount of Sc in each film was controlled by the power delivered to the Sc target. The composition of the films was investigated by Elastic recoil detection analysis (ERDA) and the results of some $Al_{(1-x)}Sc_xN$ films are presented in Figure 3.1.

In order to reach highly c-textured films, one important step in the synthesis of $Al_{(1-x)}Sc_xN$ films was the investigation of the optimal substrate temperature during deposition. To this end, one specific composition of $Al_{(1-x)}Sc_xN$ film was chosen ($x = 0.09$) and films were grown at different temperatures, in the range from room temperature up to 800 ºC. The film texture was judged by the films' rocking curve (XRD analysis), where the FWHM[16] of each film was measured afterwards.

[16] The FWHM is calculated from the rocking curve (X-ray diffraction). The lower is the FWHM (narrower curve), the better is the film texture.

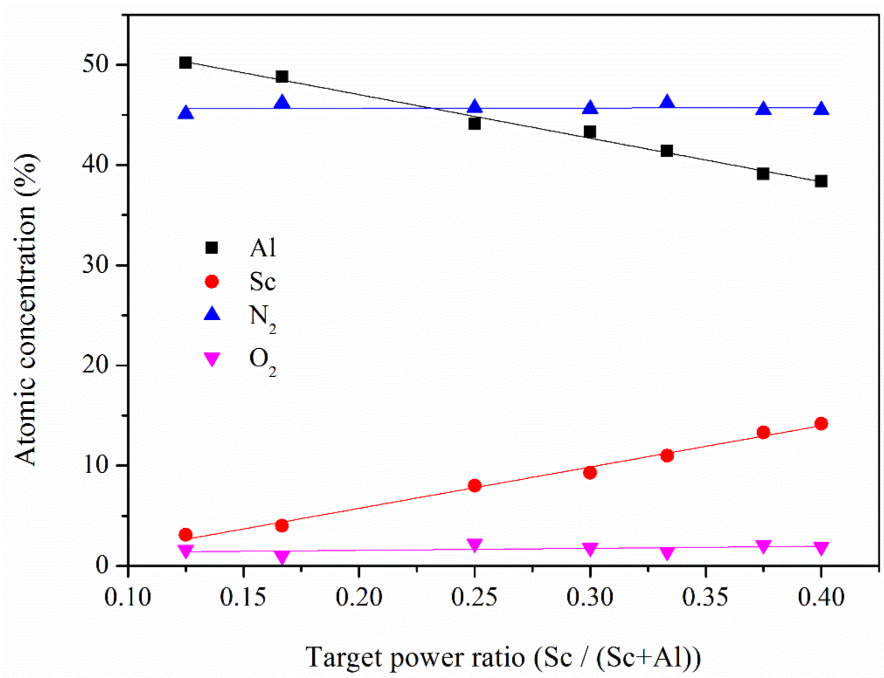

Figure 3.1 - ERDA analysis of $Al_{(1-x)}Sc_xN$ films.

As indicated in Figure 3.2, there is an improvement at the FWHM by increasing the deposition temperature up to 400 ºC, at which the film reaches the best FWHM (lowest value). For temperatures higher than 400 ºC the FWHM starts to deteriorate. Some authors explain this phenomenon by assuming that there is a threshold energy for the adatoms which defines the different growth mechanisms, ergo the film texture [62, 63]. Still according to these authors, the increment of the adatom mobility at the substrate surface contributes not only to the preferential orientation growth (002 plane), but also to the grain coarsening. Depending of the overall energy delivered to the adatoms (around the threshold energy, for instance), the AlN (002) plane growth can be promoted and other crystal orientations suppressed.

Therefore, the substrate temperature for the deposition of $Al_{(1-x)}Sc_xN$ films was set to 400 ºC since the films deposited at this temperature presented the best results in terms of texture. Obviously this temperature is valid for a specific hardware setup (target-to-substrate distance, rotation speed of the target, substrate heating method, etc.) and deposition conditions (gas flow rate, target power, etc.). Most likely, for different hardware setups and deposition conditions there will be other optimal substrate temperatures for deposition of textured $Al_{(1-x)}Sc_xN$ films due to the differences in the overall balance of energy between the systems. A summary of the hardware setup and deposition conditions used in this work are listed in Table 3.1.

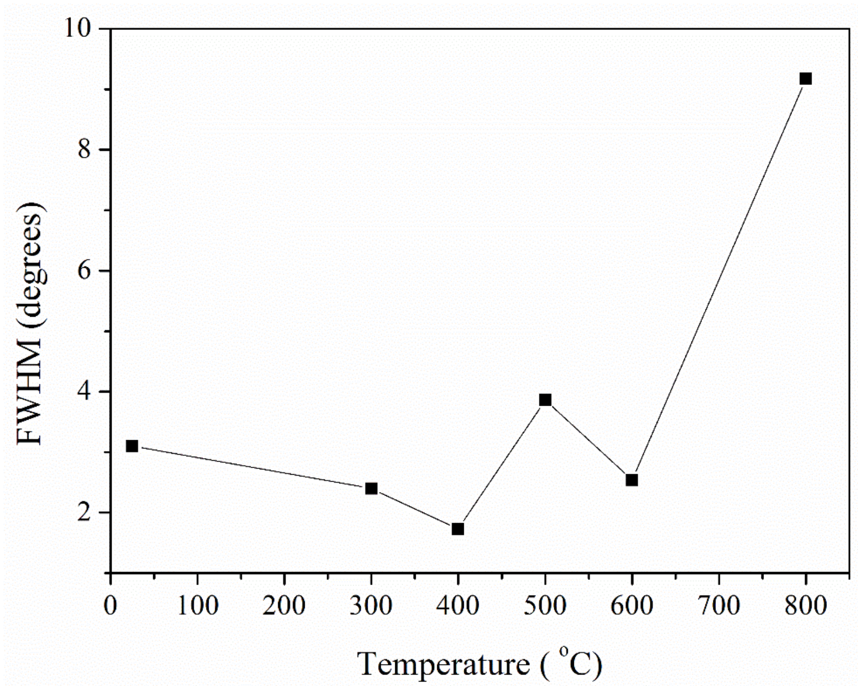

Figure 3.2 - Influence of deposition temperature on the texture of AlScN (FWHM plot).

Table 3.1 - Brief summary of the hardware setup and deposition conditions of $Al_{(1-x)}Sc_xN$ films.

Target-to-substrate distance	18 cm
Rotation speed	20 rpm
Substrate heating	Radiative heater
Base pressure	< 2 x 10^{-8} Torr
Deposition pressure	2.8 – 3.1 mTorr
Ar flow	30 sccm
N_2 flow	30 sccm

Noteworthy, substrate temperature studies were performed also for other $Al_{(1-x)}Sc_xN$ compositions. However, the temperature range variation was not as broad as for the $Al_{0.91}Sc_{0.09}N$ film. The temperatures used were 300 ºC, 400 ºC and 500 ºC. Even though the film compositions were different, the results indicated 400 ºC as the optimal substrate temperature for all cases.

Another important step in the synthesis of $Al_{(1-x)}Sc_xN$ films was the investigation of the suitable substrate to grow the films. The initial tests were performed on Si and Si/Mo (300 nm) substrates.

On Si substrates, the films showed columnar structure but high FWHM (around 7°). This value is not acceptable for use in high performance devices, which require piezoelectric films with FWHM between 1° - 2°. A possible solution to this issue is the improvement in the nucleation layer of the $Al_{(1-x)}Sc_xN$ films deposited directly on Si. However, the target-to-substrate distance in the equipment used to deposit the films is high (see Table 3.1), which makes it more difficult to achieve higher adatom mobility over the substrate surface. In this work we suggest the use of HiPIMS deposition to grow suitable nucleation layers for the $Al_{(1-x)}Sc_xN$ films (for further details see item 3.3 and Paper I).

Besides the films deposited directly on Si substrates, it was necessary to synthesize also the films deposited on top of a metal layer since the use of a bottom electrode is required for some devices applications. The metal used in here is Molybdenum (Mo) due to its intrinsic properties such as low acoustic attenuation and high electrical conductivity [64], which makes it a common choice as metal layer (electrode) for electroacoustic devices applications.

However, obtain highly textured films on top of Mo layer is not straightforward since there is a lattice mismatch between Mo and $Al_{(1-x)}Sc_xN$ structural planes. There are reports in the literature suggesting the use of a thin AlN seed layer underneath the Mo in order to improve the texture of the latter one [64, 65], ergo leading to an improvement in the texture of the main AlN layer. The same concept was used in this work in order to enhance the quality of $Al_{(1-x)}Sc_xN$ films deposited on top of Mo.

The beneficial effect of the AlN interlayer on the texture of $Al_{(1-x)}Sc_xN$ film is seen in Table 3.2, where the presented results refer to the composition x = 0.09 (deposition at room temperature). In Figure 3.3 one can see a simplified schematic of the substrates and stacked layers used to grow $Al_{(1-x)}Sc_xN$ films. Noteworthy, in order to achieve the best quality $Al_{(1-x)}Sc_xN$ films, a study was carried out where the thicknesses of the AlN and Mo layers were systematically changed.

Table 3.2 - FWHM (degrees) of $Al_{0.91}Sc_{0.09}N$ (002) and Mo (110) films.

	Mo (110)	**$Al_{0.91}Sc_{0.09}N$ (002)**
(a) Si / $Al_{0.91}Sc_{0.09}N$	-	6.7
(b) Si / Mo / $Al_{0.91}Sc_{0.09}N$	12	9.5
(c) Si / AlN interlayer / Mo / $Al_{0.91}Sc_{0.09}N$	3.2	3.1

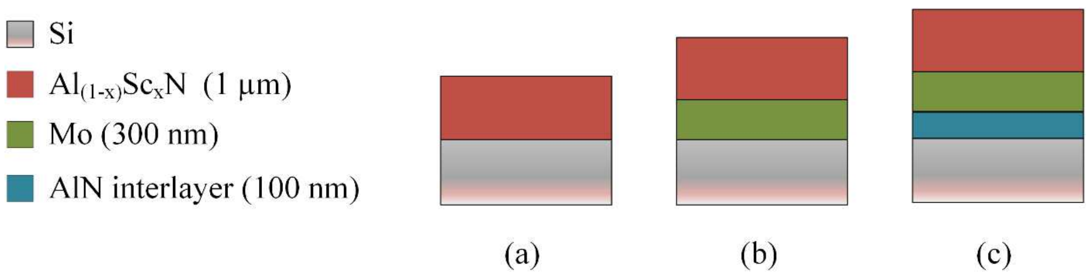

Figure 3.3 - Simplified schematic the substrates and stacked layers used to grow $Al_{(1-x)}Sc_xN$ films: (a) Si, (b) Si/AlN interlayer and (c) Si/AlN interlayer/Mo.

3.2 ELECTROACOUSTIC PROPERTIES OF ALSCN FILMS

As described in Paper IV, FBAR devices were fabricated in order to investigate the electroacoustic properties of $Al_{(1-x)}Sc_xN$ films. The results presented and discussed here refer to the compositions x = 0, 0.03, 0.09 and 0.15.

The θ-2θ XRD scans of all four film compositions are presented in Figure 3.4. The value of the FWHM extracted from the rocking curve of each film is indicated in Figure 3.4 as well. The well aligned (002) peak, the low values of FWHM and the absence of other AlN crystal orientations indicate that the $Al_{(1-x)}Sc_xN$ films are highly textured and c-axis oriented. The peaks at 38.5° and 40.5° are related to the metals used as bottom and top electrodes: Mo (110) and Al (111), respectively. It can be noted also at Figure 3.4 a slight downshift of the (002) peak at the compositions x = 0.09 and 0.15. This is due to the residual stress[17], which is more pronounced at

[17] The deposition conditions are the major reasons for the appearance of residual stress in thin films (substrate temperature, input power and gas pressure, for instance). The direction (compressive or tensile) and magnitude of the

the films with higher Sc concentration. Most likely, this behavior is caused by the increase in the lattice mismatch between the film and the substrate by adding higher amounts of Sc in the $Al_{(1-x)}Sc_xN$ films.

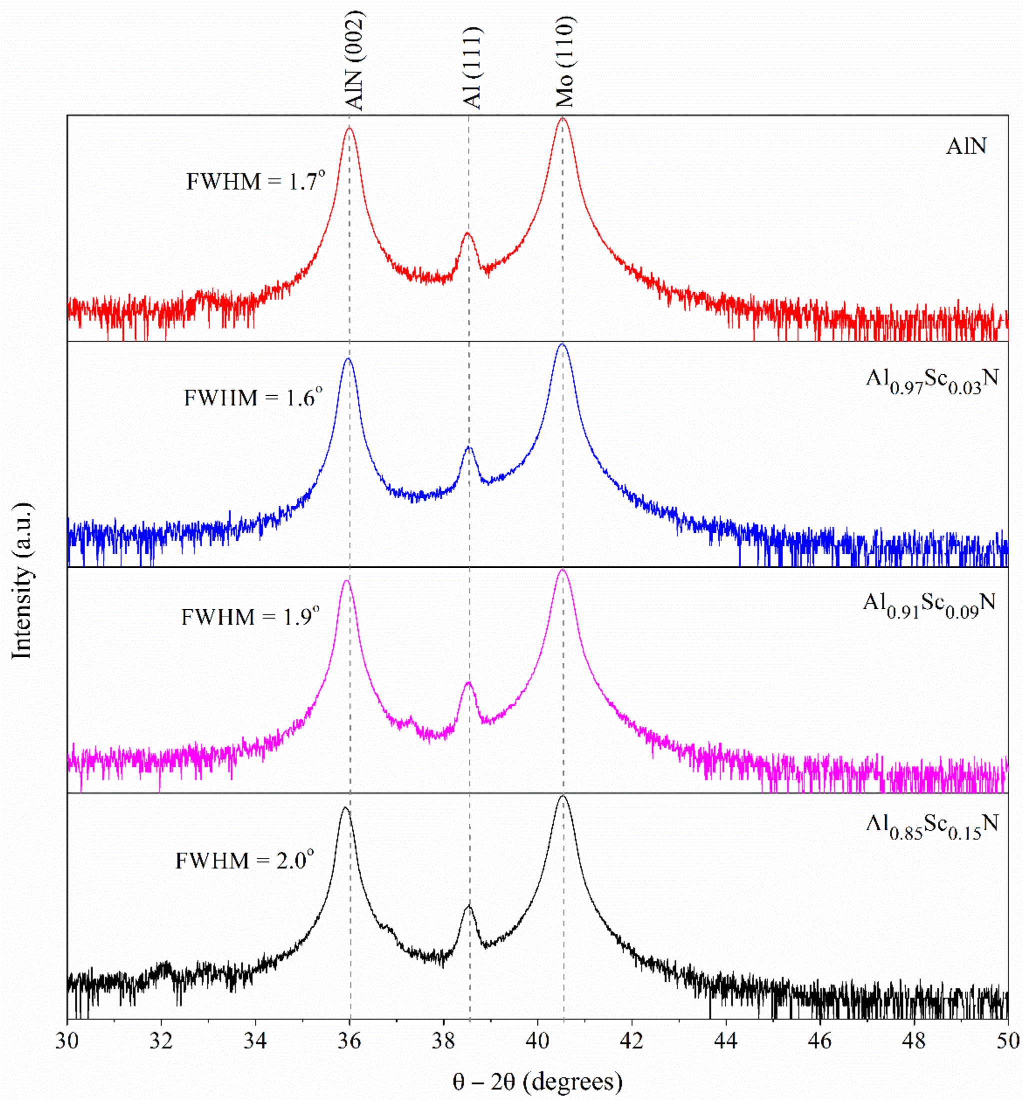

Figure 3.4 - θ-2θ scans of $Al_{(1-x)}Sc_xN$ films of the FBAR devices (x = 0, 0.03, 0.09 and 0.15).

The measurements for the electroacoustic characterization were performed in a network analyzer (standard configuration) and the wave excitation mode was the longitudinal[18] one. The

residual stress are mostly influenced by the deposition conditions. Noteworthy, the thickness of the thin film can also influence this parameter [16, 18, 36, 66].

[18] In the longitudinal wave propagation mode, the direction of particle motion is parallel to the direction of the wave propagation (see Figure 1.2).

equipment was calibrated for a 50 Ohm input impedance and central frequency around the central resonance frequency of the fabricated FBARs (2.35 MHz).

In order to extract the electrical and acoustic parameters of $Al_{(1-x)}Sc_xN$ films, the measured data were fitted to the Modified Butterworth Van-Dyke [19] (MBVD) and one-dimensional Nowotny-Benes[20] (NB) models by using the software ADS® (Agilent Technologies). The procedure is described in detail in Paper IV (item 3).

The doping of AlN films with Sc leads to a softening of the material, i.e., the $Al_{(1-x)}Sc_xN$ films become softer as the Sc concentration increases. This phenomenon has an impact on the electroacoustic properties of the film, clearly evidenced by the reduction of the quality factor (Q-factor) as indicated in Figure 3.5. Even though the films become softer their piezoelectric properties are enhanced, which leads to an improvement of the coupling coefficient (refer to Figure 3.5). Noteworthy, the coupling coefficient was increased by 100% when comparing pure AlN films and $Al_{(1-x)}Sc_xN$ with the highest Sc concentration (x = 0.15) used in the fabricated FBAR devices.

Therefore, there is a trade-off to be evaluated when doping AlN films with Sc: increase the coupling coefficient and improve the efficiency to which the piezoelectric material will convert electrical into mechanical energy (and vice-versa); or keep the quality factor as high as possible, ergo lowering the energy dissipation? Thus, the Figure of Merit (FOM) can be used as an indicator of the optimal compromising relationship. In the case of electroacoustic devices, the FOM is defined as the product k_t^2 x Q. Based on the measured values $k^2_{eff,m}$ and $Q_{B,m}$, the FOM was calculated for each $Al_{(1-x)}Sc_xN$ composition, and the maximum FOM achieved was 65.55 for the film with 9% of Sc (see Figure 3.6).

[19] For further information and references about this model, see Paper IV.
[20] Idem.

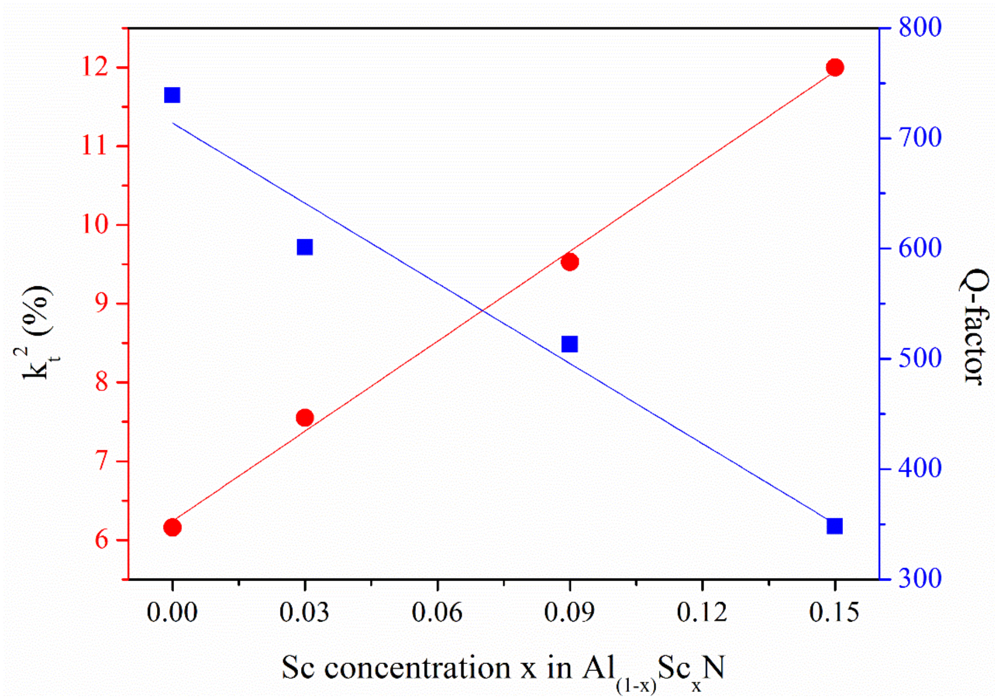

Figure 3.5 - Electromechanical coupling (k_t^2) and quality factor (Q-factor) as a function of the Sc concentration in $Al_{(1-x)}Sc_xN$ films.

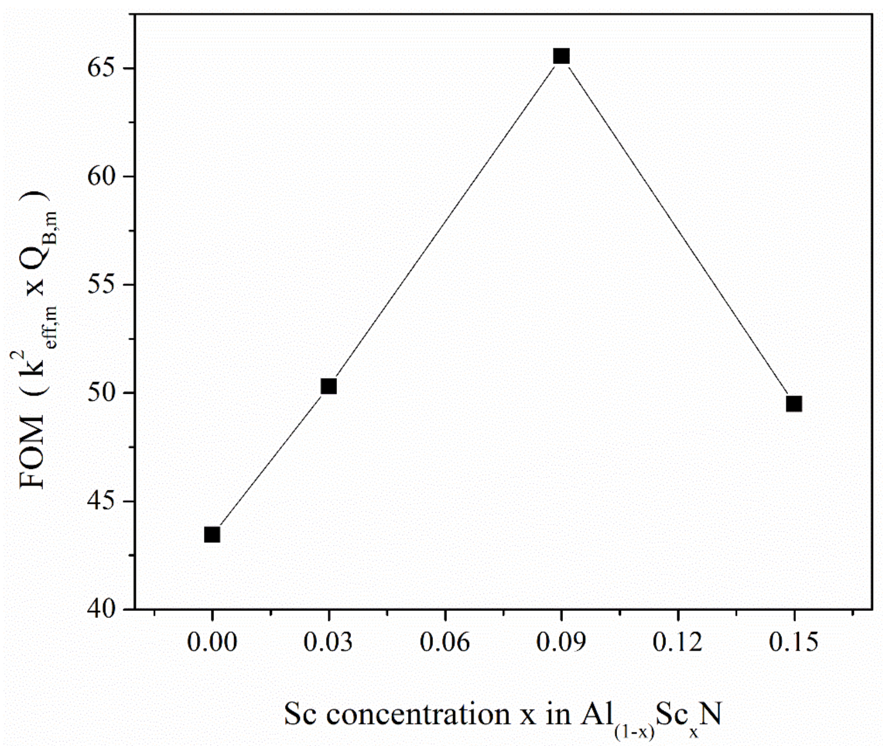

Figure 3.6 - Figure of merit (FOM) calculated for FBAR devices based on $Al_{(1-x)}Sc_xN$ and Sc concentration of 0, 3, 9 and 15%.

The temperature coefficient of frequency (TCF[21]) is also an important parameter to investigate in order to evaluate the performance of the devices operating at higher temperatures. To this end, the FBARs were heated in the temperature interval 25 - 125 ºC and their resonance frequencies were re-measured. The results are presented in Figure 3.7. It can be noted that the TCF tends to increase with the Sc concentration in the films. A possible solution to this issue is the use of a compensating layer of SiO_2 in the FBAR structure. The SiO_2 has a positive temperature coefficient of frequency and it has been largely used as a thermal compensating layer in resonators operating at high temperatures [67-69].

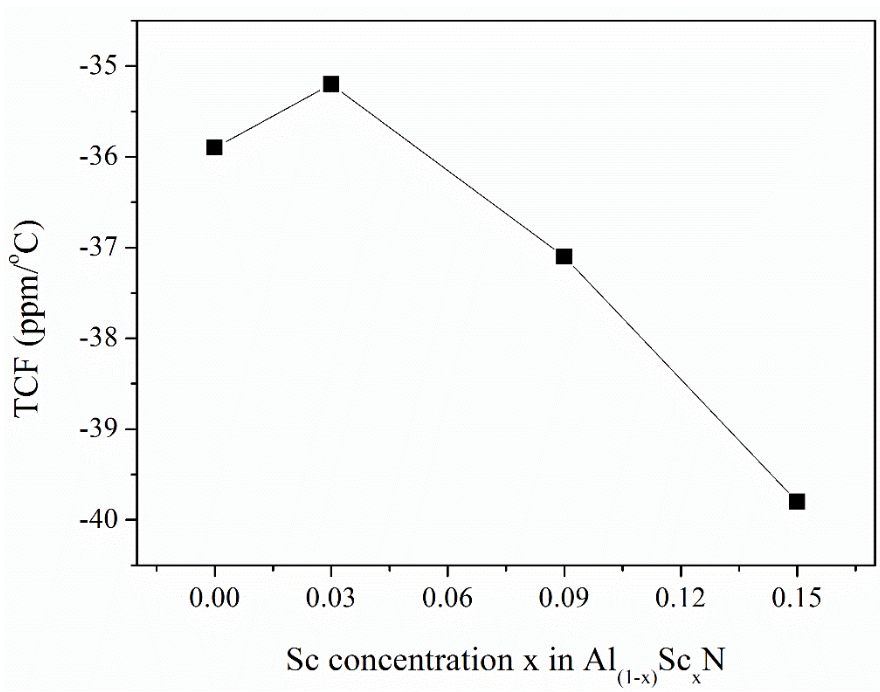

Figure 3.7 - Temperature coefficient of frequency (TCF) for FBAR devices based on $Al_{(1-x)}Sc_xN$ and Sc concentrations of 0, 3, 9 and 15%.

In addition to the acoustic properties studies, the electric parameters ε_r and tan δ[22] were investigated in order to evaluate the electrical behavior of $Al_{(1-x)}Sc_xN$ films as a function of the Sc concentration. The relative dielectric permittivity, ε_r, was calculated from the extracted static capacitance of the fabricated FBARs (see Paper IV, item 3). Metal-insulator-metal (MIM)

[21] The TCF indicates the relative change of the resonance frequency with the change of temperature. It is desirable to have this coefficient as near to zero as possible.

[22] The dielectric loss, tan δ, quantify the energy loss (heat) inherent to a dielectric material and it is calculated in here by the ratio imaginary/real part of the dielectric constant.

capacitors were fabricated to extract the dielectric losses, tan δ. These results are shown in Figure 3.8.

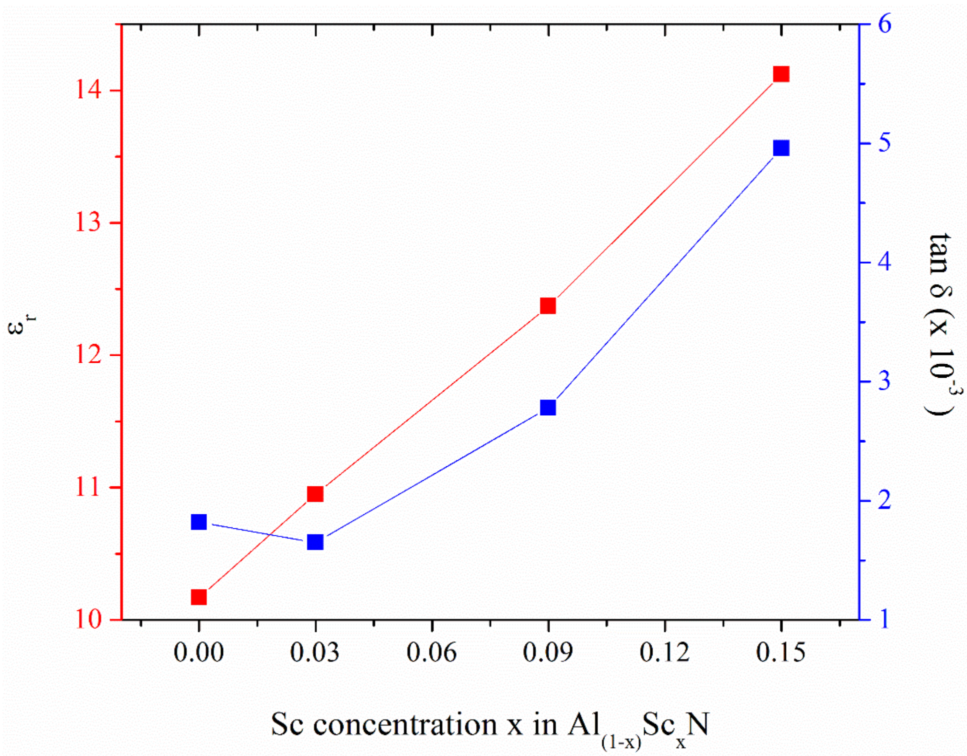

Figure 3.8 - Dielectric permittivity, ε_r, and dielectric losses, tan δ, as a function of the Sc concentration in $Al_{(1-x)}Sc_xN$ films.

It can be noted an undesirable increase in the tan δ parameter by increasing the amount of Sc in the films. However, these values are still lower (or similar to) when comparing with other concurrent piezoelectric materials, such as ZnO and PZT [70, 71].

3.3 HIPIMS AND ALN FILMS

It was already mentioned before that different parameters and conditions can influence the final texture of sputtered AlN films. Substrate material, deposition temperature, target power, pressure, gas flows and target-to-substrate distance are some of them. However, not least important is the condition of the nucleation layer of the films. More commonly, attention has been given in the literature to the growth of suitable nucleation layers when c-axis tilted AlN films are studied. In this case, the nucleation layer should be poor in (002) crystal orientations. Notwithstanding, a nucleation layer rich in (002) crystal planes is the best choice in order to grow c-axis textured AlN films.

At the work presented in Paper I, different deposition conditions were tested using the HiPIMS method and aiming the improvement of the nucleation layer properties of AlN films. Furthermore, depositions by conventional Pulsed DC (under similar conditions as the depositions done by HiPIMS) were performed for comparative studies. Since the use of a bottom electrode is required for certain devices applications, the analysis should be extended to AlN films deposited on top of metal layers as well. Thus, all films were deposited onto two different substrates: Si and textured Mo. The reasons why Mo was chosen as the metal layer and its use in the textured composition were previously presented (see item 3.1). XRD measurements were performed in order to evaluate the film properties (more specifically, θ-2θ scans and FWHM of the rocking curve).

Some authors consider that below certain N_2 flow levels, there is not enough N_2 to grow AlN. On the other hand, above certain N_2 levels there are not enough Al atoms [14]. Clearly there is an optimal range of gas flows in within which the N_2 flow is suitable to the growth of stoichiometric c-axis oriented AlN films. Obviously this range is not the same for all experimental setups, varying from machine to machine and, furthermore, varying with other deposition conditions.

Thus, in order to identify the optimal gas composition Ar/N_2 for the HiPIMS, different gas flows were used for AlN depositions on both types of substrates (Si and textured Mo). The total flow was kept constant at 70 sccm and four different compositions were tested (Ar/N_2, in sccm): (i) 30/40, (ii) 35/35, (iii) 40/30 and (iv) 45/25.

One can see in Figure 3.9b that all gas compositions tested were favorable to the growth of AlN (002) on top of textured Mo layers. However, an undesirable AlN (100) is noted on the films deposited by the composition Ar/N_2 30/40 sccm.

In the case of films deposited directly on Si, the AlN (002) peak is totally vanished at 45/25 sccm gas flows and shows the lowest intensity at 40/30 sccm composition (Figure 3.9a).

Thus, based on the above observations, the composition 35/35 sccm was chosen as the optimal gas flows ratio. Noteworthy, at this gas composition the AlN (100) peak has the lowest intensity for the films deposited on Si substrates by the HiPIMS technique.

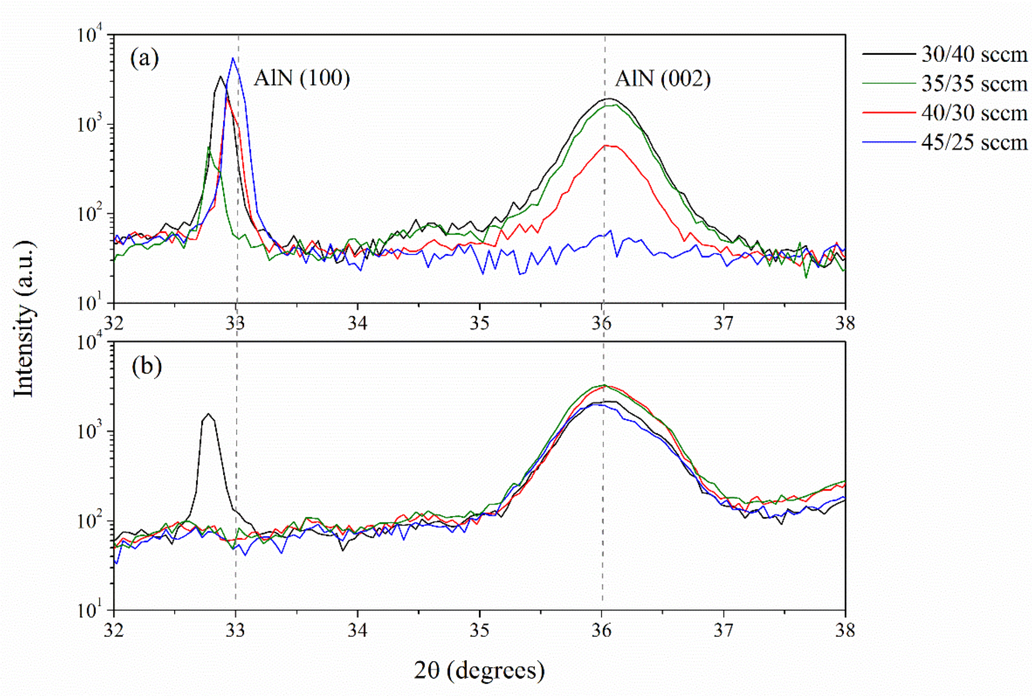

Figure 3.9 - θ-2θ scans of AlN films deposited by HiPIMS at room temperature and different gas flows ratio (Ar/N_2) on top of (a) Si substrates and (b) textured Mo substrates.

Considering that the c-axis texture is improved by the substrate temperature at Pulsed DC depositions, the study of this phenomenon was shortly investigated for the HiPIMS depositions as well. Nevertheless, the influence of the temperature was not the main focus of the investigation. Thus, only three substrate temperatures were tested: room temperature, 300 ºC and 400 ºC. The optimal gas flow composition was used (35/35 sccm) and the films were deposited on both types of substrates. The results are shown in Figure 3.10.

Even though the AlN (002) peak is very similar for the films deposited at 300 ºC and at 400 ºC on textured Mo, the peak intensity is slightly higher for the film deposited at 400 ºC on Si substrates. Thus, 400 ºC was chosen as the deposition temperature for the comparative studies. It is important to reinforce in here that the temperature analysis was not the focus of the work, ergo the analysis of its effects on the HiPIMS depositions was marginal.

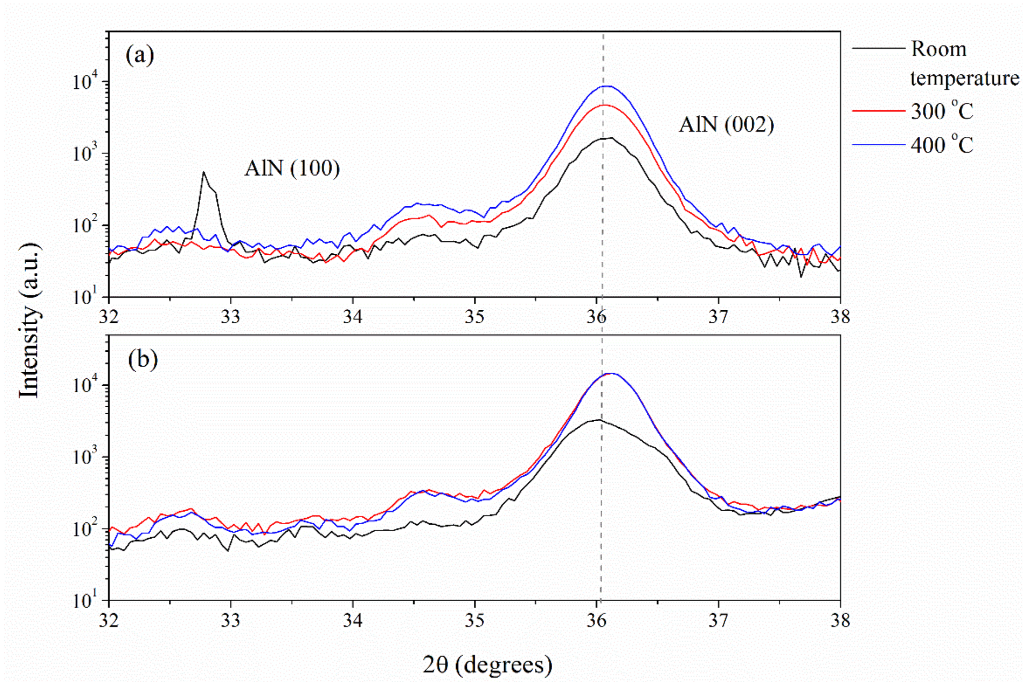

Figure 3.10 - θ-2θ scans of AlN films deposited by HiPIMS at fixed gas flow ratio (Ar/N_2 35/35 sccm) and different deposition temperatures on top of (a) Si substrates and (b) textured Mo substrates.

By knowing the optimal conditions for the growth of textured AlN films by means of HiPIMS method, the next step in the studies was the comparison of the films deposited by HiPIMS and Pulsed DC techniques. As showed in Figure 3.11 and Figure 3.12, it is clear the improvement in the AlN films brought by the HiPIMS method. Most likely, this is due to the higher degree of ionization (high plasma density) during the HiPIMS depositions, which in turns provides an enhancement in the adatoms mobility at the surface during the film growth. Noteworthy, the films were deposited under similar conditions (refer to Paper I for more details).

The results in Figure 3.11a show that at room temperature and by means of Pulsed DC depositions it was not possible to grow AlN (002) films on Si, even at different gas flows. On the other hand, even if followed by an undesirable (100) peak, the HiPIMS film shows a well pronounced (002) peak.

Since the results are quite poor for the Pulsed DC films deposited at room temperature, it was not possible to define the optimal gas flow composition. Thus, the 35/35 sccm was chosen as the gas flow for the comparison of HiPIMS and Pulsed DC deposited at higher temperature (400 °C). As expected, the quality of both films is improved by the temperature (see Figure 3.11b).

However, the HiPIMS film exceeds the Pulsed DC. Moreover, the AlN (100) peak found at the room temperature deposition was vanished for the HiPIMS at 400 ºC.

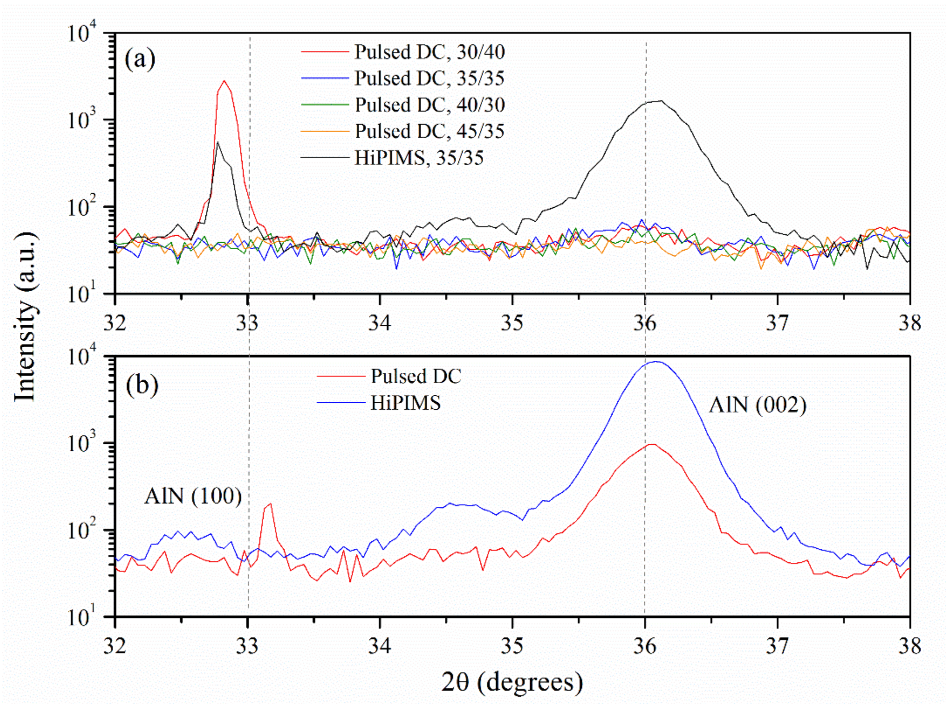

Figure 3.11 - θ-2θ scans of AlN films deposited by Pulsed DC and HiPIMS on Si substrates: (a) at room temperature and different gas compositions for the Pulsed DC films; (b) at 400 ºC and Ar/N_2 35/35 sccm as gas flow composition.

It is important to point out here that these results refer to a certain experimental setup. It doesn't mean the AlN films deposited by Pulsed DC at room temperature and on top of Si substrates will present the same poor results for all experimental setups. However, it is also important to point out that this is a comparative study, and the films were deposited under similar conditions (same target-to-substrate distance, similar base and deposition pressures, and so on). In our understanding this means that, by changing the experimental setup and keeping the deposition conditions similar for both techniques, HiPIMS will continue showing an improvement in the AlN films characteristics in comparison with the Pulsed DC ones.

As can be seen in Figure 3.12, there were no pronounced differences between the films growth by both deposition methods on textured Mo substrates at room temperature (Figure 3.12a) or at 400 ºC (gas composition 35/35 sccm, Figure 3.12b). One can consider that the textured Mo layer is already the optimal seed layer for the AlN films. Thus, in this case the deposition method does not influence so strongly the film growth (as long as it provides enough kinetic energy to the atoms).

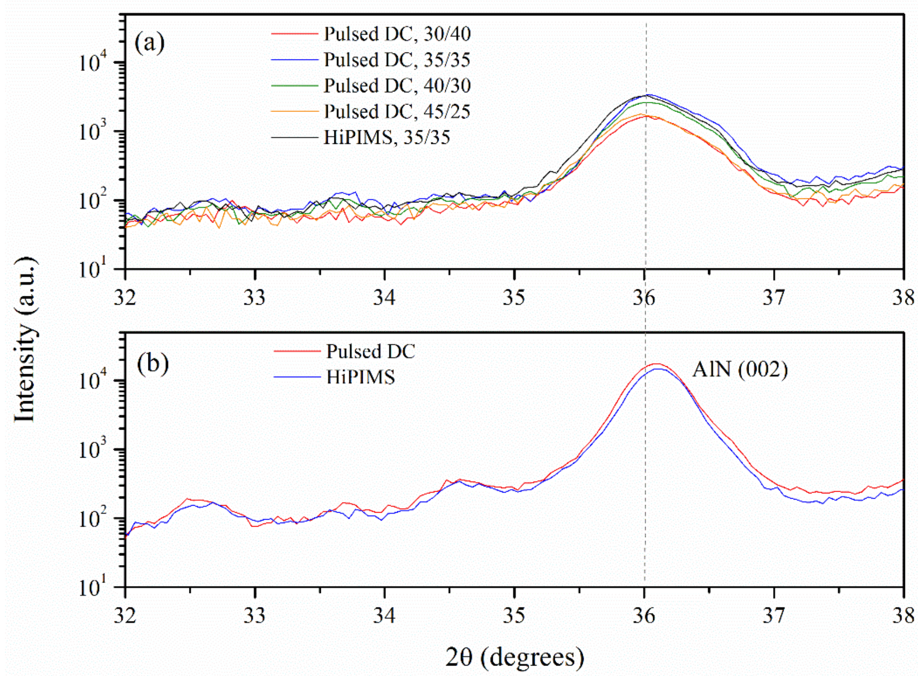

Figure 3.12 - θ-2θ scans of AlN films deposited by Pulsed DC and HiPIMS on textured Mo layers: (a) at room temperature and different gas compositions for the Pulsed DC films; (b) at 400 ºC and Ar/N_2 35/35 sccm as gas flow composition.

The beneficial effect of the HiPIMS method on the texture of the AlN films is seen in Figure 3.13. The FWHM of the (002) rocking curves presented refer to the films deposited at the gas composition Ar/N_2 35/35 sccm. There is no FWHM for the AlN films sputtered by Pulsed DC on Si substrates and at room temperature since the (002) peak was vanished at this deposition condition (refer to Figure 3.11).

One can say that the HiPIMS method can be considered as a promising technique to deposit suitable nucleation layers for the growth of c-axis textured AlN films.

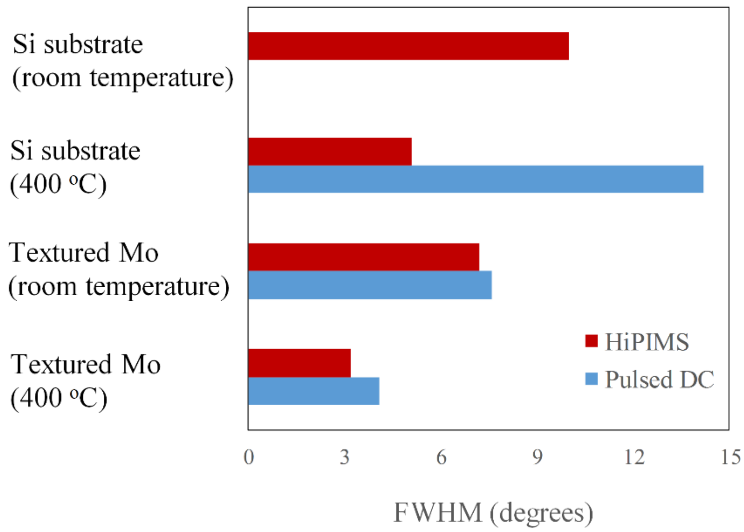

Figure 3.13 - FWHM of AlN films deposited by Pulsed DC and HiPIMS on Si and textured Mo substrates, at room temperature and 400 ºC.

4 SUMMARY OF INCLUDED PAPERS

4.1 PAPER I: THIN ALN FILMS DEPOSITED BY REACTIVE HIPIMS AND PULSED DC SPUTTERING: A COMPARATIVE STUDY

Manuscript to be submitted.

Author’s contribution: Part of planning and analysis. Major part of thin films deposition (Pulsed DC and HiPIMS) and measurements. Significant part of writing.

The motivation of this work was the deposition of textured (002) AlN thin layers directly on Si substrates, at reduced temperatures and in a setup with long target-to-substrate distance. It can be difficult to growth textured films by means of conventional Pulsed DC depositions when these three conditions are combined. For instance, in order to grow texture AlN by Pulsed DC, higher deposition temperatures are applied to compensate the long target-to-substrate distance, or suitable seed layers to the growth of (002) AlN films (such as Mo, Pt, Au) need to be used.

Thus, thin AlN films (200 nm) were deposited by HiPIMS and Pulsed DC under similar conditions and the results were compared. The depositions were performed at the same experimental setup, and the power supply was the single physical change between both processes. The deposition conditions are summarized in Table 4.1.

Table 4.1 - Summary of the deposition conditions of HiPIMS and conventional Pulsed DC.

	Pulsed DC	**HiPIMS**
Pressure	2.8 – 3.2 mTorr	
Pre-sputtering time (in pure Ar)	3 min	
Pre-sputtering power	200 W	400 W
Discharge power	800 W	830 W
Pulse frequency	250 KHz	1 KHz
Duty cycle	12.5%	5%

The gas flow ratio Ar/N_2 was optimized for the HiPIMS process. Supported by θ-2θ scans (X-ray diffraction analysis), the films deposited at 35/35 sccm presented the best results. Thus, this gas composition was used for both deposition processes (HiPIMS and Pulsed DC).

In order to evaluate the influence of the substrate material, besides the depositions directly on Si, AlN films were also grown on top of textured Mo layers. Furthermore, the influence of the deposition temperature was also analyzed.

Noteworthy, samples deposited by a standard deposition process were used as reference samples. This standard process is performed by Pulsed DC sputtering in a system with short target-to-substrate distance, which is favorable to the growth of textured films. It should be noted that the deposition conditions were similar to those presented in Table 4.1 for the Pulsed DC process.

The results indicate a substantial improvement brought by the HiPIMS method over the Pulsed DC ones. Notably, the texture of the AlN films deposited by HiPIMS excels the Pulsed DC process for the samples deposited on Si and at room temperature.

Therefore, it was demonstrated the possibility to obtain textured (002) AlN films deposited on Si substrates, at reduced temperatures and in systems with long target-to-substrate distances by means of HiPIMS depositions.

4.2 PAPER II: EFFICIENT RF VOLTAGE TRANSFORMER WITH BANDPASS FILTER CHARACTERISTICS

M. Moreira, J. Bjurström, I. Katardjiev, and V. Yantchev, "Efficient RF voltage transformer with bandpass filter characteristics," *Electronics Letters,* vol. 49, pp. 198-199, 2013.

Author’s contribution: Minor part of planning. Involved in fabrication and measurements. Minor writing.

The main objective of this work is to develop a realistic solution to a passive, addressable, remotely controlled switch using far field communication. By definition, such switches make use of the energy of the control signal the power of which decays exponentially with distance in addition to being limited by existing RF emission regulations. This necessitates both power accumulation and voltage amplification in order to generate a usable DC signal for switching.

Further, addressability requires frequency modulation which necessitates the use of bandpass filters. All these requirements make existing solutions totally impractical in terms of both performance and cost. The solution proposed addresses elegantly both of these aspects by developing a single component with a dual functionality, that is, it is both a highly efficient voltage transformer and a bandpass filter at the same time. Called transfilter for brevity, the device represents an electroacoustic bandpass filter with a large input/output impedance ratio (transformer characteristic).

The transfilter designed is a 2-port Lamb wave resonator using a highly c-axis oriented AlN piezoelectric thin film. Input and output are realized by interdigital transducers (IDT) and energy confinement is achieved by the use of reflectors with the same pitch as the IDT (see Figure 4.1). Whereas the resonance frequency of the transfilter is defined by the pitch of the IDT, devices with different resonance frequencies can be fabricated on a single chip having a common input and distinct outputs.

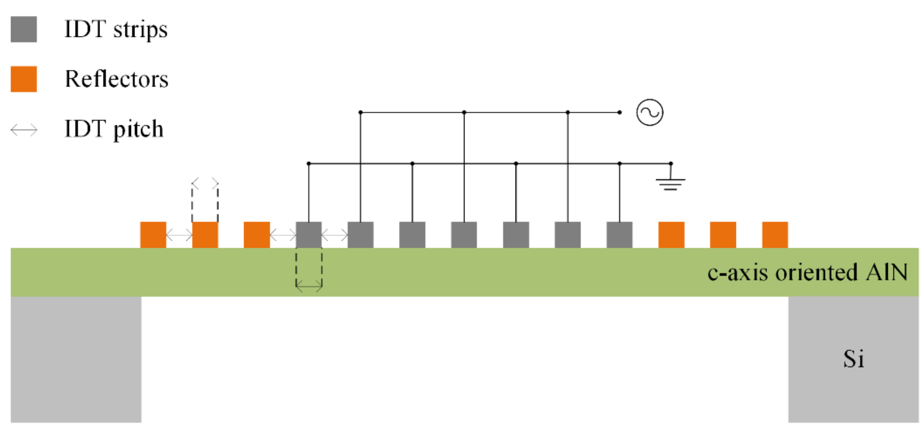

Figure 4.1 - Cross section schematic of the transfilter.

The transfilter was fabricated (Figure 4.2) using standard planar technology and was electrically characterized around its resonance frequency (888 MHz) by a Network Analyzer. Under open circuit conditions, an AC voltage input of 0.2 V was applied, returning a voltage output of approximately 2 V, thereby confirming the voltage amplification of the input signal. This voltage transformer ratio can be varied in a wide range by varying the ratio between input and output impedances (varying the number of pairs of the input and output IDT).

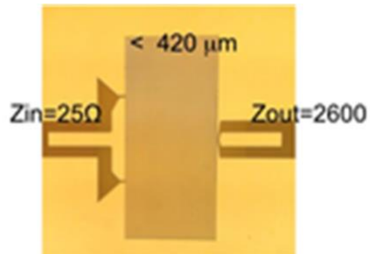

Figure 4.2 - Top view of the fabricated transfilter.

By the use of transfilters, truly passive and addressable RTS (radio triggered switch) can be built by employing capacitive MEMS (microelectromechanical systems) switches (Figure 4.3).

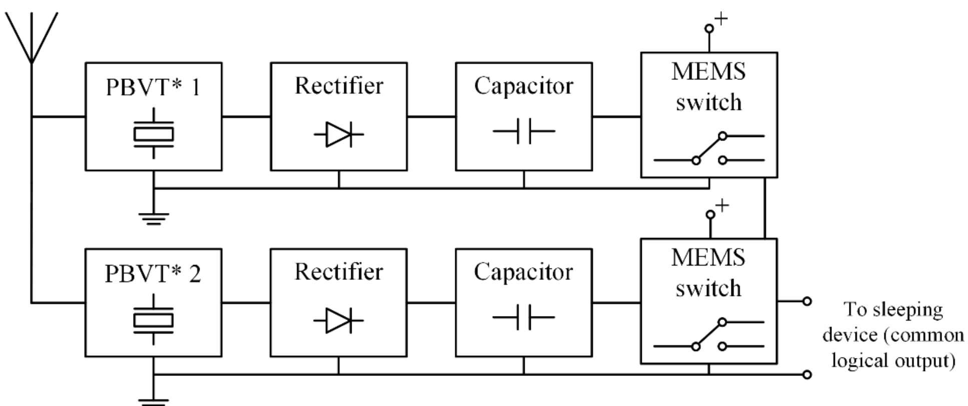

Figure 4.3 - Schematic of a truly passive and addressable RTS by the use of transfilters (*PBVT: see footnote).

In comparison with existing commercial wireless technologies (notably radio-frequency identification, RFID, tags), the obvious advantages of the transfilter are (i) quite low internal energy accumulation in the device, (ii) it is a linear device, it operates at all input power levels, i.e. no threshold, (iii) low cost and size and (iv) high efficiency. As a stand-alone component it can also be used in efficient AC/DC charge pumps.

Noteworthy, the design of the transfilter is not solely confined to Lamb wave devices and AlN thin films. Analogously, similar or even better performances can be obtained by using other piezolelectric materials and acoustic waves. Specifically, an insertion loss of -1 dB in the

*PBVT: piezoelectric bandpass voltage transformer.

passband is quite feasible with today's filter design technologies, making the transfilter an extremely efficient component unrivalled by existing solutions.

4.3 PAPER III: PREPARATION AND CHARACTERIZATION OF HIGH-K ALUMINIUM NITRIDE (ALN) THIN FILM FOR SENSOR AND INTEGRATED CIRCUITS APPLICATIONS

J. F. Souza, M. A. Moreira, I. Doi, J. A. Diniz, P. J. Tatsch, and J. L. Gonçalves, "Preparation and characterization of high-k aluminium nitride (AlN) thin film for sensor and integrated circuits applications," *Physica Status Solidi (c),* vol. 9, pp. 1454-1457, 2012.

Author's contribution: Minor part of planning. Major part of synthesis and characterization of AlN for the application as the transistor gate. Minor writing.

There a continuous trend to downsize scaling of transistor based devices (MISFET and ISFET, for instance)[23]. To this end, all layers and dimensions of these devices should follow the same trend. However, there are some limitations related with the materials properties. For example, SiO_2 is the most common used material as gate dielectric and the downsizing of its thickness implies in an increasing of the leakage current through it. Therefore, this downsize scaling has been driving the research efforts to find dielectric materials with high-k to replace the SiO_2 as gate dielectric while keeping (or improving) the performance of the device.

This paper reports the use of AlN films as gate dielectric for MISFETs and ion sensitive membrane for EISFETs devices.

The sputtered AlN films were prior synthesized in order to reach the desirable characteristics (polycrystalline, c-axis oriented, smooth surface and stoichiometric films). The devices were fabricated following the standard transistors fabrication process. The thickness of the AlN films deposited is 30 nm. A thin layer of SiO_2 (5 nm) was stacked to the AlN layer in order to reduce the mobile charges in the interface dielectric-semiconductor.

C-V measurements were done with the aim of determine the electrical quality of the AlN/SiO_2 stacked layer and AlN/SiO_2/Si(100) interface. These measurements were performed at

[23] According to the Moore's law, the amount of transistors in an integrated circuit double around every two years.

the MIS capacitor intrinsic to the MISFET device (see Figure 4.4). The results (see Table 4.2) confirm that the AlN/SiO_2 stacked layer is a good insulator on silicon substrates.

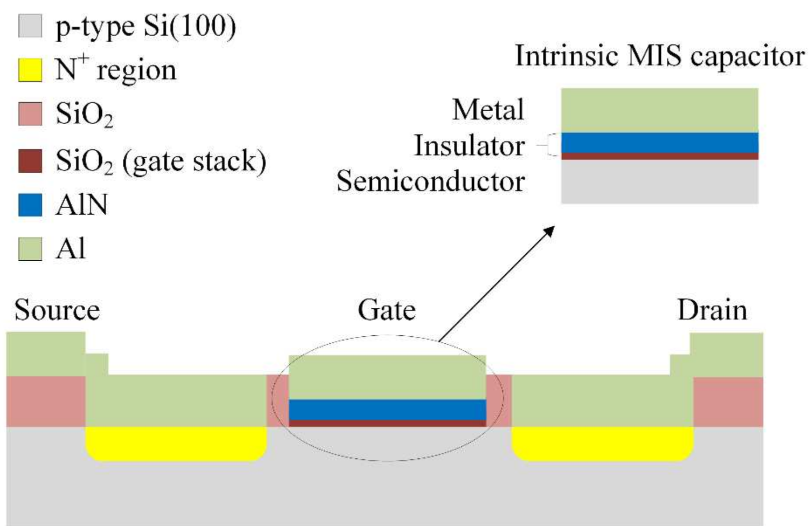

Figure 4.4 - Schematic cross-section of a MISFET device and an inset of its intrinsic MIS capacitor.

Table 4.2 - Electrical parameters (measured and calculated) of the AlN/SiO_2 stacked layer.

Maximum capacitance C_{max}	158.5 pF
Minimum capacitance C_{min}	40.66 pF
Substrate acceptor concentration N_A	1.87×10^{17} cm^{-3}
Flat-band capacitance C_{fb}	116.71 pF
Equivalent oxide thickness EOT	8.71 nm
Flat-band voltage V_{fb}	-0.59 V
Work function metal-semiconductor ϕ_{ms}	-1.02 V
Charge trap density (negative) N_t	-1.02×10^{12} cm^{-2}
Threshold voltage V_{th}	0.84 V

Furthermore, the MISFET and EISFET[24] devices were electrically characterized by means of their I_{DS} x V_{GS} curves. The calculated values are summarized in Table 4.3.

[24] A standard pH 7 solution was used for the EISFET measurements.

Table 4.3 - Electrical parameters of MISFET and EISFET devices.

	MISFET	**EISFET**
Transconductance G_m	96 µs	329 µs
Current-off I_{off}	5×10^{-11} A	1.88×10^{-9} A
Subthreshold swing S_t	103 mV/dec	171 mV/dec

The possibility to use AlN as gate insulator in MISFET and EISFET devices was demonstrated by fabricating and characterizing such devices.

4.4 PAPER IV: ALUMINUM SCANDIUM NITRIDE THIN-FILM BULK ACOUSTIC RESONATORS FOR WIDE BAND APPLICATIONS

M. Moreira, J. Bjurström, I. Katardjiev, and V. Yantchev, "Aluminum scandium nitride thin-film bulk acoustic resonators for wide band applications," *Vacuum,* vol. 86, pp. 23-26, 2011.

Author's contribution: Part of planning. Involved in synthesis and characterization of AlScN films. Involved in fabrication and characterization of FBARs. Minor writing.

This paper is the first to present an experimental electroacoustic characterization of highly c-textured $Al_{(1-x)}Sc_xN$ piezoelectric films as a function of Sc concentration in view of wide band telecom applications in the low GHz range. For this purpose, one port FBAR test devices were fabricated with four different Sc concentrations, namely x = 0, 0.03, 0.09 and 0.15 respectively. The films were grown by reactive sputter deposition under identical conditions as illustrated in Table 4.4.

Table 4.4 - Deposition conditions of the $Al_{(1-x)}Sc_xN$ layers.

Base pressure	< 2×10^{-8} Torr
Deposition pressure	2.8 mTorr
Substrate temperature	400 °C
Ar flow	30 sccm
N_2 flow	30 sccm

In order to obtain films with a high crystallographic texture a double seed layer consisting of a 120 nm thick (002) AlN layer and a 300 nm thick (110) textured Mo layer was used. The high c-axis texture of the $Al_{(1-x)}Sc_xN$ films was confirmed by X-ray diffraction analysis. The XRD measurements showed that all films are c-axis oriented and highly textured, with a FWHM of the (002) peaks varying from 1.6° up to 2° with increasing Sc concentration.

A simplified cross-section of the FBAR structure is shown in Figure 4.5.

Figure 4.5 - Cross-section view of the resonator structure.

The electroacoustic characterization of the FBARs was performed with a network analyzer and the scattering parameters were acquired at frequencies around the fundamental longitudinal resonance of each device. It is noted that a slight downshift of the resonance frequency with increasing the Sc concentration was observed.

The measured data were fitted to the MBVD equivalent circuit, which yielded a negligible shunt resistance (R_0) and a series parasitic resistance (R_s) of around 0.3 Ohms for all resonators. The unknown stiffness C_{33} and piezoelectric constant e_{33} parameters were determined by a combination of the one-dimensional Nowotny-Benes model and the MBVD extraction. Both parameters were varied to best fit the series resonance frequency f_s and the effective electromechanical coupling k_{eff}^2 from the MBVD extraction. The relative dielectric permittivity ε_r was extracted from the static FBAR capacitance C_0.

Other parameters such as the parallel resonance (f_p), the Q-factor at parallel resonance (Q_p) and the unloaded Q-factor (Q_B) were obtained from the electroacoustic measurements.

Table 4.5 shows the most relevant parameters measured/extracted, including the intrinsic electromechanical coupling k_t^2 for all four different Sc concentrations.

Table 4.5 - Measured and extracted $Al_{(1-x)}Sc_xN$ parameters.

Composition	**f_s (GHz)**	**Q_B**	**k_{eff}^2 (%)**	**FOM**	**ε_r**	**C_{33} (GPa)**	**e_{33} (C/m^2)**	**k_t^2 (%)**
AlN	2.3605	790	5.50	40	10.1	370	1.48	6.16
$Al_{0.97}Sc_{0.03}N$	2.2935	730	6.89	50	10.9	346	1.66	7.55
$Al_{0.91}Sc_{0.09}N$	2.2339	690	9.50	65	12.4	326	1.94	9.53
$Al_{0.85}Sc_{0.15}N$	2.1522	410	12.07	60	14.1	270	2.14	12.00

It is seen in Table 4.5 that the electromechanical coupling increases steadily with increasing Sc concentration to exceed by 100% that of pure AlN at a Sc concentration of x = 0.15. In other words, the latter films may be used for the fabrication of bandpass filters with a twice as large bandwidth than that of pure AlN. Another important finding is that the Q-value correspondingly decreases with increasing Sc concentration owing to increased acoustic losses associated with a correspondingly increased softness of the films as manifested by the decrease in the C_{33} elastic constant.

However, more important for filter design is the FOM defined as the product between the electromechanical coupling and the Q value. As seen in Table 4.5 this FOM exhibits a maximum for x = 0.09.

The above results demonstrate unequivocally that highly textured $Al_{(1-x)}Sc_xN$ films can be used for the fabrication of high performance telecom components with a large bandwidth.

4.5 PAPER V: SYNTHESIS OF C-TILTED ALN FILMS WITH A GOOD TILT AND THICKNESS UNIFORMITY

M. Moreira, J. Bjurström, T. Kubart, B. Kuzavas, and I. Katardjiev, "Synthesis of c-tilted AlN films with a good tilt and thickness uniformity," in *IEEE International Ultrasonics Symposium Proceedings*, 2011, pp. 1238-1241.

Author's contribution: Minor part of planning. Involved in thin films depositions and measurements. Minor writing.

AlN films with a nonzero tilt of the c-axis have been studied for use in electroacoustic devices in the shear thickness propagation mode (see Figure 4.6) operating in liquid media. In the latter case propagation of the shear mode is confined to the resonating cavity (piezoelectric layer including electrodes), since shear motion is not supported in liquid media and hence the resonator retains its high Q-factor. Certain degradation of Q is inevitable due to viscous loading from the liquid but the overall Q-value is still sufficiently high to guarantee low noise performance. In terms of biosensor applications, for instance, this leads to a higher mass and viscosity resolution.

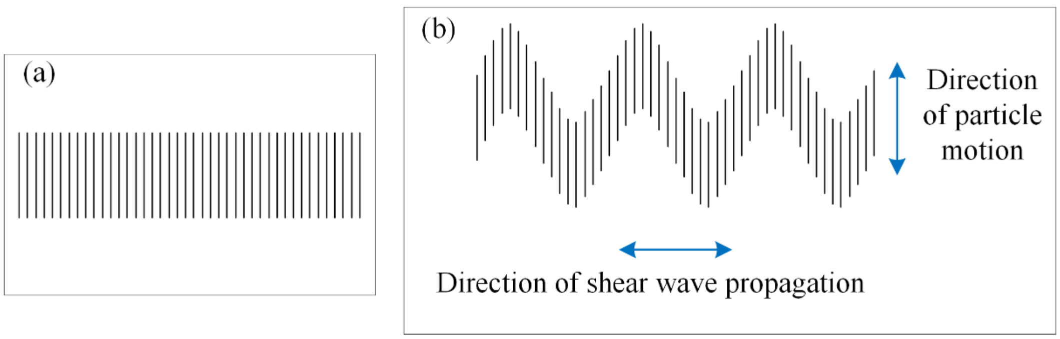

Figure 4.6 - One dimensional representation of particle displacement in a medium (a) without any wave motion, and (b) with shear thickness wave propagation.

This paper describes a method for the deposition of c-tilted AlN films by pulsed DC sputtering with good uniformity of both tilt and thickness throughout the wafer. Other existing methods for the deposition of c-tilted AlN films suffer from serious drawbacks such as low deposition rates and non-uniform thickness and tilt. In this sense, the method presented here intends to overcome these shortcomings. To this end, it is primordial to have an adequate handle on both the nucleation and the growth stages. The strategy of the method presented here is as follows. During nucleation, optimal conditions are chosen which hamper the nucleation of grains with the c-plane parallel to the surface and instead promote nucleation of a sizable population of grains with a crystallographic orientation non-parallel to the average film surface. During the growth stage, optimal conditions are chosen which promote the growth of non c-oriented grains whose c-axis lies in a specific half-plane perpendicular to the film surface. Growth of grains with other crystallographic orientations is suppressed. In this way, a film with a monodirectional tilt of the c-axis is obtained. This growth stage is typically achieved by assuring a certain directionality of the deposition flux, say by operating the process at relatively low pressures which minimizes scattering in the gas phase.

A suitable nucleation layer for tilted AlN growth can be achieved by: (i) rough substrate surface and/or (ii) crystallographic mismatch between substrate and the film (non-hexagonal structure in case of AlN films) and/or (iii) a non-textured AlN seed layer, which can be obtained under diffusion limited nucleation conditions, e.g., at high deposition pressures and low substrate temperatures.

The growth of tilted films proposed in this paper suggests the use of an array of linear magnetrons instead of the conventional magnetrons with circular symmetry (see Figure 4.7).

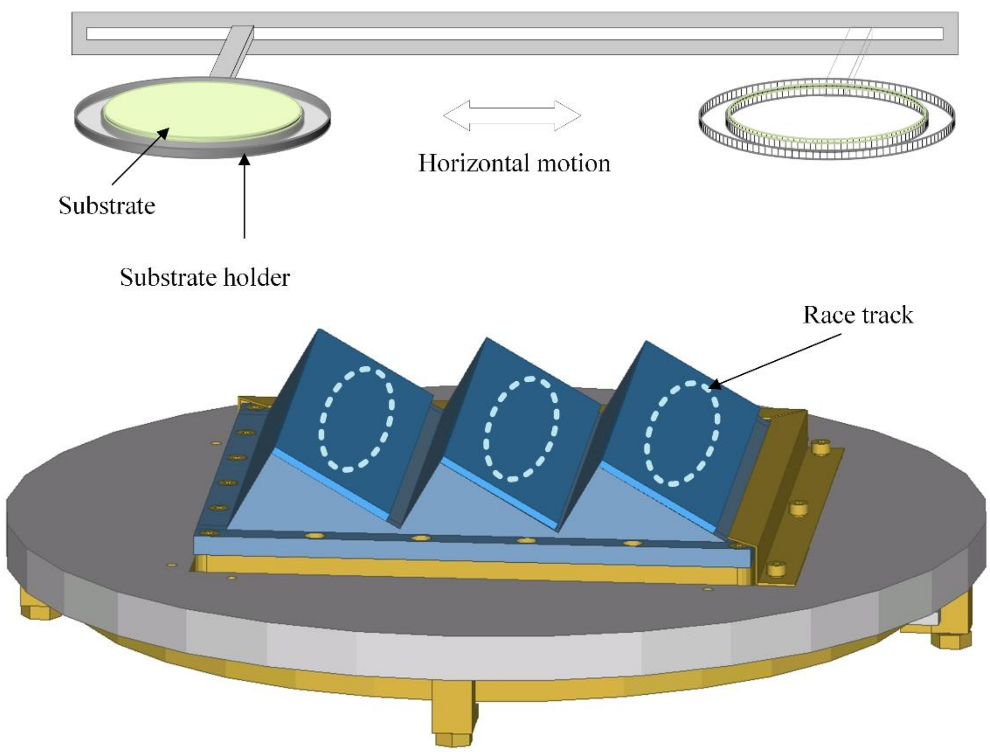

Figure 4.7 - Array of tilted magnetrons.

Assuming that the majority of the sputtered atoms arrive at the substrate at angles close to the surface normal, the tilt of the magnetron segments relative to the surface normal sets the incident angle of the deposition flux. However, it is also necessary to achieve thickness uniformity. To this end, the substrate is moved horizontally along the projection of the atoms flux from the target towards the substrate (refer to Figure 4.7).

XRD pole plot figures clearly demonstrate the significant improvement in the tilt distribution resulting from the magnetron array proposed (see Figure 4.8). Even though a c-tilted film was previously demonstrated by conventional magnetron deposition (Figure 4.8a), it exhibited a broad tilt distribution as indicated by the kidney shape of the XRD pole plot. On the other hand, the narrower tilt distribution of the film deposited by the use of the magnetron array shows that a higher texture was attained (Figure 4.8b).

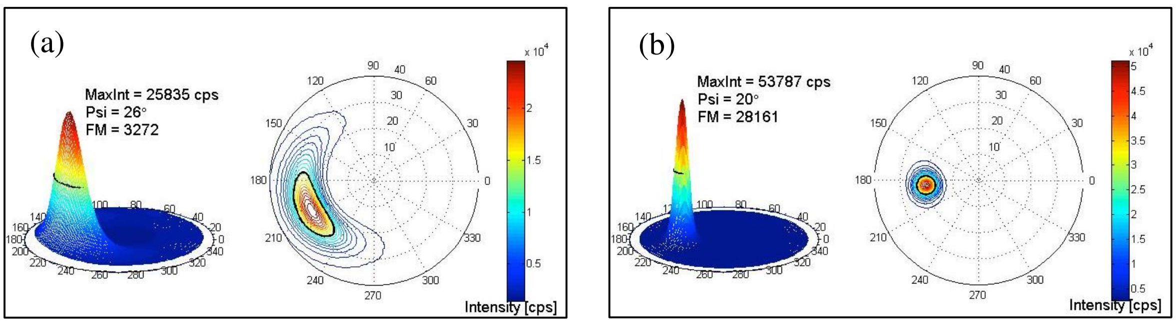

Figure 4.8 - XRD pole plot figures of tilted AlN films deposited by use of (a) a conventional magnetron with circular symmetry and (b) an array of tilted magnetrons.

It is likely that the use of the array of linear magnetrons in addition to an adequate control of the nucleation stage are suitable to the growth of not only tilted AlN films, but other wurtzite thin films as well.

4.6 PAPER VI: ELECTRICAL CHARACTERIZATION AND MORPHOLOGICAL PROPERTIES OF ALN FILMS PREPARED BY DC REACTIVE MAGNETRON SPUTTERING

M. A. Moreira, I. Doi, J. F. Souza, and J. A. Diniz, "Electrical characterization and morphological properties of AlN films prepared by dc reactive magnetron sputtering," *Microelectronic Engineering,* vol. 88, pp. 802-806, 2011.

Author's contribution: Part of planning. All fabrication and measurements. Significant part of writing.

The paper describes the physical and electrical characterization of sputtered AlN films deposited by different conditions. Notwithstanding AlN is a well-known material and the influence of the deposition conditions on its quality have been presented in the literature by other groups, there is still a lack of results regarding it. In this sense, more studies will contribute in the further development of high quality AlN thin films.

The deposition conditions that changed in this paper were N_2 flow ratio and discharge power. The physical parameters analyzed were roughness, crystallographic texture, absorbance, resistivity and refractive index. In addition, electrical parameters were analyzed such as dielectric constant, hysteresis, equivalent oxide thickness and flat band voltage. To this latter end, Metal-Insulator-Semiconductor (MIS) capacitors were fabricated (Figure 4.9) and some of them where annealed. Therefore, the electrical parameters were studied not only as a function of N_2 flow and target power, but also as a function of insulator thickness and heat treatment of the MIS structures.

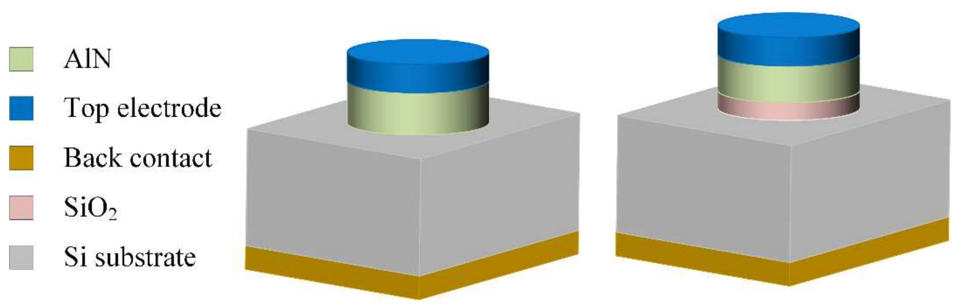

Figure 4.9 - Schematic of the MIS capacitors fabricated.

The achieved results showed the formation of reasonably good AlN thin films, applicable in some electronic devices. The equipment used to deposit those films was not fully explored yet and it has a great potential to develop uniform and highly textured films (short target-to-substrate distance and large targets, for instance).

5 CONCLUDING REMARKS

The intrinsic properties of AlN make it an outstanding material among other piezoelectric materials. It can be used in a wide variety of applications such as:

- Microelectromechanical systems,
- Electroacoustic sensors (including biosensors),
- High frequency filters and oscillators,
- Transistor-based devices (MOSFET, ISFET, etc.),
- Optoelectronics, and
- Coating layers.

It is therefore understandable why AlN thin films have been extensively studied by many research groups over the last couple of years.

The focus of this thesis was the study and improvement of AlN films in view of its application on devices operating at high frequencies. This includes, for instance, sensors, biosensors, filters and oscillators. To this end, the investigation was driven by the improvement of AlN films in different aspects, such as its c-axis orientation, piezoelectric and electroacoustic properties.

The major findings and contributions of this work are summarized below:

1. Improvements of the AlN films properties by doping with Sc. The electromechanical coupling k_t^2 have shown a two fold increase for 15% of Sc concentration (Paper IV).
2. First work to present an experimental characterization of $Al_{(1-x)}Sc_xN$ films as a function of the Sc concentration (electrical and acoustic properties). The optimal Sc concentration (9%) was demonstrated by means of Figure-of-Merit calculations (Paper IV).
3. Deposition of c-axis textured AlN films by HiPIMS directly on Si, at reduced temperatures and in a system with large target-to-substrate distance (Paper I).
4. Sputtering of c-axis tilted films with well-defined thickness and tilt uniformity. The method includes a proposed experimental setup and deposition conditions (Paper V).
5. Design, fabrication and experimental characterization of a device that possesses both properties of voltage transformer and bandpass filter (transfilter) (Paper II).

6. It was demonstrated the possibility to use AlN films as the gate dielectric (high-k material) by means of the fabrication and characterization of MISFET and EISFET devices (Paper III).

My personal opinion about the use of AlN films on devices operating at high frequencies is that the material is close to reach its limits. Certainly the performance of these devices can be improved by changes in the design (electrodes, interdigital transducers, and so on). However, in terms of materials, AlN films may not be substantially improved. The conditions to obtain highly c-axis oriented and tilted films (for application in sensors operating in viscous media, for instance) are well-known and deeply studied. Significant enhancements can most certainly not be achieved from pure AlN films. However, by doping the AlN films with metalloids and transition metals this scenario can be changed. Thus, improvements in the piezoelectric properties of AlN films by means of film doping have received strong attention over the last years. This thesis used Sc as a dopant, and the results confirm that $Al_{(1-x)}Sc_xN$ films are promising, which has been confirmed by other studies as well. I believe that a new range of possibilities is open by doping AlN films.

REFERENCES

[1] M. Ishihara, S. J. Li, H. Yumoto, K. Akashi, and Y. Ide, "Control of preferential orientation of AlN films prepared by the reactive sputtering method," *Thin Solid Films,* vol. 316, pp. 152-157, 1998.

[2] F. Engelmark, G. F. Iriarte, I. V. Katardjiev, M. Ottosson, P. Muralt, and S. Berg, "Structural and electroacoustic studies of AlN thin films during low temperature radio frequency sputter deposition," *Journal of Vacuum Science & Technology A,* vol. 19, pp. 2664-2669, 2001.

[3] X.-H. Xu, H.-S. Wu, C.-J. Zhang, and Z.-H. Jin, "Morphological properties of AlN piezoelectric thin films deposited by DC reactive magnetron sputtering," *Thin Solid Films,* vol. 388, pp. 62-67, 2001.

[4] F. Engelmark, J. Westlinder, G. F. Iriarte, I. V. Katardjiev, and J. Olsson, "Electrical Characterization of AlN MIS and MIM Structures," *IEEE Transactions on Electron Devices,* vol. 50, pp. 1214-1219, 2003.

[5] A. Fathimulla and A. A. Lakhani, "Reactively rf magnetron sputtered AlN films as gate dielectric," *Journal of Applied Physics,* vol. 54, pp. 4586-4589, 1983.

[6] G. F. Iriarte, J. G. Rodríguez, and F. Calle, "Synthesis of c-axis oriented AlN thin films on different substrates: A review," *Materials Research Bulletin,* vol. 45, pp. 1039-1045, 2010.

[7] G. Wingqvist, F. Tasnadi, A. Zukauskaite, J. Birch, H. Arwin, and L. Hultman, "Increased electromechanical coupling in w-$Sc_xAl_{(1-x)}N$," *Applied Physics Letters,* vol. 97, 2010.

[8] S.-T. Lee, B.-G. Park, M.-D. Kim, J.-E. Oh, S.-G. Kim, Y.-H. Kim*, et al.*, "Control of polarity and defects in the growth of AlN films on Si (111) surfaces by inserting an Al interlayer," *Current Applied Physics,* vol. 12, pp. 385-388, 2012.

[9] B. Liu, J. Gao, K. M. Wu, and C. Liu, "Preparation and rapid thermal annealing of AlN thin films grown by molecular beam epitaxy," *Solid State Communications,* vol. 149, pp. 715-717, 2009.

[10] M.-J. Lai, L.-B. Chang, T.-T. Yuan, and R.-M. Lin, "Improvement of crystal quality of AlN grown on sapphire substrate by MOCVD," *Crystal Research and Technology,* vol. 45, pp. 703-706, 2010.

[11] J.-W. Soh, S.-S. Jang, I.-S. Jeong, and W.-J. Lee, "C-axis orientation of AlN films prepared by ECR PECVD," *Thin Solid Films,* vol. 279, pp. 17-22, 1996.

[12] C.-M. Yang, K. Uehara, S.-K. Kim, S. Kameda, H. Nakase, and K. Tsubouchi, "Highly c-axis-oriented AlN film using MOCVD for 5GHz-band FBAR filter," in *IEEE International Ultrasonics Symposium Proceedings*, 2003, pp. 170-173.

[13] M. Clement, E. Iborra, J. Sangrador, A. Sanz-Hervás, L. Vergara, and M. Aguilar, "Influence of sputtering mechanisms on the preferred orientation of aluminum nitride thin films," *Journal of Applied Physics,* vol. 94, pp. 1495-1500, 2003.

[14] T. Kumada, M. Ohtsuka, K. Takada, and H. Fukuyama, "Influence of sputter power and N_2 gas flow ratio on crystalline quality of AlN layers deposited at 823 K by RF reactive sputtering," *Physica Status Solidi (c),* vol. 9, pp. 515-518, 2012.

[15] Y. Z. You and D. Kim, "Influence of incidence angle and distance on the structure of aluminium nitride films prepared by reactive magnetron sputtering," *Thin Solid Films,* vol. 515, pp. 2860-2863, 2007.

[16] K. A. Aissa, A. Achour, J. Camus, L. L. Brizoual, P.-Y. Jouan, and M.-A. Djouadi, "Comparison of the structural properties and residual stress of AlN films deposited by dc magnetron sputtering and high power impulse magnetron sputtering at different working pressures," *Thin Solid Films,* vol. 550, pp. 264-267, 2013.

[17] A. Guillaumot, F. Lapostolle, C. Dublanche-Tixier, J. C. Oliveira, A. Billard, and C. Langlade, "Reactive deposition of Al–N coatings in Ar/N_2 atmospheres using pulsed-DC or high power impulse magnetron sputtering discharges," *Vacuum,* vol. 85, pp. 120-125, 2010.

[18] K. Kusaka, D. Taniguchi, T. Hanabusa, and K. Tominaga, "Effect of sputtering gas pressure and nitrogen concentration on crystal orientation and residual stress in sputtered AlN films," *Vacuum,* vol. 66, pp. 441-446, 2002.

[19] K.-H. Chiu, H.-R. Chen, and S. R.-S. Huang, "High-Performance Film Bulk Acoustic Wave Pressure and Temperature Sensors," *Japanese Journal of Applied Physics,* vol. 46, pp. 1392-1397, 2007.

[20] A. Choujaa, N. Tirole, C. Bonjour, G. Martin, D. Hauden, P. Blind*, et al.*, "AlN/silicon Lamb-wave microsensors for pressure and gravimetric measurements," *Sensors and Actuators A: Physical,* vol. 46, pp. 179-182, 1995.

[21] L. Zhou, J.-F. Manceau, and F. Bastien, "Interaction between gas flow and a Lamb waves based microsensor," *Sensors and Actuators A: Physical,* vol. 181, pp. 1-5, 2012.

[22] R. Gabl, E. Green, M. Schreiter, H. D. Feucht, H. Zeininger, R. Primig*, et al.*, "Novel integrated FBAR sensors: a universal technology platform for bio- and gas-detection," in *IEEE Sensors*, 2003, pp. 1184-1188.

[23] G. Wingqvist, "AlN-based sputter-deposited shear mode thin film bulk acoustic resonator (FBAR) for biosensor applications — A review," *Surface and Coatings Technology,* vol. 205, pp. 1279-1286, 2010.

[24] M. Nirschl, A. Blüher, C. Erler, B. Katzschner, I. Vikholm-Lundin, S. Auer*, et al.*, "Film bulk acoustic resonators for DNA and protein detection and investigation of in vitro bacterial S-layer formation," *Sensors and Actuators A: Physical,* vol. 156, pp. 180-184, 2009.

[25] I. Katardjiev and V. Yantchev, "Recent developments in thin film electro-acoustic technology for biosensor applications," *Vacuum,* vol. 86, pp. 520-531, 2012.

[26] L. Liljeholm, M. Junaid, T. Kubart, J. Birch, L. Hultman, and I. Katardjiev, "Synthesis and characterization of (0001)-textured wurtzite $Al_{(1-x)}B_xN$ thin films," *Surface and Coatings Technology,* vol. 206, pp. 1033-1036, 2011.

[27] L. Liljeholm and J. Olsson, "Electrical characterization of wurtzite (Al,B)N thin films," *Vacuum,* vol. 86, pp. 466-470, 2011.

[28] J.-H. Song, J.-L. Huang, T. Omori, J. C. Sung, S. Wu, H.-H. Lu*, et al.*, "Growth of highly c-axis oriented (B, Al)N film on diamond for high frequency surface acoustic wave devices," *Thin Solid Films,* vol. 520, pp. 2247-2250, 2012.

[29] E. Iborra, J. Capilla, J. Olivares, M. Clement, and V. Felmetsger, "Piezoelectric and electroacoustic properties of Ti-doped AlN thin films as a function of Ti content," in *IEEE International Ultrasonics Symposium*, Dresden, 2012, pp. 2734 - 2737.

[30] M. Akiyama, T. Kamohara, K. Kano, A. Teshigahara, Y. Takeuchi, and N. Kawahara, "Enhancement of Piezoelectric Response in Scandium Aluminum Nitride Alloy Thin Films Prepared by Dual Reactive Cosputtering," *Advanced Materials,* vol. 21, pp. 593-597, 2009.

[31] A. Teshigahara, K.-Y. Hashimoto, and M. Akiyama, "Scandium aluminum nitride: Highly piezoelectric thin film for RF SAW devices in multi GHz range " in *IEEE International Ultrasonics Symposium*, Dresden, 2012, pp. 1-5.

[32] A. Žukauskaitė, C. Tholander, J. Palisaitis, P. O. Å. Persson, V. Darakchieva, N. B. Sedrine*, et al.*, "$Y_xAl_{(1-x)}N$ thin films," *Journal of Physics D: Applied Physics,* vol. 45, p. 422001, 2012.

[33] J. T. Luo, B. Fan, F. Zeng, and F. Pan, "Influence of Cr-doping on microstructure and piezoelectric response of AlN films," *Journal of Physics D: Applied Physics,* vol. 42, p. 235406, 2009.

[34] V. V. Felmetsger and M. K. Mikhov, "Reactive Magnetron Sputtering of Piezoelectric Cr-Doped AlN Thin Films," in *IEEE Ultrasonic Symposium 2011*, 2011, pp. 835-839.

[35] H. Liu, F. Zeng, G. Tang, and F. Pan, "Enhancement of piezoelectric response of diluted Ta doped AlN," *Applied Surface Science,* vol. 270, pp. 225-230, 2013.

[36] E. Iborra, J. Olivares, M. Clement, L. Vergara, A. Sanz-Hervás, and J. Sangrador, "Piezoelectric properties and residual stress of sputtered AlN thin films for MEMS applications," *Sensors and Actuators A: Physical,* vol. 115, pp. 501-507, 2004.

[37] Erik Särhammar, Erik Strandberg, Nicolas Martin, and T. Nyberg, "Sputter Rate Distribution and Compositional Variations in Films Sputtered from Elemental and Multi-Element Targets at Different Pressures," *International Journal of Materials Science and Applications,* vol. 3, pp. 29-36, 2014.

[38] G. F. Iriarte, F. Engelmark, and I. V. Katardjiev, "Reactive Sputter Deposition of Highly Oriented AlN Films at Room Temperature," *Journal of Materials Research,* vol. 17, pp. 1469-1475, 2002.

[39] G. F. Iriarte, J. Bjurstrom, J. Westlinder, F. Engelmark, and I. V. Katardjiev, "Synthesis of c-axis-oriented AlN thin films on high-conducting layers: Al, Mo, Ti, TiN, and Ni," *IEEE Transactions on Ultrasonics, Ferroelectrics and Frequency Control,* vol. 52, pp. 1170-1174, 2005.

[40] J. Bjurström, G. Wingqvist, and I. Katardjiev, "Synthesis of Textured Thin Piezoelectric AlN Films With a Nonzero C-Axis Mean Tilt for the Fabrication of Shear Mode Resonators," *IEEE Transactions on Ultrasonics Ferroelectrics and Frequency Control,* vol. 53, pp. 2095-2100, 2006.

[41] Y.-C. Chen, W.-T. Chang, K.-S. Kao, C.-H. Yang, and C.-C. Cheng, "The Liquid Sensor Using Thin Film Bulk Acoustic Resonator with C-Axis Tilted AlN Films," *Journal of Nanomaterials,* vol. 2013, p. 8, 2013.

[42] J. Xiong, H.-S. Gu, W. Wu, M.-Z. Hu, P.-F. Du, and H. Xie, "Synthesis of c-Axis Inclined AlN Films in an Off-Center System for Shear Wave Devices," *Journal of Electronic Materials,* vol. 40, pp. 1578-1583, 2011.

[43] R. Deng, P. Muralt, and D. Gall, "Biaxial texture development in aluminum nitride layers during off-axis sputter deposition," *Journal of Vacuum Science & Technology A,* vol. 30, pp. 051501-1 - 051501-9, 2012.

[44] F. Martin, M. E. Jan, S. Rey-Mermet, B. Belgacem, D. Su, M. Cantoni, *et al.*, "Shear mode coupling and tilted grain growth of AlN thin films in BAW resonators," *Ultrasonics, Ferroelectrics and Frequency Control, IEEE Transactions on,* vol. 53, pp. 1339-1343, 2006.

[45] A. A. Turkin, Y. T. Pei, K. P. Shaha, C. Q. Chen, D. I. Vainshtein, and J. T. M. De Hosson, "On the evolution of film roughness during magnetron sputtering deposition," *Journal of Applied Physics,* vol. 108, pp. 094330-094330-9, 2010.

[46] D. Deniz, J. M. E. Harper, J. W. Hoehn, and F. Chen, "Tilted fiber texture in aluminum nitride thin films," *Journal of Vacuum Science & Technology A,* vol. 25, pp. 1214-1218, 2007.

[47] N. S. Dellas and J. M. E. Harper, "Effect of deposition angle on fiber axis tilt in sputtered aluminum nitride and pure metal films," *Thin Solid Films,* vol. 515, pp. 1647-1650, 2006.

[48] T. Karabacak, "Thin-film growth dynamics with shadowing and re-emission effects," *Journal of Nanophotonics,* vol. 5, pp. 052501-052501-18, 2011.

[49] P. Stempflé, A. Besnard, N. Martin, A. Domatti, and J. Takadoum, "Accurate control of friction with nanosculptured thin coatings: Application to gripping in microscale assembly," *Tribology International,* vol. 59, pp. 67-78, 2013.

[50] G. Wingqvist, "Thin-film electro-acoustic sensors based on AlN and its alloys: possibilities and limitations," *Microsystem Technologies,* vol. 18, pp. 1213-1223, 2012.

[51] J.-C. Yang, X.-Q. Meng, C.-T. Yang, and Y. Zhang, "Influence of sputtering power on crystal quality and electrical properties of Sc-doped AlN film prepared by DC magnetron sputtering," *Applied Surface Science,* vol. 287, pp. 355-358, 2013.

[52] M. Akiyama, K. Kano, and A. Teshigahara, "Influence of growth temperature and scandium concentration on piezoelectric response of scandium aluminum nitride alloy thin films," *Applied Physics Letters,* vol. 95, pp. 162107-162107-3, 2009.

[53] F. Tasnadi, B. Alling, C. Hoglund, G. Wingqvist, J. Birch, L. Hultman*, et al.*, "Origin of the Anomalous Piezoelectric Response in Wurtzite $Sc_xAl_{1-x}N$ Alloys," *Physical Review Letters,* vol. 104, pp. 137601-1 - 137601-4, 2010.

[54] A. A. Vives, *Piezoelectric Transducers and Applications*: Springer, 2008.

[55] D. Eom, S. Y. No, C. S. Hwang, and H. J. Kim, "Properties of Aluminum Nitride Thin Films Deposited by an Alternate Injection of Trimethylaluminum and Ammonia under Ultraviolet Radiation," *Journal of The Electrochemical Society,* vol. 153, pp. C229-C234, 2006.

[56] E. P. Gusev, D. A. Buchanan, E. Cartier, A. Kumar, D. DiMaria, S. Guha*, et al.*, "Ultrathin high-K gate stacks for advanced CMOS devices," in *Electron Devices Meeting, 2001. IEDM '01. Technical Digest. International*, 2001, pp. 20.1.1-20.1.4.

[57] K. Sarakinos, J. Alami, and S. Konstantinidis, "High power pulsed magnetron sputtering: A review on scientific and engineering state of the art," *Surface and Coatings Technology,* vol. 204, pp. 1661-1684, 2010.

[58] U. Helmersson, M. Lattemann, J. Bohlmark, A. P. Ehiasarian, and J. T. Gudmundsson, "Ionized physical vapor deposition (IPVD): A review of technology and applications," *Thin Solid Films,* vol. 513, pp. 1-24, 2006.

[59] J. Böhlmark, "Fundamentals of high power impulse magnetron sputtering," 2006.

[60] J. T. Gudmundsson, "Ionized physical vapor deposition (IPVD): magnetron sputtering discharges," *Journal of Physics: Conference Series,* vol. 100, p. 082002, 2008.

[61] J. T. Gudmundsson, N. Brenning, D. Lundin, and U. Helmersson, "High power impulse magnetron sputtering discharge," *Journal of Vacuum Science & Technology A,* vol. 30, pp. -, 2012.

[62] H. Jin, B. Feng, S. Dong, C. Zhou, J. Zhou, Y. Yang, *et al.*, "Influence of Substrate Temperature on Structural Properties and Deposition Rate of AlN Thin Film Deposited by Reactive Magnetron Sputtering," *Journal of Electronic Materials,* vol. 41, pp. 1948-1954, 2012.

[63] A. Artieda, M. Barbieri, C. S. Sandu, and P. Muralt, "Effect of substrate roughness on c-oriented AlN thin films," *Journal of Applied Physics,* vol. 105, pp. 024504-024504-6, 2009.

[64] T. Kamohara, M. Akiyama, N. Uena, and N. Kuwano, "Improvement in crystal orientation of AlN thin films prepared on Mo electrodes using AlN interlayers," *Ceramics International,* vol. 34, pp. 985-989, 2008.

[65] T. Kamohara, M. Akiyama, N. Ueno, K. Nonaka, and H. Tateyama, "Growth of highly c-axis-oriented aluminum nitride thin films on molybdenum electrodes using aluminum nitride interlayers," *Journal of Crystal Growth,* vol. 275, pp. 383-388, 2005.

[66] H. Y. Liu, G. S. Tang, F. Zeng, and F. Pan, "Influence of sputtering parameters on structures and residual stress of AlN films deposited by DC reactive magnetron sputtering at room temperature," *Journal of Crystal Growth,* vol. 363, pp. 80-85, 2013.

[67] C.-M. Lin, T.-T. Yen, V. V. Felmetsger, M. A. Hopcroft, J. H. Kuypers, and A. P. Pisano, "Thermally compensated aluminum nitride Lamb wave resonators for high temperature applications," *Applied Physics Letters,* vol. 97, pp. 083501-1 - 083501-3, 2010.

[68] G. Wingqvist, L. Arapan, V. Yantchev, and I. Katardjiev, "A micromachined thermally compensated thin film Lamb wave resonator for frequency control and sensing applications," *Journal of Micromechanics and Microengineering,* vol. 19, p. 035018, 2009.

[69] J. H. Kuypers, L. Chih-Ming, G. Vigevani, and A. P. Pisano, "Intrinsic temperature compensation of aluminum nitride Lamb wave resonators for multiple-frequency references," in *Frequency Control Symposium, 2008 IEEE International*, 2008, pp. 240-249.

[70] Ahmad Safari and E. K. Akdoğan, *Piezoelectric and Acoustic Materials for Transducer Applications*: Springer, 2008.

[71] S. Trolier-McKinstry and P. Muralt, "Thin Film Piezoelectrics for MEMS," *Journal of Electroceramics,* vol. 12, pp. 7-17, 2004.

APPENDIX

APPENDIX A – LIST OF INCLUDED PAPERS

This thesis is based on the following papers, which are referred to in the text by their Roman numerals.

I **M. A. Moreira**, T. Törndahl, I. Katardjiev, T. Kubart, “Thin AlN films deposited by reactive HiPIMS and Pulsed DC sputtering: a comparative study,” (Manuscript to be submmited).

II **M. Moreira**, J. Bjurström, I. Katardjiev, and V. Yantchev, "Efficient RF voltage transformer with bandpass filter characteristics," *Electronics Letters,* vol. 49, pp. 198-199, 2013.

III J. F. Souza, **M. A. Moreira**, I. Doi, J. A. Diniz, P. J. Tatsch, and J. L. Gonçalves, "Preparation and characterization of high-k aluminium nitride (AlN) thin film for sensor and integrated circuits applications," *Physica Status Solidi (c),* vol. 9, pp. 1454-1457, 2012.

IV **M. Moreira**, J. Bjurström, I. Katardjiev, and V. Yantchev, "Aluminum scandium nitride thin-film bulk acoustic resonators for wide band applications," *Vacuum,* vol. 86, pp. 23-26, 2011.

V **M. Moreira**, J. Bjurström, T. Kubart, B. Kuzavas, and I. Katardjiev, "Synthesis of c-tilted AlN films with a good tilt and thickness uniformity," in *IEEE International Ultrasonics Symposium Proceedings*, 2011, pp. 1238-1241.

VI **M. A. Moreira**, I. Doi, J. F. Souza, and J. A. Diniz, "Electrical characterization and morphological properties of AlN films prepared by dc reactive magnetron sputtering," *Microelectronic Engineering,* vol. 88, pp. 802-806, 2011.

Reprints were made with permission from the respective publishers.

APPENDIX B - AUTHOR'S CONTRIBUTION IN THE INCLUDED PAPERS

I Part of planning and analysis. Major part of thin films deposition (Pulsed DC and HiPIMS) and measurements. Significant part of writing.

II Minor part of planning. Involved in fabrication and measurements. Minor writing.

III Minor part of planning. Major part of synthesis and characterization of AlN for the application as the transistor gate. Minor writing.

IV Part of planning. Involved in synthesis and characterization of AlScN films. Involved in fabrication and characterization of FBARs. Minor writing.

V Minor part of planning. Involved in thin films depositions and measurements. Minor writing.

VI Part of planning. All fabrication and measurements. Significant part of writing.

APPENDIX C - CONFERENCE CONTRIBUTIONS

i. Tomas Kubart, Ilia Katardjiev, **Milena Moreira**, “Thin AlN films deposited by reactive HiPIMS and pulsed DC sputtering - a comparative study,” presented at *14th International Conference on Plasma Surface Engineering (PSE 2014)*, Garmisch-Partenkirchen, Germany, 2014.

ii. J. Olivares, M. M. Ramos, E. Iborra, M. Clement, T. Mirea, **M. Moreira**, I. Katardjiev, “IR-reflectance assessment of the tilt angle of AlN-wurtzite films for shear mode resonators,” presented at *European Frequency and Time Forum & International Frequency Control Symposium (EFTF/IFC)*, Prague-Czech Republic, 2013.

iii. **M. A. Moreira**, J. Bjurström, V. Yantchev, I. Katardjiev, “Microacoustic voltage transformer with bandpass filter characteristics,” presented at *IEEE International Ultrasonics Symposium (UFFC-IUS)*, Prague-Czech Republic, 2013.

iv. **M. A. Moreira**, J. Bjurström, V. Yantchev, I. Katardjiev, “Synthesis and characterization of highly c-textured $Al_{(1-x)}Sc_xN$ thin films in view of telecom applications,” presented at *European Material Research Society E-MRS*, Strasbourg-France, 2012.

v. **M. A. Moreira**, J. Bjurström, V. Yantchev, I. Katardjiev, “Synthesis of wurtzite $Al_{(1-x)}Sc_xN$ thin films,” presented at IEEE *International Ultrasonics Symposium (UFFC-IUS)*, Dresden-Germany, 2012.

vi. J. F. Souza, **M. A. Moreira**, I. Doi, J. A. Diniz, P. J. Tatsch, “Preparation and characterization of high-k Aluminum nitride (AlN) thin film for sensors and integrated circuits applications,” presented at *International Conference on the Formation of Semiconductor Interfaces (ICFSI-13)*, Prague-Czech Republic, 2011.

vii. **M. Moreira**, J. Bjurström, T. Kubart, B. Kuzavas, I. Katardjiev, ”Synsthesis of highly textured w-AlN thin films with a tilted c-axis having good tilt and thickness uniformity,” presented at *IEEE International Ultrasonics Symposium (UFFC-IUS)*, Orlando-USA, 2011.

viii. **M. A. Moreira**, I. Doi, J. F. Souza, J. A. Diniz, “Electrical characterization and morphological properties of AlN films prepared by dc reactive magnetron sputtering,” presented at *Materials for Advanced Metallization (MAM)*, Mechelen-Belgium, 2010.

ix. **M. A. Moreira**, I. Doi, J. F. Souza, J. A. Diniz, “Electrical properties of AlN MIS capacitors prepared by DC reactive magnetron sputtering technique,” presented at International Conference on Electronic Materials (IUMRS-ICEM), Seoul-Korea, 2010.

APPENDIX D – PAPER I

"Thin AlN films deposited by reactive HiPIMS and Pulsed DC sputtering: a comparative study,"

M. A. Moreira, T. Törndahl, I. Katardjiev, T. Kubart,

(Manuscript to be submmited)

Thin AlN films deposited by reactive HiPIMS and Pulsed DC sputtering: a comparative study

M.A. Moreira[1,2], T. Törndahl, I. Katardjiev[1], T. Kubart[1*]

1. Dept. Solid State Electronics, Ångström Lab., Uppsala University, Box 534, SE-752 21, Uppsala, Sweden
2. School of Electrical and Computer Engineering, University of Campinas, CEP 13.083-852, Campinas-SP, Brazil

Abstract: *Aluminum nitride films were deposited by high power impulse magnetron sputtering and Pulsed DC on Si and textured Mo substrates. Similar deposition conditions were used for both techniques: discharge power, pressure, Ar/N_2 gas flow and substrate temperature. The films were characterized using profilometer, X-ray diffraction (θ-2θ scans and rocking curves) and atomic force microscope (AFM). The results indicate an improvement in the AlN (002) peak over the Pulsed DC methods for all films deposited by HiPIMS. No significant stresses were identified. The HiPIMS films were smooth, with roughness around 1 nm.*

Introduction:

Aluminum nitride (AlN) is a wide-band gap piezoelectric material used in various applications. AlN films have been used in microelectronics as piezoelectric layers in electroacoustic devices (including biosensors and filters) [1-3], gate dielectric for transistors (replacing SiO_2) [4] and cantilevers in microelectromechanical systems (MEMS) [5]. The broad range of possible uses of AlN thin film is due to its unique combination of material properties, such as high acoustic velocity (11300 m/s for bulk acoustic wave devices), low propagation losses, wide bandgap (6.2 eV) and high electrical resistivity (1×10^{16} Ω cm) [6]. AlN is also chemically stable and fully compatible with the fabrication process of integrated circuits.

With respect to electroacoustic devices for high frequency applications, the properties of the piezoelectric layer play a key role in the final performance of the device since these properties define the electroacoustic parameters namely electromechanical coupling coefficient (k_t^2), quality factor (Q) and insertion loss. These properties are closely related to the crystalline orientation and structure, film stress and density. Therefore, a good control of the growth conditions is crucial for the synthesis of highly textured films.

AlN films can be deposited by different techniques, such as molecular beam epitaxy (MBE) [7], chemical vapour deposition (CVD) [8] or physical vapour deposition (PVD). PVD, namely magnetron sputtering, is the technique of choice for electroacoustic devices since it requires lower deposition temperatures than MBE and CVD [9] and it is compatible with standard microelectronic fabrication processes. Furthermore, high deposition rates and good control of deposition parameters are other advantages of the sputtering method.

Because highly textured wurtzite AlN films are required, the growth of the film has attracted attention. The deposition conditions should provide sufficient energy to the growing surface in order to enhance the adatom mobility on the substrate surface and thus promote growth of (002) grains [10]. At reduced deposition temperature, kinetic energy of sputtered species or additional ion bombardment is beneficial. The former was employed by this group. The depositions parameters were tuned in previous studies and AlN films with FWHM below 2 degrees could be achieved [11]. In order to avoid thermalization of sputtered species, low sputtering pressure and short target-to-substrate distance is required.

Texture evolution in AlN can be promoted by a suitable seed layer. Mo is frequently used in electroacoustic due to its intrinsic properties and good lattice match to AlN [12, 13]. AlN grown directly on Si typically contain a transition layer and the degree of texture is inferior.

When the distance is large in comparison to the mean free path, different approaches have to be employed. [9] have shown the importance of ion bombardment on the texture formation in AlN. Especially the importance of low energy Ar^+ ions was pointed out.

Reactive Pulsed DC is the most common process for PVD AlN deposition [14, 15]. Recently high power impulse magnetron (HiPIMS) was used for deposition of AlN films [16]. In HiPIMS, very high ionization degree of the sputtered material is achieved thanks to the pulsed mode operation of the discharge. Low frequency operation with a duty cycle typically about 1% is typically used which leads to two orders of magnitude higher electron densities and corresponding increase in the ionization of deposition flux. As a result, the energy input into the growing film can be significantly increased [17]. The study [16] has shown a clear improvement in the film texture and a reduction in the thickness of the interface amorphous AlN layer. It should be noted that a setup with long target-to-substrate distance was used.

The motivation of this work is the growth of thin textured (002) AlN layers directly on Si substrates without any textured metal seed layer. The resulting layer may be used as a seed layer for deposition of thick AlN films or as a functional film for high frequency devices. HiPIMS technique is evaluated as it can provide high flux of low energy ionized sputtered material and thus be suitable for arbitrary system geometries. The goal is to find the optimal conditions to achieve films with quality superior to the short target-to-substrate distance process in a more robust geometrical configuration which can also be used for deposition of complex films by co-sputtering.

Experimental:

AlN films were deposited by Pulsed DC and HiPIMS techniques and in the same sputtering system, CMS-18 (Kurt J. Lesker). The power supply was the single modification performed at the machine in order to switch between the deposition processes. The system has one load-lock chamber and one process chamber and it is pumped by a cryopump (CTI CryoTorr 8). The CMS-18 is equipped with four magnetron sputtering sources in a co-sputtering configuration and the distance target-to-substrate is 18 cm.

The power in HiPIMS mode was supplied by a SIPP 1000 pulsing unit fed by an Advanced Energy Pinnacle DC generator. Both the target current and voltage were monitored using a current and voltage transducer, and recorded in Agilent Infiniium (DSO9064A) digital oscilloscope, which was also used to calculate the instantaneous power delivered to the discharge. The pulsing unit was controlled by an arbitrary function generator (Tektronix AFG 3200). Pulsing frequency of 1 KHz and pulse on-time of 50 μs was used. An average discharge power of 830 W was maintain by adjusting the discharge voltage. The substrates were electrically floating during the deposition.

For Pulsed DC sputtering, an Advanced Energy Pinnacle plus power supply was used with a pulsing frequency of 250 KHz and 0.5 μs on-time pulse. The discharge power was 800 W.

The setup characteristics are summarized on *Table 1* and the deposition conditions of each method are summarized on *Table 2*.

Table 1. Summary of the setup characteristics for the Pulsed DC and the HiPIMS depositions.

Al target (4")	**99.99% purity**
Ar	99.9995% purity
N_2	99.9995% purity
Base pressure	$1 - 5 \times 10^{-8}$ Torr
Distance target-to-substrate	180 mm
Substrate rotation speed	20 rpm
Substrate heating (if used)	Radiative heater

Table 2. Summary of the deposition conditions of Pulsed DC and HiPIMS methods.

	Pulsed DC	HiPIMS
Pre-sputtering power	200 W	400 W
Discharge power	800 W	830 W
Pulse frequency	250 KHz	1 KHz
Duty cycle	0.5 μs	50 μs

* Corresponding author
tomas.kubart@angstrom.uu.se

The deposition pressure was kept between 2.8 – 3.2 mTorr for both processes and the films were deposited at four different gas flow compositions (Ar/N_2, in sccm): (i) 30/40, (ii) 35/35, (iii) 40/30, and (iv) 45/25. Noteworthy, the total gas flow ($Ar + N_2$) was kept at 70 sccm. Prior to each deposition, the Al target was sputter-conditioned in pure Ar during 3 min. No bias voltage was applied and the substrates were on floating mode.

Reference samples were deposited by Pulsed DC in a Von Ardenne balanced magnetron sputtering system (CS 730S, Von Ardenne). This system has a low distance target-to-substrate (5.5 cm), which is favourable to the growth of highly textured films. Details of the deposition system are provided elsewhere [11].

The substrates used were Si (p-100) and textured Mo and all three deposition process were used to sputter AlN films on top of these substrates: Pulsed DC, HiPIMS and the standard process. Regarding the deposition temperatures, two conditions were used: no substrate heating (deposition at room temperature) and substrate heated to 400 °C.

The crystallographic properties of the films were evaluated from the θ-2θ scans and rocking curves performed at a Philips MRD X-ray diffractometer. Considering that the FWHM is dependent of the film thickness, and in order to be fair in the comparison between films, all AlN films were deposited with thicknesses around 200 nm (deposition rates determined by prior depositions). The thicknesses were measured by mean of a Dektak profilometer (Dektak 150, Veeco).

Results and Discussions:

The properties of 200 nm thick AlN films were studied as a function of the deposition technique (HiPIMS or Pulsed DC), N_2 gas flow, substrate material (Si or textured Mo) and deposition temperature (room temperature or 400 °C). The temperature of 400 °C was selected as optimal based on previous evaluation. For comparison, AlN films were also deposited by Pulsed DC using otherwise identical conditions.

As a reference, two sets of samples were prepared using the standard deposition setup [11]. 200 nm AlN films were deposited by the optimized process on Si and textured Mo substrates.

HiPIMS process characteristics

Typical HiPIMS discharge current and voltage waveforms are shown in *Figure 1.* The discharge current increased with increasing flow of N_2 in agreement with other studies [18]. Because of the short on-time of 50 μs, no saturation of the discharge current was reached. Short on-times are also beneficial to supress formation of arcs and very stable operation of the discharge was observed.

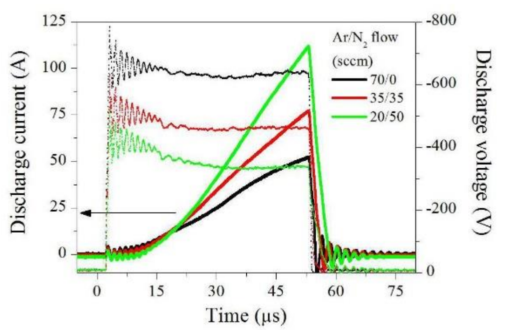

Figure 1. Discharge current and voltage waveforms in the HiPIMS mode for selected values of N_2 gas flow.

The discharge voltage and deposition rate as a function of the N_2 flow are shown in *Figure 2* and *Figure 3*, respectively. From the results presented in *Figure 2* it is clear that higher N_2 flow is required to reach a stable discharge voltage in the HiPIMS mode as compared to Pulsed DC. This is a result of gas rarefaction which occurs during HiPIMS on-time [17]. Although the discharge voltage is typically attributed to the poisoning of the sputtering target surface, only a small reduction in the HiPIMS rate was observed above 30 sccm despite the continuous change in the discharge voltage. The deposition rate was 20 – 30 % lower in the HiPIMS mode, indicating moderate level of the self-sputtering [17].

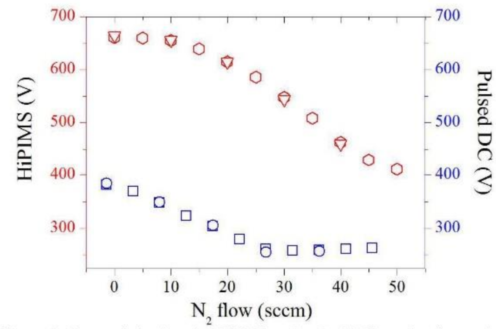

Figure 2. Process behaviour in HiPIMS and pulsed DC mode of operation illustrated by the discharge voltage versus the N_2 gas flow.

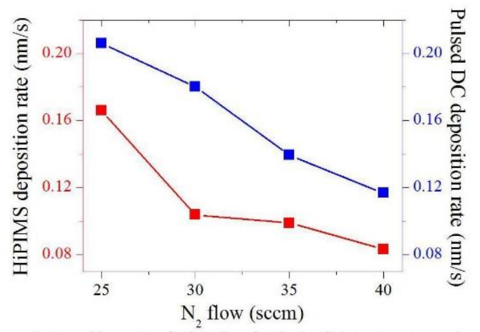

Figure 3. Deposition rates of HiPIMS and Pulsed DC (room temperature) as a function of the N_2 gas flow (on Si substrates).

Film characterization

From comparison of films deposited at different N_2 gas flows, not shown, the gas flow ratio Ar/N_2 of 35/35 sccm gave best results and was therefore used for all depositions analysed in this work. It may be noted that the influence of the gas flow ratio was relatively weak but the films deposited at the optimum gas flow showed lower residual stress both on Si and textured Mo substrates.

Overview θ-2θ spectra of AlN films deposited on Si substrates, *Figure 4,* clearly show the benefit of the HiPIMS process. Already at room deposition temperature the intensity of HiPIMS AlN (002) peak is comparable to the reference process as displayed in a detailed view in *Figure 5*. At elevated temperature, the intensity clearly exceeds the reference value. The film deposited by Pulsed DC on Si at room temperature shows only a very weak (002) peak. Even the intensity of the high temperature Pulsed DC film is lower than that of all of the HiPIMS films.

The effect of deposition temperature is in agreement with previous studies [19-21] and the films deposited at 400°C show higher (002) peak intensity for both deposition processes (Pulsed DC and HiPIMS, on Si, *Figure 4*). The beneficial effect the temperatures is usually attributed to the enhanced surface mobility of adatoms which promotes the evolution of (002) orientation [22, 23]. Obviously the optimal deposition temperature varies for different experimental setups, deposited materials, substrates, etc. Considering that the adatom mobility is directly related to the deposition temperature in the system, one should find the optimal temperature for each experimental setup and deposition processes. As previously mentioned, 400 °C is the optimized temperature to deposit c-axis textured AlN films in our systems.

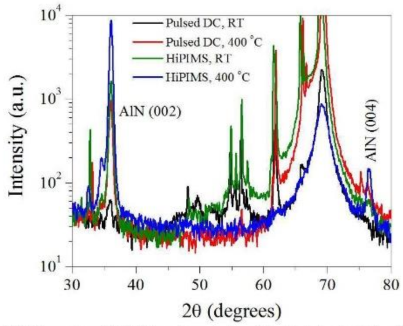

Figure 4. θ-2θ spectra of AlN films deposited on Si substrates by Pulsed DC and HiPIMS, at room temperature (RT) and at 400 ºC (35/35 gas flow ratio).

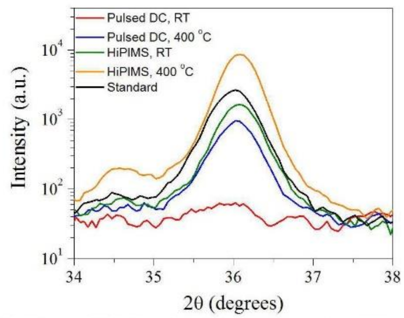

Figure 5. θ-2θ scans of AlN films deposited at room temperature (RT) and 400 ºC on Si by Pulsed DC, HiPIMS and standard process (zoomed in at the AlN (002) peak).

The shift of (002) AlN peak on the θ-2θ scans was analysed for all films in order to estimate the internal stresses. No considerable peak shift was found which indicates very low stress levels. This is in contrast to previous HiPIMS study by Aissa et al. [16]. Lower stress in our case is caused by the long target-to-substrate distance and hence thermalization of the energetic ions produced in HiPIMS discharges [24]. The energy of the ions arriving to the substrate are then determined mainly by the plasma potential. It should be noted, however, that higher stress may develop in thicker films deposited at the same conditions than the thin ones, even further on the films deposited at 400 ºC.

A significant fraction of the sputtered atoms gets ionized in HiPIMS with up to 70% ionization of the sputtered metal reported for HiPIMS of Al [25]. Moreover, in reactive HiPIMS the ion flux is dominated by reactive gas ions which further increases the ion flux to the substrate [26]. The high flux of low energy ions promotes surface diffusion of atoms and thus contributes to the preferred orientation of the coating. At the same time, the high energy tail of the ion energy distribution function seems to be sufficiently suppressed and therefore no excessive internal stresses evolved.

For applications where AlN films are deposited on a metal bottom electrode, growth on metal layers is of interest. Therefore, in addition to Si substrates, the films were also grown on textured Mo substrates to evaluate the influence of the substrate. Mo is the metal of choice as a bottom electrode in microelectronics, for instance at electroacoustic devices applications. Previous studies showed that a textured Mo layer enhances textured growth of AlN films because of better lattice match between the materials [12, 13].

The results of XRD measurement around the (002) AlN peaks for each deposition method is shown in *Figure 6* for films grown on textured Mo substrates. All three deposition processes achieved similar results. Even the effect of temperature is similar for pulsed DC and HiPIMS. Noteworthy, the HiPIMS films on Si deposited at 400ºC shown intensity comparable to the films deposited on textured Mo.

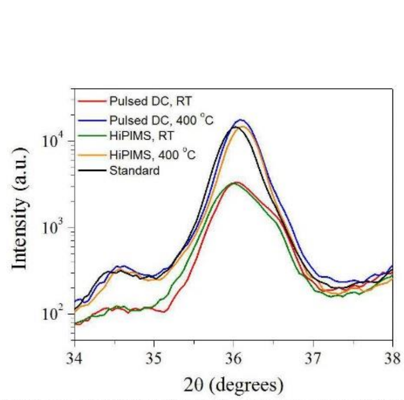

Figure 6. θ-2θ scans of AlN films deposited at room temperature (RT) and 400 ºC on textured Mo by Pulsed DC, HiPIMS and standard process (zoomed in at the AlN (002) peak).

To further illustrate the improvement in the nucleation layer provided by the HiPIMS method, the (002) full width at half maximum (FWHM) values of X-ray rocking curves are presented in *Table 3*. The texture of AlN films deposited by HiPIMS is superior to any of those deposited by Pulsed DC and the standard process. The FWHM of all films is considerably high. However, it is important to consider the thicknesses of the films studied here was only 200 nm. Thus, a lower FWHM is expected for thicker films [27].

Such thicker films may be grown even without a Mo seed layer directly on Si either by the HiPIMS process or by a standard DC sputtering using the thin HiPIMS films as seed layers. The later approach could benefit from higher deposition rate of the DC sputtering as compared to HiPIMS.

Table 3. (002) FWHM of AlN films deposited by Pulsed DC, HiPIMS and standard process on Si and textured Mo substrates, at room temperature and 400 ºC.

Substrate		**FWHM (degrees)**		
		Pulsed DC	**HiPIMS**	**Standard process**
Si	**Room temperature**	Poor quality	10	-
	400ºC	14,2	5,1	8,5
Mo	**Room temperature**	7,6	7,2	-
	400ºC	4,1	3,2	3,6

The roughness of some films was measured by AFM (non-contact mode). All measured films were smooth, with roughness around 1 nm. Further investigation should be performed in order to study the influence of deposition method, substrate and deposition temperatures in the films' roughness.

***Conclusions*:**

Thin AlN films were grown by HiPIMS directly on Si substrates and compared with films deposited by Pulsed DC (at the same sputtering machine) and a standard deposition process (reference process). The results indicate a significant improvement over the Pulsed DC and the standard process for the films deposited at room temperature and at 400 ºC as well. Moreover, the HiPIMS process is more robust and can be used in a co-sputtering configuration. The results also indicate very low stresses in the AlN films deposited by HiPIMS, probably as a result of thermalization of ionized species.

References:

[1] G. Wingqvist, "AlN-based sputter-deposited shear mode thin film bulk acoustic resonator (FBAR) for biosensor applications — A review," *Surface and Coatings Technology*, vol. 205, pp. 1279-1286, 2010.

[2] C.-M. Yang, K. Uehara, S.-K. Kim, S. Kameda, H. Nakase, and K. Tsubouchi, "Highly c-axis-oriented AlN film using MOCVD for

5GHz-band FBAR filter," in *IEEE International Ultrasonics Symposium Proceedings*, 2003, pp. 170-173.

[3] M. Moreira, J. Bjurström, I. Katardjiev, and V. Yantchev, "Efficient RF voltage transformer with bandpass filter characteristics," *Electronics Letters,* vol. 49, pp. 198-199, 2013.

[4] J. F. Souza, M. A. Moreira, I. Doi, J. A. Diniz, P. J. Tatsch, and J. L. Gonçalves, "Preparation and characterization of high-k aluminium nitride (AlN) thin film for sensor and integrated circuits applications," *Physica Status Solidi (c),* vol. 9, pp. 1454-1457, 2012.

[5] A. Andrei, K. Krupa, M. Jozwik, P. Delobelle, L. Hirsinger, C. Gorecki, *et al.*, "AlN as an actuation material for MEMS applications: The case of AlN driven multilayered cantilevers," *Sensors and Actuators A: Physical,* vol. 141, pp. 565-576, 2008.

[6] X.-H. Xu, H.-S. Wu, C.-J. Zhang, and Z.-H. Jin, "Morphological properties of AlN piezoelectric thin films deposited by DC reactive magnetron sputtering," *Thin Solid Films,* vol. 388, pp. 62-67, 2001.

[7] B. Liu, J. Gao, K. M. Wu, and C. Liu, "Preparation and rapid thermal annealing of AlN thin films grown by molecular beam epitaxy," *Solid State Communications,* vol. 149, pp. 715-717, 2009.

[8] M.-J. Lai, L.-B. Chang, T.-T. Yuan, and R.-M. Lin, "Improvement of crystal quality of AlN grown on sapphire substrate by MOCVD," *Crystal Research and Technology,* vol. 45, pp. 703-706, 2010.

[9] M. Clement, E. Iborra, J. Sangrador, A. Sanz-Hervás, L. Vergara, and M. Aguilar, "Influence of sputtering mechanisms on the preferred orientation of aluminum nitride thin films," *Journal of Applied Physics,* vol. 94, pp. 1495-1500, 2003.

[10] M.-A. Dubois and P. Muralt, "Stress and piezoelectric properties of aluminum nitride thin films deposited onto metal electrodes by pulsed direct current reactive sputtering," *Journal of Applied Physics,* vol. 89, pp. 6389-6395, 2001.

[11] G. F. Iriarte, F. Engelmark, and I. V. Katardjiev, "Reactive Sputter Deposition of Highly Oriented AlN Films at Room Temperature," *Journal of Materials Research,* vol. 17, pp. 1469-1475, 2002.

[12] T. Kamohara, M. Akiyama, N. Uena, and N. Kuwano, "Improvement in crystal orientation of AlN thin films prepared on Mo electrodes using AlN interlayers," *Ceramics International,* vol. 34, pp. 985-989, 2008.

[13] T. Kamohara, M. Akiyama, N. Ueno, K. Nonaka, and H. Tateyama, "Growth of highly c-axis-oriented aluminum nitride thin films on molybdenum electrodes using aluminum nitride interlayers," *Journal of Crystal Growth,* vol. 275, pp. 383-388, 2005.

[14] F. Engelmark, J. Westlinder, G. F. Iriarte, I. V. Katardjiev, and J. Olsson, "Electrical Characterization of AlN MIS and MIM Structures," *IEEE Transactions on Electron Devices,* vol. 50, pp. 1214-1219, 2003.

[15] A. Guillaumot, F. Lapostolle, C. Dublanche-Tixier, J. C. Oliveira, A. Billard, and C. Langlade, "Reactive deposition of Al–N coatings in Ar/N_2 atmospheres using pulsed-DC or high power impulse magnetron sputtering discharges," *Vacuum,* vol. 85, pp. 120-125, 2010.

[16] K. A. Aissa, A. Achour, J. Camus, L. L. Brizoual, P.-Y. Jouan, and M.-A. Djouadi, "Comparison of the structural properties and residual stress of AlN films deposited by dc magnetron sputtering and high power impulse magnetron sputtering at different working pressures," *Thin Solid Films,* vol. 550, pp. 264-267, 2013.

[17] D. Lundin and K. Sarakinos, "An introduction to thin film processing using high-power impulse magnetron sputtering," *Journal of Materials Research,* vol. 27, pp. 780-792, 2012.

[18] M. Aiempanakit, A. Aijaz, D. Lundin, U. Helmersson, and T. Kubart, "Understanding the discharge current behavior in reactive high power impulse magnetron sputtering of oxides " *Journal of Applied Physics,* vol. 113, p. 133302, 2013.

[19] F. Engelmark, G. Fuentes, I. V. Katardjiev, A. Harsta, U. Smith, and S. Berg, "Synthesis of highly oriented piezoelectric AlN films by reactive sputter deposition," *Journal of Vacuum Science Technology A,* vol. 18, pp. 1609-1612, 2000.

[20] F. Medjani, R. Sanjinés, G. Allidi, and A. Karimi, "Effect of substrate temperature and bias voltage on the crystallite orientation in RF magnetron sputtered AlN thin films," *Thin Solid Films,* vol. 515, pp. 260-265, 2006.

[21] M. Akiyama, K. Kano, and A. Teshigahara, "Influence of growth temperature and scandium concentration on piezoelectric response of scandium aluminum nitride alloy thin films," *Applied Physics Letters,* vol. 95, pp. 162107-162107-3, 2009.

[22] H. Jin, B. Feng, S. Dong, C. Zhou, J. Zhou, Y. Yang, *et al.*, "Influence of Substrate Temperature on Structural Properties and Deposition Rate of AlN Thin Film Deposited by Reactive Magnetron Sputtering," *Journal of Electronic Materials,* vol. 41, pp. 1948-1954, 2012.

[23] A. Artieda, M. Barbieri, C. S. Sandu, and P. Muralt, "Effect of substrate roughness on c-oriented AlN thin films," *Journal of Applied Physics,* vol. 105, pp. 024504-024504-6, 2009.

[24] P. Y. Jouan, L. Le Brizoual, M. Ganciu, C. Cardinaud, S. Tricot, and M. Djouadi, "HiPIMS Ion Energy Distribution Measurements in Reactive Mode," *Plasma Science, IEEE Transactions on,* vol. 38, pp. 3089-3094, 2010.

[25] C. Huo, M. A. Raadu, D. Lundin, J. T. Gudmundsson, A. Anders, and N. Brenning, "Gas rarefaction and the time evolution of long high-power impulse magnetron sputtering pulses," *Plasma Sources Science and Technology,* vol. 21, p. 045004, 2012.

[26] M. Aiempanakit, A. Aijaz, D. Lundin, U. Helmersson, and T. Kubart, "Understanding the discharge current behavior in reactive high power impulse magnetron sputtering of oxides," *Journal of Applied Physics,* vol. 113, pp. -, 2013.

[27] W.-K. Liu, K.-W. Tay, S.-C. Kuo, and M.-J. Wu, "Fabrication of piezoelectric AlN thin film for FBARs," *Science in China Series G: Physics, Mechanics and Astronomy,* vol. 52, pp. 226-232, 2009.

APPENDIX E – PAPER II

"Efficient RF voltage transformer with bandpass filter characteristics,"

M. Moreira, J. Bjurström, I. Katardjiev, and V. Yantchev,

Electronics Letters, vol. 49, pp. 198-199, 2013.

Efficient RF voltage transformer with bandpass filter characteristics

M. Moreira, J. Bjurström, I. Katardjiev and V. Yantchev

A microwave bandpass filter with a large ratio between the output and the input impedance has been designed and fabricated. Consequently, it functions both as a voltage transformer and a bandpass filter, or transfilter for brevity. It represents a two-port micro-acoustic resonator employing Lamb waves in a thin piezoelectric AlN film grown onto a Si carrier substrate with a centre frequency of around 887 MHz. The transfilter has a transformer ratio of 10 and a voltage efficiency of over 80%. The component has a small size ($<0.5\ \mathrm{mm}^2$) and is shown to sustain power levels of 250 mW. It can be used in a variety of cases where both voltage amplification and frequency filtering are required. Examples include: charge pumps in RFID tags, energy scavenging, remotely triggered switches, wake-up radios in wireless networks, stand-by units in home electronics etc.

Introduction: Passive CMOS-based RFID tags attain energy from the interrogation signal which is rectified and subsequently accumulated over a period of time. Practical reading distances require voltage amplification which is achieved by various variants of the Dickson multistage rectifier [1], also referred to as charge pump, representing a network of rectifying devices (transistors or Schottky diodes) and capacitors. Their voltage efficiency, however, is low and declines rapidly with the degree of amplification.

In a different context, remotely triggered switches (RTSs) are needed in remotely controlled devices such as wake-up radios in wireless sensor networks, home electronics etc. The basic circuit of an RTS was proposed by Gu and Stankovic [2] and is illustrated in Fig. 1.

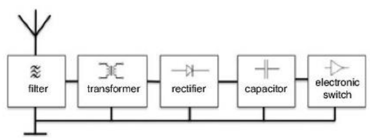

Fig. 1 *Schematic of remotely triggered switch*

The idea is to make use of the energy of the interrogation signal to trigger a low threshold electronic switch. Since the power levels at practical distances are insufficiently low, the energy is accumulated over a period of time and stored into a capacitor. A voltage transformer is typically needed to increase both the output voltage and the energy accumulated. A filter is placed between the antenna and the transformer to provide addressing. For instance, several such RTSs, tuned at different frequencies, may be connected in parallel to provide addressing, as illustrated in Fig. 2.

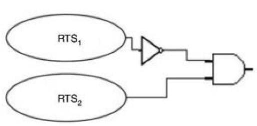

Fig. 2 *Example of 2-bit remotely triggered switch, hard coded as (0,1)*

Notable drawbacks of the RTS described above are its cost and size. To overcome the deficiencies in the above-described cases we have designed and fabricated a micro-acoustic bandpass filter with a large ratio between the output and the input impedance which makes it an efficient voltage transformer at the same time. In other words, it is both a transformer and a filter, for brevity also called a transfilter. Thus, a single transfilter replaces the first two components in Fig. 1.

Experiment: The transfilter represents a two-port Lamb wave resonator made of a 2.2 μm-thick c-textured AlN thin film grown onto a Si carrier substrate. The latter is etched from the backside to release the film and form a free-standing membrane. Wave excitation and signal output are realised by inter-digital transducers (IDTs) with a 6 μm pitch while energy confinement is achieved by Bragg reflectors consisting of metal strips with the same pitch as that of the IDTs. Both the IDTs and the reflectors were made of 300 nm-thick Al. For more information on the design of Lamb wave devices see [3]. Fig. 3 shows a cross-sectional schematic of the component.

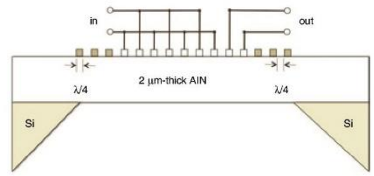

Fig. 3 *Cross-sectional schematic of transfilter*

The area of the transfilter is less than $0.5\ \mathrm{mm}^2$. The transfilter was electrically characterised with a network analyser in a 50/50Ω configuration around its central frequency of about 887 MHz. Fig. 4*a* shows the device S_{21} transfer function while Fig. 4*b* shows its voltage transformer characteristics at the centre frequency.

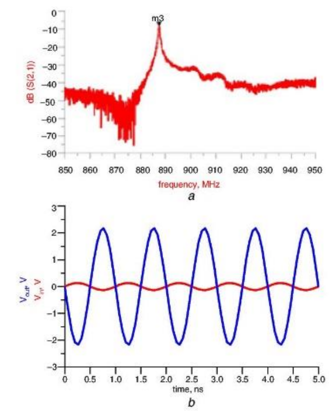

Fig. 4 *S_{21} characteristics, and open circuit voltage characteristics*
a S_{21} characteristics
b Open circuit voltage characteristics

Specifically, Fig. 4*a* shows that the component is a bandpass filter with an insertion loss of about −5 dB which after design optimisation can readily be brought down to −1 dB. The unloaded Q was 3000 while the device input and output impedance at centre frequency were measured to be 25Ω and 2600Ω, respectively, resulting in a voltage transformer ratio of about 10. The latter is confirmed by Fig. 4*b* which shows the input and output voltage amplitudes under open circuit conditions. Specifically, an input amplitude of 0.2 V is transformed into an output amplitude of 2 V with a 180° phase shift.

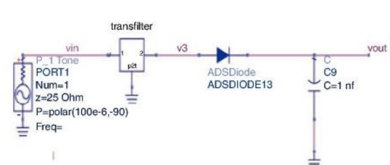

Fig. 5 *Simulated circuit with input power of 100 μW*

To illustrate further the usability of the transfilter in a RTS, the above measurements were used to simulate the circuit illustrated in Fig. 5.

Fig. 6 shows the voltage at the output capacitor against time at the centre frequency. For comparison, a simulation was also performed for the case without the transfilter.

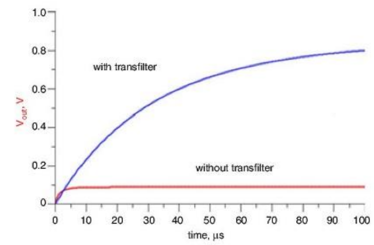

Fig. 6 *Voltage accumulation at output capacitor at centre frequency*

Specifically, for the case without a transfilter, the output voltage saturates at around 0.1 V irrespective of frequency. In the case with a transfilter, the output voltage increases to 0.8 V for the initial 100 µs when operated at the centre frequency, indicating an overall voltage efficiency for the whole circuit of 80% in view of the open circuit transformer ratio of 10. Outside centre frequency the voltage at the output capacitor is practically zero, as also seen from Fig. 4*a* which shows that the signal is significantly attenuated outside the passband. Hence, the circuit illustrated in Fig. 5 operates as a highly efficient RTS. Further, recalling that the centre frequency of the transfilter is determined by the pitch of the IDT, that is lithographically, it is seen that a number of such transfilters operating at different centre frequencies can be fabricated on a single chip having a common input and separate outputs. In other words, addressing in the context of Fig. 2 is readily and efficiently achieved.

Naturally, the complete device (the whole set of transfilters) needs to be carefully designed as each separate transfilter sees the rest as a net parasitic capacitance connected in parallel affecting thus the bandwidth of each transfilter. As noted above, the transformer ratio is determined by the ratio between the output and the input impedance, which can be varied in a wide range. Thus, assuming a limited interrogation power of 10 mW in the ISM band and interrogation distances of several metres, output voltages in the order of several volts become feasible [2]. This, of course, would be at the expense of longer integration time intervals in the range of milliseconds. In this context, truly passive RTSs become possible by employing capacitive MEMS switches which require pull-in voltages of the order of several volts [4]. Hard coding in this case is achieved by both normally open '1' and normally closed '0' MEMS switches.

It is noted that the thin film electro-acoustic technology is a low-cost technology indicating low transfilter fabrication costs, most likely in the order of 10 US cents in large volumes. In addition, it is fully compatible with the IC technology, suggesting that transfilters can be fabricated on top of an IC provided the areas of the two are comparable. Naturally, the area of the transfilter is inversely proportional to frequency.

With respect to semiconductor charge pumps the transfilter excels in terms of efficiency, cost and size. Another distinct feature is the fact that there is practically no initial energy accumulation, unlike charge pumps where all coupling capacitors need to be sequentially charged. A further advantage of the transfilter is that it is a linear device operating at all input power levels, practically eliminating the so-called 'dead zone' of charge pumps. Not least, for a full cycle rectifier the number of forward-biased rectifying devices in this case is two, in contrast to charge pumps where this number is proportional to the degree of voltage amplification. Noteworthy, the transfilter has been operated at a power level of 250 mW for a period of several weeks without degradation.

Other possible uses of the transfilter include stand-by units in remotely controlled home electronics such as TV, video etc, wake-up radio circuits in wireless sensor networks, addressable passive (non-IC) sensors, RFID tags, impedance matching etc.

Conclusion: A highly efficient, small size, low-cost RF voltage transformer with filter functionality has been designed, fabricated and electrically characterised. A voltage transformer ratio of 10 at a centre frequency of 887 MHz has been demonstrated. An insertion loss of -5 dB has been measured. Alternative designs are expected to decrease the insertion loss to around -1 dB, while higher transformer ratios are readily achievable. A wide range of possible applications has been identified.

14 November 2012
doi: 10.1049/el.2012.3982
One or more of the Figures in this Letter are available in colour online.

M. Moreira, J. Bjurström, I. Katardjiev and V. Yantchev (*Department of Solid State Electronics, Uppsala University, Box 534, S-75121 Uppsala, Sweden*)

E-mail: Ilia.Katardjiev@Angstrom.uu.se

References

1 Dickson, J.F.: 'On-chip high-voltage generation in NMOS integrated circuits using an improved voltage multiplier technique', *IEEE J. Solid-State Circuits*, 1976, **SSC-11**, (3), pp. 374–378
2 Gu, L., and Stankovic, J.: 'Radio triggered wake-up in wireless sensor networks', *Real-Time Syst.*, 2005, **29**, pp. 157–182
3 Bjurström, J., Katardjiev, I., and Yantchev, V.: 'Lateral-field-excited thin-film Lamb wave resonator', *Appl. Phys. Lett.*, 2005, **86**, (15)
4 Kaajakari, V.: 'Practical MEMS' (Small Gear Publishing, Las Vegas, 2009, ISBN: 978-0-9822991-0-4)

APPENDIX F – PAPER III

"Preparation and characterization of high-k aluminium nitride (AlN) thin film for sensor and integrated circuits applications,"

J. F. Souza, M. A. Moreira, I. Doi, J. A. Diniz, P. J. Tatsch, and J. L. Gonçalves,

Physica Status Solidi (c), vol. 9, pp. 1454-1457, 2012.

(Reprint made with the permission from the publisher)

Phys. Status Solidi C 9, No. 6, 1454–1457 (2012) / DOI 10.1002/pssc.201100461

physica status solidi c
www.pss-c.com
current topics in solid state physics

Preparation and characterization of high-k aluminium nitride (AlN) thin film for sensor and integrated circuits applications

J. F. Souza[1,2,3], M. A. Moreira[1,2], I. Doi[*,1,2], J. A. Diniz[1,2], P. J. Tatsch[1,2], and J. L. Gonçalves[2,3]

[1] School of Electrical and Computer Engineering, University of Campinas, Av. Albert Einstein 400, 13.083-852 Campinas-SP, Brazil
[2] Center for Semiconductor Components (CCS), University of Campinas, João Pandiá Calógeras 90, 13.083-870 Campinas-SP, Brazil
[3] Center for Information Technology Renato Archer (CTI), Rodovia D. Pedro I (SP – 65) Km 143,6, 23.069-901 Campinas-SP, Brazil

Received 25 July 2011, revised 12 September 2011, accepted 14 September 2011
Published online 20 February 2012

Keywords high-k, aluminium nitride, thin films, dc reactive magnetron sputtering, MISFET, EISFET

* Corresponding author: e-mail doi@ccs.unicamp.br

In last years considerable interest has been shown in aluminium nitride (AlN) films because of their optical, electrical, dielectric and acoustic properties. Owing to these characteristics, AlN thin films are suitable for the use in micro-electronic applications. In this work, AlN thin films were deposited on p-Si(100) and SiO_2/p-Si(100) substrates by dc reactive magnetron sputtering technique under the same deposition conditions (500 W of discharge power, 30 sccm N_2 flow, 80 sccm Ar flow and deposition pressure of $3x10^{-3}$ Pa). These conditions were defined by prior analysis in order to achieve films with smooth surface morphology, hexagonal wurtzite phase, and refractive index compatible with polycrystalline AlN films (between 2.0 and 2.2). The films were physically characterized using a variety of techniques such as atomic force microscopy (AFM), X-ray diffraction spectroscopy (XRD), Fourier infrared spectroscopy (FTIR) and ellipsometry. Electrical characteristics of films were compared by using metal-insulator-semiconductor (MIS) structures. Using a set of metal insulator semiconductor field effect transistors (MISFETs) and electrolyte-insulator-semiconductor field effect transistors (EISFETs) fabricated, electrical characteristics and sensing properties were investigated. The electrical quality of the AlN film and AlN/SiO_2/p-Si interface obtained suggests that AlN is an adequate insulator on silicon device and pH sensors application.

1 Introduction

AlN films, an III-V compound, has a symmetric band model with a wide band gap (6.2 eV), a refractive index value about 2.15, a breakdown voltage range of 4-9 $MV.cm^{-1}$, piezoelectric properties, high chemical stability, good thermal conductivity (k=0.31–1.4 W/cmK) and a thermal expansion coefficient matching with the silicon [1, 2]. These properties have made AlN a useful material in many applications, such as surface passivation of semiconductors, thin film resonator (TFR), acoustic optic (AO) devices, surface acoustic wave (SAW) devices, micro-electromechanical (MEM) devices, pH sensing devices, metal insulator semiconductor (MIS) devices and integrated circuit packaging. Besides, AlN is one of the blue and UV light emitting nitrides, which gives it an edge over other high-k dielectrics. Using AlN-Si MIS structures with acceptable qualities will thus open the path to co-integration of light emitting nitrides with silicon microelectronics. In order to achieve devices with high quality, many techniques have been used to obtain AlN films and AlN nanostructures (nanotubos and nanoparticles) such as sputtering, MOCVD, PECVD and dc-arc plasma [3-16]. Among these methods, the dc reactive magnetron sputtering process is an attractive deposition technique due to the combination of many advantages, such as compatibility with microelectronic processes, low temperature depositions, low cost method and fine tuning of the material characteristics [3, 4, 7-11].

This work reports the use of AlN/SiO_2 stacked layer as gate dielectric in MIS devices and AlN thin film as ion sensitive membrane in pH-EISFET devices as well as the device structures and the characterizations of both, films and devices.

Phys. Status Solidi C 9, No. 6 (2012) 1455

2 Experiments

2.1 AlN thin film preparation

The AlN thin films were deposited by dc reactive magnetron sputtering technique (Ulvac, MCH-9000, Massachusetts, USA). The target used was 99% Al-1% Si (99.99% purity) and the atmosphere were composed by a high purity nitrogen (N_2)/ argon (Ar) gas mixture (6N N_2 and 5N Ar), the Ar gas takes advantage of ions bombardment, while N_2 gas takes a function of reactive ions. The characteristic of the sputtering system includes pre-chamber, water-cooled magnetron, target with a diameter of 250 mm, target to substrate distance around 55 mm, and the discharge mode is power-constant. The target was pre-sputtered for 5 min in Ar in order to remove the residual contamination on its surface. The flow rate of Ar was fixed at 80 standard cubic centimeters per minute (sccm), while the flow rate of N_2 was 30 sccm. The discharge power was fixed at 500 W. The base and work pressure of the chamber was $2x10^{-6}$ Pa and $3x10^{-3}$ Pa, respectively. The thickness of thin film was 30 nm. These conditions were defined by prior analysis in order to achieve films with smooth surface morphology, high degree of c-axis orientation (002), refractive index compatible with polycrystalline AlN films (between 2.0 and 2.2) [17], and high device sensitivity. All deposition parameters are shown in Table 1.

Table 1 Parameters for the deposition of AlN film

Ar flow rate	80 sccm
N_2 flow rate	30 sccm
Substrate temperature	Room Temperature
Discharge power	500 W
Target to substrate distance	55 mm
Deposition rate	6 Å/second
Film thickness	30 nm
Target	99% Al-1%Si(99.99% purity), 250 mm diam.

2.2 MIS capacitor fabrication

The MIS capacitors were fabricated on p-type Si (100) with AlN and AlN/SiO_2 as the insulate layers. The SiO_2 layer was obtained by a thermal oxidation process at 1000 °C in an oxygen environment. A 300 nm thick layers of sputtered Al were used as the top and the backside electrodes. The MIS structures have circular geometry with 200 μm diameter, and the top electrodes were patterned by the lift-off method.

2.3 MISFET structure fabrication

The AlN film for the MISFET was grown using the conditions listed in Table 1 on p-type (1-10 Ω.cm) Si (100) substrate. The substrates were cleaned using a standard RCA wet process. The MISFET structure fabrication process consisted of twelve steps:

1) Substrate material: 3 inch diameter, 1-10 Ω.cm, (100), p-type silicon wafer;
2) Boron ion implantation: dose 10^{13} ion.cm^{-2}, 65 keV;
3) Thermal oxide: 8000 Å;
4) 1st photomask and oxide etching;
5) Phosphorus ion implantation of the source and drain regions : dose 10^{15} ion.cm^{-2}, 80 keV;
6) Activation anneal in nitrogen and thermal oxide: 5000 Å;
7) 2nd photomask and oxide etching;
8) Thermal gate oxide: 50 Å;
9) 3rd photomask and gate AlN thin film deposition: 300 Å (liftoff process);
10) 4th photomask and oxide etching;
11) Al sputtering: 3000 Å;
12) 5th photomask and Al etching.

Figure 1a shows a schematic cross section of the complete MISFET device.

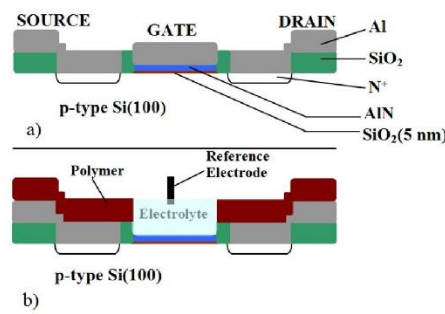

Figure 1 Schematic of the cross-sectional structure of the AlN/SiO_2 stacked layer a) on Si MISFET and b) on Si EISFET.

2.4 EISFET structure fabrication

Four additional process steps are required to transform the MISFET structure in an EISFET structure:

1) 6th photomask and Al etching of gate electrode;
2) Photopolymer thick layer (AZ 4620) deposition by spin-coat: ≈ 6 μm;
3) 7th photomask and polymer etching of the gate region;
4) Hard bake.

Figure 1b shows a schematic cross section of the complete EISFET device.

2.5 Film characterization

The AlN thin films used in these studies were characterized by X-ray diffraction spectroscopy (structural characterization), Fourier transform infrared spectrometry (infrared spectra), atomic force microscopy in contact image mode (surface morphology), and ellipsometry (film thickness and refractive index).

2.6 Measurements setup

In order to study electrical and sensing properties, current-voltage (I_{DS}-V_{GS}), high frequency (1 MHz) capacitance-voltage (C-V) and quasi-static C-V characteristics of MISFETs and EISFETs structures were measured by a semiconductor parameter analyzer Keithley 4200-SCS, and a capacimeter Keithley 590. The gate voltages were applied to an aluminium metal gate of MISFETs and a gold reference electrode for EISFETs.

3 Results and discussion

3.1 Physical characteristics of AlN film

The XRD patterns of the obtained AlN films as shown in Fig. 2a exhibited diffraction peaks at 2θ = 35.9° and 2θ = 37.8°, corresponding to the (002) and (101) crystal planes of the hexagonal wurtzite phase of AlN, respectively. The FTIR spectra of these films, Figure 2b showed absorbing band at 669 cm^{-1}, confirming that the film is aluminium nitride [17, 18].

Figure 3 shows the morphology of the used AlN films. The AFM image shows the formation of very smooth and uniform AlN films, with average (R_a) and root mean square (R_{rms}) roughness of 0.58 nm and 0.73 nm, respectively.

3.2 Electrical properties of devices

MIS capacitor – Figure 4 shows experimental plot of the (1 MHz) C-V curves for AlN/Si and AlN/SiO_2/Si capacitors. The C-V measurements showed hysteresis between forward and reverse sweeps. This phenomenon occurs due to mobile charges in the interface dielectric-semiconductor and it is strongly evident in the structures without a thin SiO_2 film stacked to the AlN layer. This behavior occurs because the oxide impedes the free movement of mobile charges in the interface dielectric-semiconductor of the AlN/SiO_2/Si capacitor.

MISFET – Figure 5 shows high frequency and quasi-static C-V curves for an MIS capacitor intrinsic to MISFET. The maximum capacitance is C_{max}=158.5 pF, the minimum capacitance is C_{min}=40.66 pF, and area is 4×10^4 μm^2 (200 µm x 200 µm). The substrate acceptor concentration (N_A), flat-band capacitance (C_{fb}), equivalent oxide thickness (EOT), flat-band voltage (V_{fb}), work function metal-semiconductor (ϕ_{ms}), effective charge (Q_{ef}/q), and threshold voltage (V_{th}) were calculated from C_{max}, C_{min}, and area, yielding $N_A=1.87\times10^{17}$ cm^{-3}, C_{fb} = 116.71 pF, EOT=8.71 nm, V_{fb}=-0.59 V, ϕ_{ms}=-1.02 V, and V_{th}= 0.84 V. The flat-band voltage value represents a shift of +0.37 V from ideal value (-0.96 V), for a negative charge trap density of $N_t= Q_{ef}/q = -1.02\times10^{12}$ cm^{-2}. No hysteresis in the flat-band voltage was observed. Quasi-static behavior of the MIS capacitor was obtained using the source and drain electrodes connected to the bulk electrode to supply minority carriers. Formation of the inversion layer is evidenced by the sharp turn on at +400 mV.

The electrical quality of the AlN/SiO_2 stacked layer and AlN/SiO_2/Si(100) interface as determined by CV measurements suggests that AlN/SiO_2 stacked layer is a quite good insulator on silicon for device applications. To test this issue, we fabricated AlN/SiO_2/Si MISFETs as shown in Fig. 1.

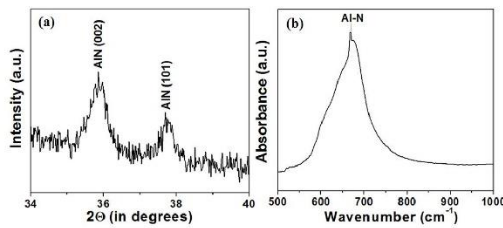

Figure 2 Physical characteristics of AlN film on SiO_2 thin film. (a) XRD spectra and (b) FTIR spectra.

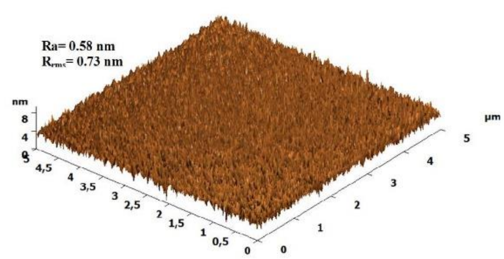

Figure 3 Surface morphology of AlN film on SiO_2 thin film.

Electrical characteristics of MISFETs including transconductance (G_m), current-off (I_{off}) and subthreshold swing (S_t) were calculated through drain-source current versus gate-source voltage (I_{DS}-V_{GS}) curves of the stack AlN/SiO_2 gate MISFET (Fig. 6). The I_{off} extracted at $V_{GS}=V_T$-0.5 V was $5x10^{-11}$ A. This I_{off} value is acceptable for FET operation. The calculated maximum transconductance of the stack AlN/SiO_2 gate MISFET was 96 µS. The high G_m value is due to the high dielectric constant ($E_{ox}\approx16$) of the AlN/SiO_2 layer. S_t is the slope of V_{GS} versus log I_{DS}. The S_t

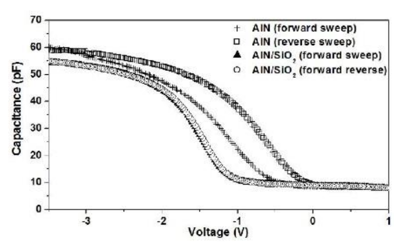

Figure 4 C-V curves of MIS capacitors with AlN and AlN/SiO_2 as insulate layer.

was obtained from the inverse of slope in subthreshold region and is 103 mV/dec to the stack AlN/SiO_2 gate MISFET (Figs. 6a and b).

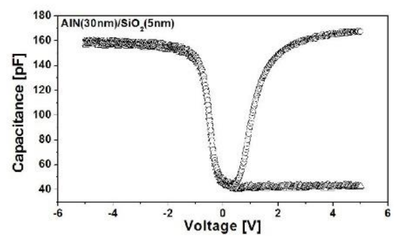

Figure 5 High frequency and quasi-static capacitance-voltage (C-V) curves for an MIS capacitor intrinsic to MISFET.

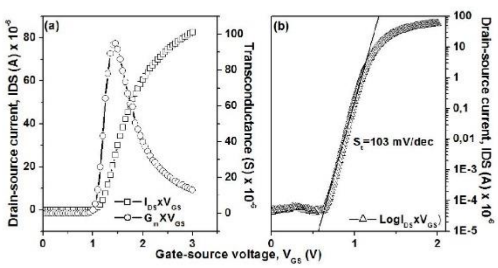

Figure 6 (a) I_{DS}-V_{GS} and G_m-V_{GS} and (b) log I_{DS}-V_{GS} characteristics of the stack AlN/SiO_2 gate MISFET.

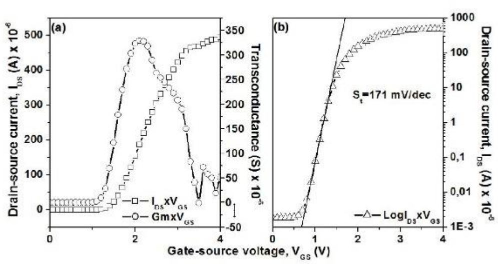

Figure 7 (a) I_{DS}-V_{GS} and G_m-V_{GS} and (b) log I_{DS}-V_{GS} characteristics of the stack AlN/SiO_2 gate EISFET in standard pH7 buffer solution.

3.3 Sensing properties of devices

The I_{DS}-V_{GS} curve of the stack AlN/SiO_2 gate EISFET in standard pH 7 buffer solution shows de normal FET operation. The I_{off} (1.88×10^{-9}A), S_t (171 mV/dec) and G_m (329 μS) characteristics of the stack AlN/SiO_2 gate EISFET were obtained as shown in Figs. 7 a and b.

4 Conclusions

In this study, we use high-k AlN thin film for sensor and integrated circuits applications. C-V measurements showed that structures with AlN/SiO_2 stacked layer exhibited high electrical quality and no hysteresis in the flat-band voltage. Thereby, we have fabricated MISFETs and EISFETs using this stacked layer. By fabricating and characterizing stack AlN/SiO_2 gate MISFET we have demonstrated a necessary step for the integration of the optoelectronic capabilities of the group III nitrides with silicon microelectronics transistors fabrication. EISFETs exhibit similar electrical characterizations as MISFETs for process and device design verification. With high G_m, the stack AlN/SiO_2 gate EISFET is suitable for sensing applications.

Acknowledgements The authors would like to thanks the CCS staff for technical assistance and the Brazilian agencies CNPq, CAPES, FAPESP, and INCT-NAMITEC for the financial support.

References

[1] J.H. Edgar (ed.), Properties of Group III Nitrides, EMIS Data Rev. Ser. No. 11 (INSPEC, IEE, 1994, UK).
[2] J. Szmidt, A. Werbowy, L. Jarzebowski, T. Gębicki, I. Pietrakowa, A. Sokolowska, and A. Olszyna, J. Mater. Sci. **31**, 2609 (1996).
[3] F. Engelmark, J. Westlinder, G. F. Iriarte et al., IEEE Trans. Electron. Dev. **50**, 1214-1219 (2003).
[4] J. X. Zhang, H. Cheng, Y. Z. Chen et al., Surf. Coat. Technol. **198**, 68-73 (2005)
[5] A. Sanz-Hervás, E. Iborra, M. Clemente et al., Diam. Relat. Mater. **12**, 1186-1189 (2003).
[6] Y. C. Kong, L. Q. Hu, Y. D. Zheng et al., Appl. Phys. A **90**, 545-548 (2008).
[7] A. Khanna and D. G. Bhat, J. Vac. Sci. Technol. A **25**, 557-565 (2007).
[8] J. A. Ruffner, P. G. Clem, B. A. Tuttle et al., Thin Solid Films **354**, 256-261 (1999).
[9] V. Dimitrova, D. Manova, and E. Valcheva, Mater. Sci. Eng. B **68**, 1-4 (1999).
[10] T. P. Drusedau and J. Bläsing, Thin Solid Films **377/378**, 27-31 (2000).
[11] X. Song, R. Fu, and H. He, Microelectron. Eng. **86**, 2217-2221 (2009).
[12] M.-J. Lai, L.-B. Chang, T.-T. Yuan, and R.-M. Lin, Cryst. Res. Technol. **45**, 703-706 (2010).
[13] J.-W. Soh, S.-S. Jang, I.-S. Jeong, and W.-J. Lee, Thin Solid Films **279**, 17-22.
[14] K. Hironaka, T. Nagashima, S. Ikeda et al., J. Cryst. Growth **312**, 2527-2529 (2010).
[15] S. Bellucci, C. Balasubramanian, A. Ivanov, A. Popov, and H. Schober, J. Neutron Res. **14**, 287-291 (2006).
[16] C. Balasubramanian, S. Bellucci, P. Castrucci, M. De Crescenzi, and S.V. Bhoraskar, Chem. Phys. Lett. **383**, 188–191 (2004).
[17] M.A. Moreira, I. Doi, J.F. Souza, and J.A. Diniz, Microelectron. Eng. **88**, 802-806 (2011).
[18] C. Balasubramanian, S. Bellucci et al., J. Phys.: Condens. Matter **18**, S2095-S2104 (2006).

APPENDIX G – PAPER IV

"Aluminum scandium nitride thin-film bulk acoustic resonators for wide band applications,"

M. Moreira, J. Bjurström, I. Katardjiev, and V. Yantchev,

Vacuum, vol. 86, pp. 23-26, 2011.

Vacuum 86 (2011) 23–26

Contents lists available at ScienceDirect

Vacuum

journal homepage: www.elsevier.com/locate/vacuum

Aluminum scandium nitride thin-film bulk acoustic resonators for wide band applications

Milena Moreira, Johan Bjurström, Ilia Katardjev, Ventsislav Yantchev*

Dept. Solid State Electronics, Angstrom Lab., Uppsala University, Box 534, S-75121 Uppsala, Sweden

ARTICLE INFO

Article history:
Received 7 March 2011
Received in revised form
28 March 2011
Accepted 29 March 2011

Keywords:
Thin film devices
Composite thin films
Acoustic microwave devices

ABSTRACT

Piezoelectric c-textured $Al_{(1-x)}Sc_xN$ thin films, where the Sc relative concentration, x, varies in the range 0–0.15 have been studied in view of radio frequency (RF) electro-acoustic applications. Thin film bulk acoustic wave resonators (FBARs) employing these films were fabricated and characterized as a function of the Sc concentration for the first time. The measured electromechanical coupling is found to increase by as much as 100% in the above concentration range. The results from this work underline the potential of the c-textured $Al_{(1-x)}Sc_xN$ based FBARs for wide band RF applications.

1. Introduction

C-axis oriented wurtzite aluminum nitride (w-AlN) thin films are currently used in commercial thin film bulk acoustic wave resonators (FBAR) and filters operating in the lower GHz range. The development of such devices has been driven by the need for low cost, high performance frequency control components in wireless communications, where the cellular phone industry is by far the largest user of this technology. AlN is a wide bandgap material with a relatively high piezoelectric constant as well as low acoustic and dielectric losses, just sufficient to satisfy the stringent requirements for bandwidth, low insertion loss, steep filter roll-off and good power handling capabilities. An important filter design parameter is the frequency bandwidth, which is determined by the electromechanical coupling coefficient of the piezoelectric layer (k_t^2). Well textured AlN films exhibit an electromechanical coupling coefficient of around 6% [1]. Using an optimized resonator design and a careful choice of materials and thicknesses of non-piezoelectric layers that comprise the resonator, the effective coupling (k_{eff}^2) of the resonator can be boosted to values of around 7%. This is just about what is required to meet the specifications of the most demanding filter applications [2]. However, the interest in new materials with higher electromechanical coupling is still very strong since, in addition to opening for new applications, they would result in a relaxed device design as well as fabrication margins and eventually to lower fabrication costs.

Recently, the piezoelectric response of w-AlN thin films alloyed with scandium (Sc) was shown to gradually increase with the scandium concentration up to 43 at.% Sc [3,4]. This experimental work was followed by first-principles calculations of the piezoelectric coefficient in wurtzite $Al_{(1-x)}Sc_xN$ that confirmed and revealed the origin of the increase of the piezoelectric constant [5]. It is also noted that the limited experimental findings with regard to c-textured wurtzite $Al_{(1-x)}Sc_xN$ films so far are deduced mostly from static measurements [3,4], while potential applications lie in the RF band. Thus, the ultimate and most realistic determination of the electromechanical properties is the experiment through RF evaluation of test FBAR resonators. Initial attempts in this respect have been recently presented for c-axis tilted films only [6], while experimental characterization as a function of Sc concentration is still missing for c-textured high quality films. Hence, the goal of this work is to characterize the properties of c-textured $Al_{(1-x)}Sc_xN$ thin films with varying Sc concentration in the lower GHz range by fabricating and measuring FBAR test structures.

2. Experimental

One port FBARs were fabricated on double side polished (100) silicon wafers. All devices have been micromachined using identical deposition processes and parameters (excluding the $Al_{(1-x)}Sc_xN$ layer), thus the FBARs with different Sc concentrations are compared under equal other parameters (layer thicknesses, area). More specifically, a seed layer of a 120 nm thick AlN film followed by a 330 nm thick molybdenum film was sputter deposited onto silicon substrates. The Mo film serves as a bottom (ground)

* Corresponding author.
E-mail address: veya@angstrom.uu.se (V. Yantchev).
URL: http://hermes.teknikum.uu.se/~veya/

0042-207X/$ – see front matter
doi:10.1016/j.vacuum.2011.03.026

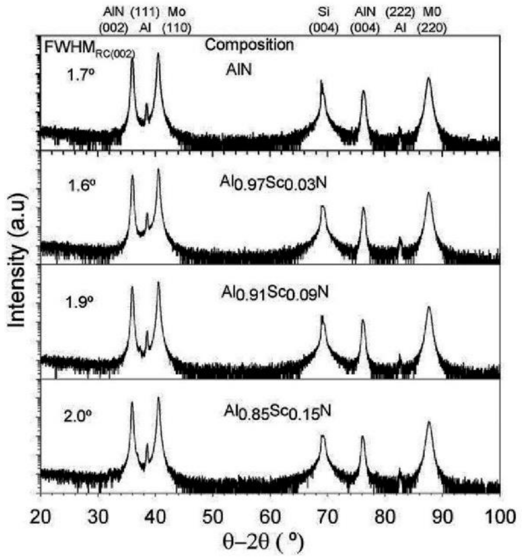

Fig. 1. X-ray diffraction θ–2θ scans of four wafers with different composition of the piezoelectric layer.

electrode to the FBAR structures. Deposition of 1.2 μm thick $Al_{(1-x)}Sc_xN$ films was performed in a dual magnetron, high vacuum system ($<2 \times 10^{-8}$ Torr) at 400 °C. Two metallic targets (Al 99.99%, Ø 100 mm and Sc 99.9%, Ø 100 mm) were reactively co-sputtered using pulsed DC mode in an argon (Ar 30 sccm) and nitrogen (N_2 30 sccm) gas mixture at a constant pressure of 2.8 mTorr. The Al and Sc atomic concentrations of the resulting film were controlled by adjusting the discharge power on the respective target.

Contact via holes through the $Al_{(1-x)}Sc_xN$ films down to the bottom Mo electrode were opened through wet etching using a 500 nm thick sputtered silicon dioxide (SiO_2) as a hard mask. Aluminum contact pads (~1 μm thick) were then sputter deposited and patterned. The remaining SiO_2 was then removed and subsequently the Al top electrode (230 nm thick) was then formed to complete the FBAR with active area of 0.09 mm^2. Finally, the resonator membrane was released through anisotropic backside dry etch of the substrate. Note that the introduced thin AlN seed layer improves the texture of the Mo electrode in view of the subsequent growth of the $Al_{(1-x)}Sc_xN$ film [7].

Four wafers were prepared with various Al/Sc target power ratio, hence FBARs with four different $Al_{(1-x)}Sc_xN$ film compositions were studied, namely $x = 0$; 0.03; 0.09 and 0.15 as determined by X-ray Photoelectron Spectroscopy (XPS) analysis. Crystallographic film properties were obtained from θ to 2θ scans and rocking curve measurements using a Philips MRD X-ray diffractometer. All films exhibited a c-axis oriented wurtzite structure as indicated by the strong {001} diffraction peaks in the θ–2θ scans, see Fig. 1.

The full with at half maximum value of the (002) rocking curve was in the range of 1.6° up to around 2°. Additional diffraction peaks are identified as the Al{111}, Mo{110} as well as the Si(100) substrate.

3. FBAR characterization

The electro-acoustic characterization of the fabricated FBARs was carried out with a pico-probe supported network-vector analyzer. One port reflection (S11) measurement data were acquired at frequencies around the fundamental longitudinal resonance. Fig. 2(a) shows the measured FBAR impedance for various compositions of the piezoelectric film. Further, the measurement data was fitted to the modified Butterworth Van-Dyke (MBVD) equivalent six parameters electrical circuit [8] (see Fig. 3). This implementation optimizes all six MBVD circuit component values in a least mean squares procedure, to best fit the measured data as shown in Fig. 2(b).

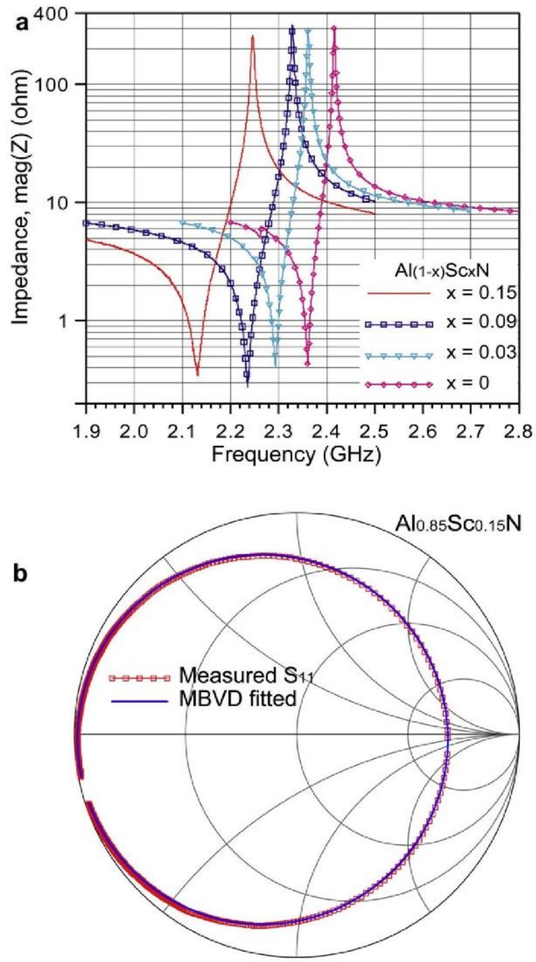

Fig. 2. Measured FBAR close in resonance response (a) Impedance for different compositions of $Al_{(1-x)}Sc_xN$. (b) S11 reflection coefficient of an $Al_{0.85}$ $Sc_{0.15}N$ based FBAR and MBVD fit to the measured data.

The MBVD fit results in a series parasitic resistance (Rs) of around 0.3 Ohms and close to 0 Ohm shunting resistance (R0) for all measured resonators. To further assess the $Al_{(1-x)}Sc_xN$ properties we have used the equivalence between the BVD model and one-dimensional resonator analysis [9] in order to account for the perturbations caused by both the electrodes and the seed layer and thus to extract important intrinsic material parameters. More specifically, the series resonance frequency f_S and the effective

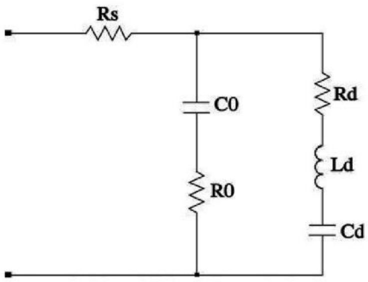

Fig. 3. Modified Butterworth Van-Dyke (MBVD) equivalent circuit.

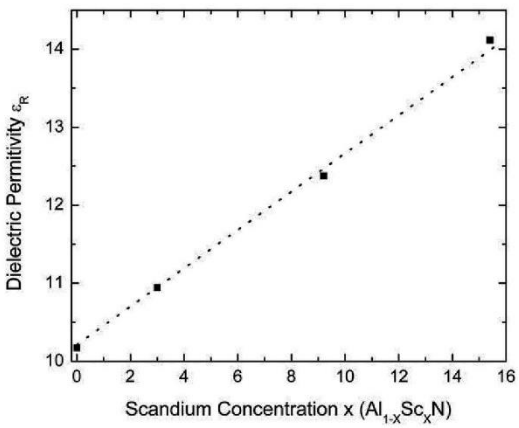

Fig. 4. $Al_{(1-x)}Sc_xN$ dielectric permittivity as a function of the relative Sc concentration.

electromechanical coupling $k^2_{eff} \approx \pi^2(f_P^2 - f_S^2)/(8f_S^2)$, where f_P is the parallel resonance frequency, both as determined from the one-dimensional Nowotny–Benes (NB) model [10] are fitted to their corresponding values, obtained from the MBVD extraction. In this fitting procedure the unknown parameters (C_{33} and e_{33}) are varied to best fit the above two parameters. All other parameters are initially determined as follows. The bulk material constants for the electrodes and the seed AlN layer have been used in this procedure. The layer thicknesses, reported in Section 2, have been measured in advance by scanning electron microscopy. The relative dielectric permittivity ε_r of the $Al_{(1-x)}Sc_xN$ is separately extracted from the static FBAR capacitance C0 (see Fig. 4), applying the formula $C' = A\varepsilon_0\varepsilon_R/t$. Here C' represents the static capacitance defined by the active FBAR area (A) only and 't' is the $Al_{(1-x)}Sc_xN$ film thickness. The parasitic contribution formed by the contact pads (including the underling SiO_2 500 nm layer) is accounted for by taking into account the actual FBAR topology. The obtained in Fig. 4 linear

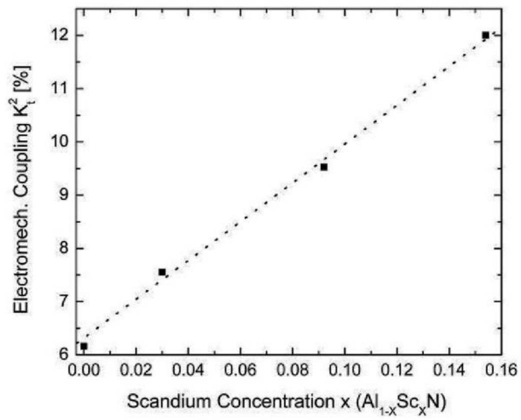

Fig. 5. $Al_{(1-x)}Sc_xN$ electromechanical coupling as a function of the relative Sc concentration.

dependence of the dielectric permittivity as function of the Sc concentration is in a good agreement with previously reported measurements [11] although the obtained values here are somewhat larger. Further, the mass density of the $Al_{(1-x)}Sc_xN$ films is accounted as a slowly varying linear function of the Sc concentration, in accordance with the experimental results for the $Al_{(1-x)}Sc_xN$ lattice parameters [12]. In particular the mass density is calculated using the atomic masses of Al, Sc and N along with the volume of the $Al_{(1-x)}Sc_xN$ unit cell. Accordingly, the mass density increase does not exceed 2% for relative Sc concentrations 'x' varying in the range 0–20%.

Table 1 summarizes the most relevant measured and extracted parameters as a function of the Sc concentration. Here $f_{s,m}$ is the measured series resonance frequency of the FBAR, $Q_{P,m}$ is the measured FBAR Q-factor at parallel resonance, $f_{P,m}$, $Q_{B,m} = \omega\tau_{GR}|S11|/(1-|S11|^2)|_{MAX}$ (here the group delay $\tau_{GR} = -\partial\varphi_{S11}/\partial\omega$ is determined as the derivative of phase φ_{S11} of the S11 coefficient with respect to the angular frequency $\omega = 2\pi f$, while $|S11|$ is the magnitude of the reflection coefficient S11) is the measured device unloaded Q-factor [13] and $k^2_{eff,m}$ is the measured device electromechanical coupling. C_{33} and e_{33} are the $Al_{(1-x)}Sc_xN$ stiffness and piezoelectric constants, respectively, extracted through the NB model [10]. Evidently, the increase of electromechanical coupling is accompanied by a decrease of the Q-factor, which is not unexpected since generally stronger piezoelectrics tend to be softer materials. Calculating the device figure of merit, FOM $= k^2_{eff,m} \times Q_{B,m}$, for the various $Al_{(1-x)}Sc_xN$ compositions we found that the maximum FOM of 65 is achieved at 0.09 Sc concentration.

Finally the intrinsic electromechanical coupling $k_t^2 = K^2/(1+K^2)$, where $K^2 = e_{33}^2/\varepsilon_R\varepsilon_0C_{33}$, is presented in the Table 1. The electromechanical couplings (both measured and extracted) have shown a linear two fold increase (see also Fig. 5) for Sc concentrations varying in the

Table 1
Measured ($f_{s,m}$, $Q_{p,m}$, $Q_{B,m}$, $k^2_{eff,m}$, $k^2_{eff,m} \times Q_{B,m}$) FBAR quantities and extracted (ε_r, C_{33}, e_{33}, k_t^2) film parameters.

Composition	$f_{s,m}$(GHz)	$Q_{p,m}$	$Q_{B,m}$	$k^2_{eff,m}$ (%)	$k^2_{eff,m} \times Q_{B,m}$	ε_r	C_{33} (GPa)	e_{33} (C/m^2)	k_t^2 (%)
AlN	2.3605	739	790	5.50	40	10.1	370	1.48	6.16
$Al_{0.97}Sc_{0.03}N$	2.2935	601	730	6.89	50	10.9	346	1.66	7.55
$Al_{0.91}Sc_{0.09}N$	2.2339	513	690	9.50	65	12.4	326	1.94	9.53
$Al_{0.85}Sc_{0.15}N$	2.1522	348	410	12.07	60	14.1	270	2.14	12.00

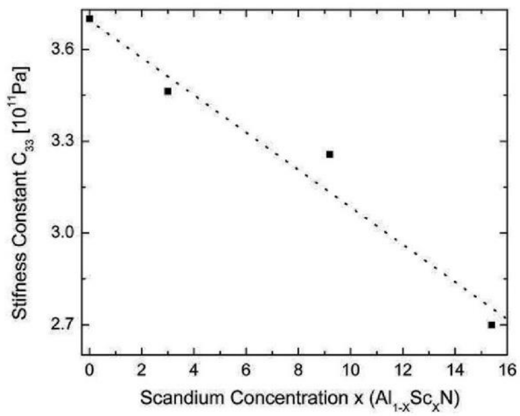

Fig. 6. $Al_{(1-x)}Sc_xN$ elastic stiffness C_{33} as a function of the relative Sc concentration.

range 0–0.15. The observed decrease in the extracted stiffness constant (see also Fig. 6) with the Sc concentration is in a very good agreement with the theoretical predictions [5]. This result further confirms the above findings that the decrease of resonance frequency with the Sc concentration is predominantly due to material softening.

4. Conclusions

FBARs employing highly c-textured $Al_{(1-x)}Sc_xN$ thin films have demonstrated improved RF performance. Further, the ability to tune the electromechanical coupling (and thus the filter bandwidth) by varying the Sc concentration underlines the potential of this technology for telecom applications. In view of filter applications, special care for preserving the device figure of merit (FOM) is needed, due to Q-factor degradation with Sc concentration. It is noted that the Q values reported here are by far not optimal as judged from the comparison between the Q values obtained for pure AlN in this work and those of the state of the art [13]. The reason for this difference is due to the use of a general purpose deposition system and not a fully optimized and dedicated equipment. This by the same token indicates that the actual Q values of $Al_{(1-x)}Sc_xN$ films are very likely to be higher than reported here. Finally, the above results suggest the existence of an optimal Sc concentration for which a larger coupling and an improved FOM are simultaneously attained.

Acknowledgments

The work has been financially supported by the Foundation for Strategic research (SSF) through the MS2E Center as well as by the Swedish Research Council (VR) and WISENET (Vinnova).

References

[1] Naik RS, Lutsky JJ, Reif R, Sodini CG, Becker A, Fetter L, et al. IEEE Trans Ultrason Ferroelectr Freq Control 2000;47:292–6.
[2] Clement M, Iborra E, Olivares J, Rimmer N, Giraud S, Bila S, et al. IEEE Trans Ultrason Ferroelectr Freq Control 2010;57:518–23.
[3] Akiyama M, Kamohara T, Kano K, Teshigahara A, Takeuchi Y, Kawahara N. Adv Mater 2009;21:593–6.
[4] Akiyama M, Tabaru T, Nishikubo K, Teshigahara A, Lano K. J Ceram Soc Jpn 2010;118:1166–9.
[5] Tasnadi F, Alling B, Höglund C, Wingqvist G, Birch J, Hultman L, Abrikosov I. Phys Rev Lett 2010;104:137601–3.
[6] Yanagitani T, Arakawa K, Kano K, Teshigara A, Akiyama M. In: IEEE Int'l. Ultrasonics, Symp; 2010. Abstract Book, P5-A1-4.
[7] Kamohara T, Akiyama M, Ueno N, Kuwano N. Ceram Int 2008;34:985–9.
[8] Larson III JD, Bradley PD, Wartenberg S, Ruby RC. In: IEEE Int'l. Ultrasonics, Symp; 2000. p. 863–8.
[9] Rosenbaum JF. Bulk acoustic wave theory and devices. Artech House; 1988.
[10] Nowotny H, Benes E. J Acoust Soc Am 1987;82:513–21.
[11] Wingqvist G, Tasna'di F, Zukauskaite A, Birch J, Arwin H, Hultman L. Appl Phys Lett 2010;97:112902–4.
[12] Hoglund C, Birch J, Alling B, Bareno J, Czigany Z, Persson P, et al. J Appl Phys 2010;107:123515–7.
[13] Ruby R, Parker R, Feld D. In: IEEE Int'l. Ultrasonics, Symp; 2008. p. 1815–8.

APPENDIX H – PAPER V

"Synthesis of c-tilted AlN films with a good tilt and thickness uniformity,"

M. Moreira, J. Bjurström, T. Kubart, B. Kuzavas, and I. Katardjiev,

IEEE International Ultrasonics Symposium Proceedings, 2011, pp. 1238-1241.

10.1109/ULTSYM.2011.0305

Synthesis of c-tilted AlN films with a good tilt and thickness uniformity

Milena Moreria, Johan Bjurström, Tomas Kubart, Björn Kuzavas and Ilia Katardjiev
Department of Engineering Sciences,
Uppsala University
Box 534, Uppsala, Sweden
Ilia.Katardjiev@angstrom.uu.se

***Abstract*—This communication describes a method for the deposition of thin piezoelectric AlN films with an inclined c-axis relative to the surface normal. Further, the tilt over the wafer is sufficiently uniform and exhibits a planar symmetry as well as good thickness uniformity. Careful control of both the nucleation and growth stages is needed to obtain tilted films with excellent quality. Thus in the nucleation state, it is argued that two independent mechanisms, namely seed layer texture and/or surface roughness, are mainly responsible for the subsequent titled growth. To achieve the latter, however, a certain directionality of the deposition flux is also necessary. The directionality of the deposition flux is achieved through the use of an array of linear magnetrons tilted under a certain angle with respect to the substrate normal.**

Keywords - AlN; c-axis tilt; piezoelectric; shear waves;

I. INTRODUCTION

Thin piezoelectric films with a wurtzite crystallographic structure such as AlN and ZnO exhibiting a nonzero tilt of the c-axis have been extensively studied in view of biosensor applications – see for instance references 1 and 2 and the references therein. More specifically, such films are employed for the fabrication of thin film bulk acoustic resonators (FBAR) operating in the shear thickness mode. This mode does not propagate in liquids and hence such resonators retain their high Q value when operated in liquids and hence are used as highly mass sensitive devices (transducers) in biosensors. Deposition of such films, however, is not straightforward and existing methods suffer from various drawbacks. Thus, the method employed in reference 1 results in films with a cylindrical symmetry on the wafer in addition to having a certain tilt non-uniformity. The method employed in reference 2 suffers from very low deposition rates. The method suggested inhere attempts to alleviate both these shortcomings.

II. DESCRIPTION OF THE METHOD

As indicated above, it is essential that one has good control over both the nucleation and the growth stages.

A. Nucleation stage

As first described by Katardjiev et al[3] tilted growth can be achieved if one or more of the following conditions are met during the nucleation stage:

a) the crystallographic texture of the substrate is not suitable for c-textured growth (i.e. does not possess hexagonal symmetry, etc).

b) the roughness of the substrate surface is sufficiently large, say, larger than 1 nm.

c) an AlN (or similar) seed layer which is not c-textured is grown on the substrate. This can be conveniently achieved by growing a 100nm thick AlN seed layer at relatively high pressures and/or relatively low substrate temperatures (diffusion limited growth), resulting in a film with mixed textures (more specifically (103), (002), etc).

Under one or more of the above conditions and in the presence of deposition flux directionality the same authors demonstrate growth of c-tilted AlN films as illustrated in Figure 1a,b.

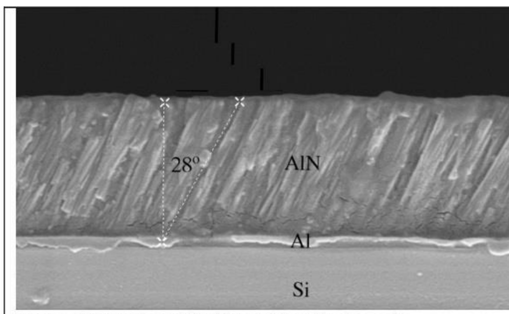

Fig 1a. SEM of an AlN film with a tilted c-axis

It is further noted that roughness of the substrate surface can readily be achieved by, say, varying the deposition parameters of the substrate film (pressure, temperature, etc). The tilt of the c-axis is confirmed by the (002) XRD pole figure shown in Figure 1b.

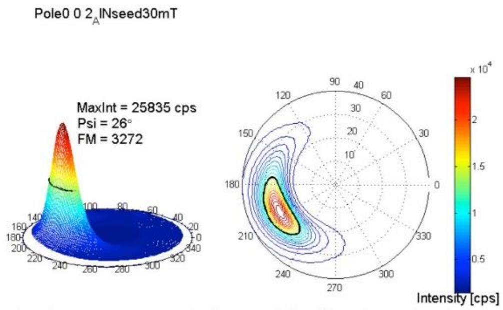

Fig 1b. (002) XRD pole figure of the film shown in Fig. 1a.

It is seen from Fig. 1b that the mean tilt angle is about 26 degrees and that the tilt has a relatively broad, kidney shaped distribution caused by the circular shape of the race track.

B. Directionality of the deposition flux

In the original method above[3] directionality of the flux is achieved by operating the process at sufficiently low pressures such that the mean free path of the sputtered particles is smaller than or comparable to the target-to-substrate distance. Under these conditions it is readily shown that the net deposition flux at any given point on the wafer (apart from the very center) has a non-zero angle of incidence as illustrated in Fig. 2.

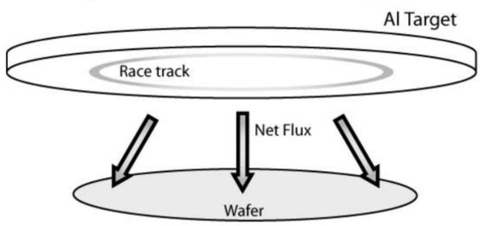

Owing to the circular symmetry of standard magnetrons this resulted in films having a cylindrical symmetry of the tilt. A small exclusion zone in the center of the wafer exhibited a biaxial tilt. To alleviate this problem a new target design is proposed in this communication as shown in Figure 3a.

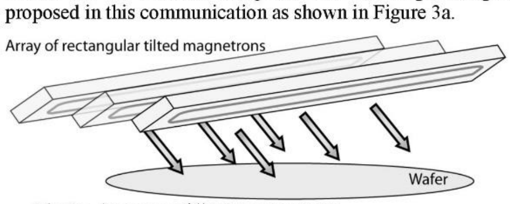

Fig 3a. An array of linear magnetrons

As seen, the array of linear magnetrons is designed in such a way as to provide to a first approximation a unidirectional flux at the substrate (owing to the fact that normally the sputtered flux exhibits a cosine angular distribution, i.e. the majority of the sputtered flux is along the normal to the target surface). The tilt of the magnetron segments relative to the normal of the substrate surface (typically 30 degrees, although it can be varied according to the specific situation) then defines the incidence angle of the deposition flux.

The resulting film, as expected, exhibits a tilted c-axis as confirmed by the (002) pole figure shown in Fig. 3b.

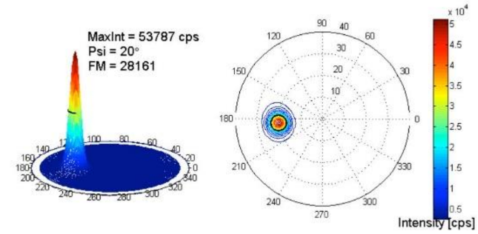

Fig. 3b. (002) XRD pole figure of a film grown using the magnetron shown in Fig. 3a.

Clearly the film in Fig. 3b has a much narrower distribution of the tilt angle as evidenced from the figure of merit FM defined as the maximum intensity divided by the peak area at half maximum. This distribution can further be improved by using flux collimators which improve the directionality of the flux. Thickness uniformity is achieved by a translational motion of the substrate along the horizontal projection of the flux direction.

III. Discussion

We now discuss in greater detail the nucleation stage of the process and illustrate the various mechanisms leading to tilted growth. They all boil down to one common goal, namely, to suppress nucleation of (002) nuclei. As already indicated this is achieved by either growing a special non c-textured seed layer, and/or introduce surface roughness, and/or use substrate crystallography which is not suitable for (002) nucleation, and/or anything to that effect.

A. Synthesis of the seed layer and its inlfuence on the film growth

Typically, a seed layer is made again of AlN and grown in situ prior to film growth. Best results are obtained if the seed layer has a preferred non c-texture. Thus for instance, dominant (103) texture is obtained under diffusion limited nucleation conditions. The latter mean low mobility of the condensing species which is achieved at relatively high process pressures (20 mTor or higher) resulting in complete thermalization of the sputtered flux. The latter thus arrives at the substrate in a diffusion like manner. More important is the fact that the kinetic energy of the condensing species is negligibly small resulting in limited surface diffusion upon condensation. Diffusion limited nucleation also implies low substrate temperatures (typically room temperature). It is noted that the c-axis of a (103) grain concludes and angle of 28 degrees with the surface normal. The in-plane orientation of the same c-axis in the seed layer, however, is uniform due to the lack of any anisotropy (both in terms of substrate properties as well as deposition flux directionality). This in-plane isotropy of the projection of the c-axis implies that at any given small area on the substrate there always exist (103) grains whose c-axis has a projection along an arbitrarily predefined in-plane direction. In simple words this means that at any given point on the substrate there always exist (103) grains whose c-planes face the incident deposition flux. Consequently, it is these grains that grow fastest along the c-direction resulting in a tilted films with a mean tilt around 28 degrees, i.e. the inclination of the c-axis in a (103) grain as illustrated in Figure 4.

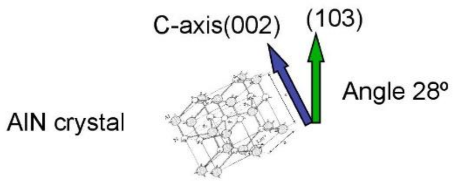

Figure 4. Illustration of the c-axis in a (103) grain

This hypothesis is confirmed by Fig. 5 which represents a series of psi-diffractograms taken at equidistant points along the radius of a 4''wafer.

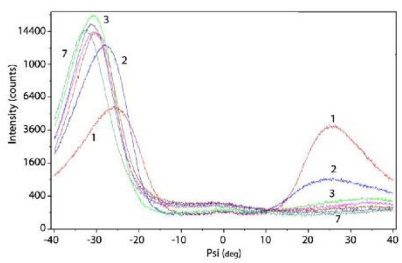

Figure 5. XRD psi-difractograms taken at equidistant ponts along the radius the wafer

It is seen from Fig. 5 that right at the center of the wafer (curve 1) the film exhibits a biaxial tilt distribution, i.e. two opposite in sign tilts. The r.h.s peak of this distribution, however, diminishes quickly as the measurement point moves along the radius of the wafer. It is noted that the mean tilt angle varies in the range 26 to 32 degrees. This observation, together with the fact that the mean angle of incidence of the deposition flux varies significantly along the wafer radius, supports the above hypothesis that the film grows preferentially along the c-axis of the (103) grains resulting in an average tilt angle of around 28 degrees.

B. Surface roughness and its influence on the growing film

It is noted that the process in the growth stage is typically a diffusion enhanced growth process since the transport of the sputtered species is practically collisionless due to the requirement for directionality. Hence, they arrive at the surface with their original kinetic energy whose mean value is roughly half the surface sublimation energy of Al, i.e. 1.68 eV. Hence, the majority of the sputtered species arrive at the surface with a mean kinetic energy equivalent to around 18000^{o}C. This means that in the absence of a seed layer the growth process typically yields highly c-textured films, since nucleation under such conditions is always along the surface normal. If the substrate surface, however, has some non-negligible surface roughness then the growth will favor those grains whose c-axis concludes the smallest angle with the incidence flux. This results in a preferential tilt of the film which is preferentially oriented along the flux direction. Noteworthy, the magnitude of the tilt angle is directly related to the surface roughness. In other words, the larger the surface undulations the larger the chance of finding local surface orientations with normals concluding minimal angles with the flux direction. In this way, surface roughness primarily determines (limits) surface tilt. Thus, relatively smooth surfaces should result in relatively small tilts and conversely relatively rough surfaces should result in tilts closer to the incidence flux direction. This hypothesis is confirmed by the observations of Figure 6a,b,c,d which represents (002) XRD pole figure plots of tilted AlN films grown on various polycrystalline films with different surface roughnesses at otherwise identical deposition conditions as well as grown in one and the same run. The roughness of the initial films, namely natively oxidized Si, Ni, Cr and Mo increases steadily. More specifically, the rms values are 0.4, 1.2, 1,8 and 2.5 nm respectively. In all cases we observe c-textured growth (defined as c-textured growth normal to the substrate surface). With increasing surface roughness, however, this c-textured growth is increasingly aligned with the incidence flux since the growth along this direction is the fastest due to geometrical considerations.

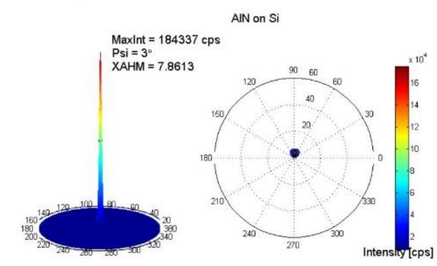

Figure 6a. (002) pole plot of AlN grown on (100) Si

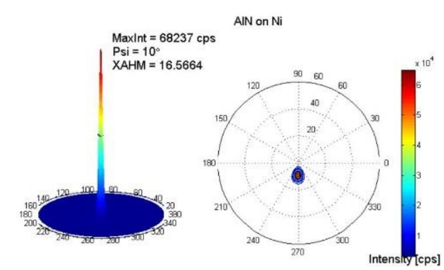

Figure 6b. . (002) pole plot of AlN grown on (111) Ni

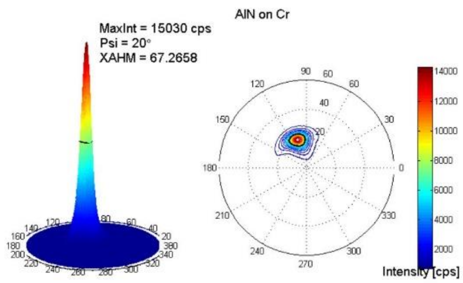

Figure 6b. (002) pole plot of AlN grown on (100) Cr

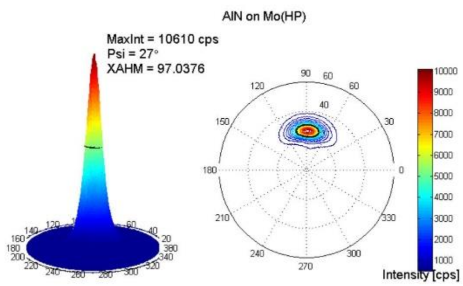

Figure 6b. (002) pole plot of AlN grown on (110) Mo

Clearly, by just varying the surface roughness of the substrates we have been able to obtain films with 0°, 10°, 20° and 27° tilt of the c-axis respectively.

So far we have been able to present experimental evidence in support of the hypothesis that films with a tilted c-axis can be grown on substrates with a sufficient roughness or on films with a suitable non c-texture. In both cases, the properties of the substrate along with the deposition flux direction determine the resulting tilt angle. As a final proof of this statement one can imagine a substrate with a relatively small surface roughness but having at the same time a scattered population of (103) nuclei. From the above observations it is expected that the relatively low surface roughness to yield a relatively low tilt angle, while the (103) nuclei population is expected to result in a tilt around 28°. Indeed, this thought experiment is confirmed by Figure 7 which shows the (002) pole figure of a film grown exactly on such a substrate surface. The resulting low and high tilt angle populations are clearly observed.

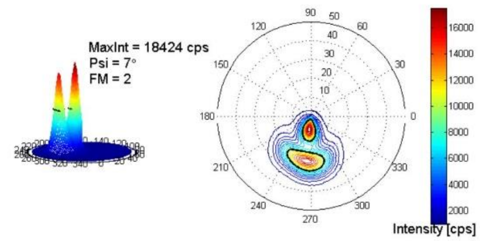

Figure 7. (002) pole figure of a film grown on a surface with a small roughness and some (103) texture.

In this way, we have been able to demonstrate that tilted AlN films can be grown on substrates with a relatively high roughness and/or substrates with a dominant crystallographic texture other than c-texture. The second necessary condition is the existence of directionality in the deposition flux.

The last thing remaining to demonstrate is the possibility of growing films with a sufficient tilt and thickness uniformity. In view of the above observations such a demonstration is straightforward. Thus, the combination of a suitable AlN seed layer (as described above) and the flux directionality of the array of linear magnetrons shown in Figure 3a results in a c-tilted AlN film with a relatively good tilt uniformity as seen from Figure 8 which represents graphically the tilt direction and angle over a 4" wafer.

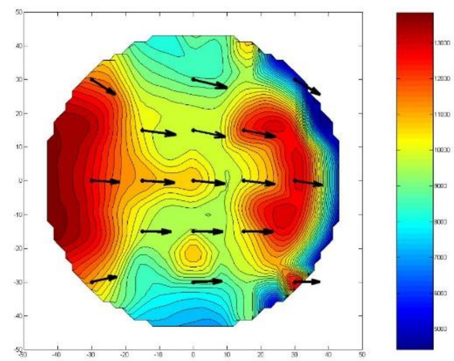

Figure 8. Tilt direction and angle (arrow length) distribution over a 4" wafer.

Finally, the above findings are expected to hold for other wurtzite thin films, including ZnO

References

[1] Bjurstrom J, Wingqvist G, Yantchev V, Katardjiev I. Temperature compensation of liquid FBAR sensors. Journal of Micromechanics and Microengineering 2007;17:651

[2] Schreiter M, Link M, Weber J. Application potential of integrated thin film resonators in liquid and gaseous media. Tm-Technisches Messen 2008;75:120

[3] Katardjiev I, Bjurstrom J, Wingqvist G. Synthesis of thin piezoelectric films with a tilted c-axis. Swedish patent application, 0500647-3, 2005; PCT/SE2006/050041, 2006

APPENDIX I – PAPER VI

"Electrical characterization and morphological properties of AlN films prepared by dc reactive magnetron sputtering,"

M. A. Moreira, I. Doi, J. F. Souza, and J. A. Diniz,

Microelectronic Engineering, vol. 88, pp. 802-806, 2011.

Microelectronic Engineering 88 (2011) 802–806

Contents lists available at ScienceDirect

Microelectronic Engineering

journal homepage: www.elsevier.com/locate/mee

Accelerated Publication

Electrical characterization and morphological properties of AlN films prepared by dc reactive magnetron sputtering

M.A. Moreira, I. Doi *, J.F. Souza, J.A. Diniz

School of Electrical and Computer Engineering, University of Campinas, Av. Albert Einstein 400, 13.083-852 Campinas, SP, Brazil
Center for Semiconductor Components, University of Campinas, P.O. Box 6061, 13.083-870 Campinas, SP, Brazil

ARTICLE INFO

Article history:
Available online 25 June 2010

Keywords:
Aluminum nitride thin films
Reactive DC sputtering
Surface morphology
Electrical properties
MIS devices

ABSTRACT

Aluminum nitride (AlN) films were deposited by dc reactive magnetron sputtering on p-Si-(1 0 0) substrate in Ar–N_2 gas mixtures. The effects of nitrogen concentration and sputtering power on AlN films deposition rate, crystallographic orientation, refractive index, and surface morphology are investigated by means of several characterization techniques. The results show that AlN films reasonably textured in (0 0 2) orientation with low surface roughness can be obtained with the deposition rate as high as 70 nm/min by the control of either target power or N_2 concentration in the gas mixture. Increasing the dc discharge power, Al atoms are not completely nitridized and the Al phases appear, as well as the AlN phases. MIS (Metal–Insulator–Semiconductor) structures were fabricated and electrically evaluated by *I–V* (current–voltage) and *C–V* (capacitance–voltage) measurements at high frequency (1 MHz). The results obtained from *C–V* curves indicate that charges at the dielectric/semiconductor interface occur, and the dielectric constant values (extracted under strong accumulation region) are compatible with those found in literature.

1. Introduction

Recently, aluminum nitride (AlN) thin films have presented an increased interest because of its superior physical properties such as good thermal stability, high ultrasonic velocity, large thermal conductivity, high electrical resistivity, good piezoelectric response, low deposition temperature and low toxicity. Due to its excellent properties AlN is suitable for a wide variety of applications [1–4]. In addition to the communication market, nowadays AlN has been used for sensing and actuation purposes. Specifically in the microelectronic field, AlN films can be easily integrated with silicon technology and monolithic systems. Moreover, due to the excellent acoustic properties, AlN is a well-established piezoelectric material for the fabrication of electro-acoustic devices [5,6], e.g., SAW (surface acoustic wave) devices widely used as resonators and band-pass filters in communication systems.

The aluminum nitride films have been prepared by several different methods, including chemical vapor deposition (CVD) and molecular beam epitaxy (MBE). However, these methods are expensive and the required high temperatures to reach satisfying properties are often incompatible with microelectronic processes. Among other techniques, the reactive magnetron sputtering process (RMS) is an attractive deposition technique because it presents advantages of being low temperature and low cost methods, and it allows fine tuning of the material characteristics [1,4,7–9].

The properties of AlN piezoelectric films, however, are strongly influenced by the sputtering systems, deposition conditions, and by the substrate materials. The use of silicon as the substrate is highly attractive for device applications due to the potential integration with well-developed silicon technologies. However, it makes the growth of high quality material very difficult due to the large differences in the lattice constants of AlN and Si. The physical properties of the sputtered AlN films depend on deposition parameters and conditions since they determine the way in which the Al and N atoms are arranged on the substrate, therefore the microstructure of the grown material. Although investigated by several researchers, almost all the reports show difficulties to determine a consistent and general relationship between deposition parameters and the final quality of the material. Moreover, contaminants such as oxygen and hydrogen may be present in the sputtering chamber and affect the morphology of the AlN films [8,10]. Thus, the structural and morphological properties are the main guide to determine the different types of devices to which the AlN films can be applied [9]. For applications in surface acoustic wave devices, for example, in addition to the surface smoothness, it is essential to achieve a high degree of *c*-axis orientation of the AlN films since the piezoelectric properties are strongly dependent on the crystallographic orientation of the film [11].

* Corresponding author. Tel.: +55 19 35215215; fax: +55 19 35217888.
E-mail address: doi@ccs.unicamp.br (I. Doi).

0167-9317/$ - see front matter © 2010 Elsevier B.V. All rights reserved.
doi:10.1016/j.mee.2010.06.045

The study of deposition conditions and its influence in the development of AlN films with high piezoelectric coefficient is very important and it is not yet fully exploited.

This work presents the results of AlN sputtered films fabricated with different deposition conditions and the analysis of its physical characterization. In terms of deposition conditions of the dc reactive magnetron sputtering, the changed parameters are dc discharge power and N_2 flow rate with fixed Ar flow rate of 80 sccm. Furthermore, MIS structures were fabricated and electrical properties such as dielectric constant and flat band voltage were investigated.

2. Experimental

AlN films were obtained by dc reactive magnetron sputtering (ULVAC MCH 9000) of an Al – 1% Si (99.99% purity) target in a high purity N_2/Ar (5 N Ar and 6 N N_2) gas mixture atmosphere. The distance target-to-substrate is about 150 mm and target diameter 250 mm. The sputtering chamber was pumped down to a base pressure below 2×10^{-6} Pa with a cryopump, and then the sputtering discharge gases N_2 and Ar were admitted into the chamber separately and regulated by a mass flow controller. The discharge mode was the power-constant mode and the target power was fixed either at 500 W or 1000 W, and the N_2 to Ar flow rate ratio R ($R = N_2/(Ar + N_2)$) was varied from 0.11–0.55, with a constant Ar flow rate of 80 sccm. The deposition pressure varied in the range of $3–4 \times 10^{-3}$ Pa. The target was sputter-conditioned for 10 min in Ar plasma prior to each run in order to remove any residual contamination on the target surface.

The AlN films used in these studies were deposited on p-type 3" Si (1 0 0) substrates with 1–10 Ω cm resistivity, cleaned in dilute HF solution to remove its native oxide right before deposition. All samples were deposited at room temperature without heating of the substrates, so their temperature depends only on the spontaneous heating by the dc plasma and radiation from the target. The substrate temperature measured using a thermocouple indicated values below 50 °C during the sputtering process.

The prepared samples were physically characterized using a variety of techniques. The surface roughness, crystallographic orientation, thickness, absorbance, and refractive index were determined using atomic force microscopy (AFM), X-ray diffraction spectroscopy (XRD), surface profiler, Fourier infrared spectroscopy (FTIR) and ellipsometer, respectively. The four-point probe method was used to characterize the resistivity of the samples.

Four sets of MIS structures were also fabricated on Si wafers with AlN and SiO_2/AlN as the insulating layers, and a 300 nm thick sputter deposited Al film as the top and backside electrodes. The structures have 200 μm diameter and were patterned using a standard lithographic process. The Al/AlN layers were etched in a H_3PO_4 solution at 75 °C.

The fabricated MIS structures were electrically characterized in terms of dielectric constant, hysteresis, equivalent oxide thickness (EOT) and flat band voltage. Current–voltage (*I–V*) measurements were carried out in a parameter analyzer, and capacitance–voltage (*C–V*) measurements in a *C–V* meter at 1 MHz. Some of the MIS capacitors were also submitted to a heat treatment in a H_2 environment at 430 °C, for 5 min, 10 min and 20 min, in order to improve the electrical properties.

3. Results and discussion

The deposition rate behavior of AlN films as a function of the used N_2 concentrations is shown in Fig. 1. The deposition rate was determined from the thickness of the prepared samples, divided by the sputter deposition time. The thickness of the samples

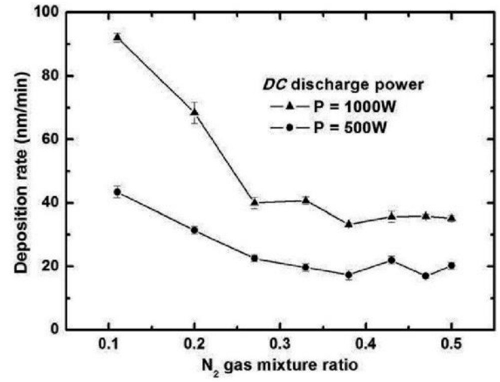

Fig. 1. Deposition rate of AlN films fabricated with different nitrogen concentrations and sputtering power of 500 W and 1000 W.

varied in the range of 218–85 nm, and 461–165 nm, as the N_2 concentration was increased, at sputtering power of 500 W and 1000 W, respectively. Increasing the sputtering discharge power also increases the sputtering efficiency, and this allows to achieve higher deposition rates, such as 68.4 nm/min at 1000 W, more than twice the rate at 500 W of 31.3 nm/min, at the same N_2 concentration ($R = 0.2$). At constant power, higher values of deposition rate are obtained with the decreasing of N_2 concentration R in the gas mixture. This behavior agrees with the results reported by many authors [1] and it occurs due to the higher mass of Ar, where the sputtering yield of Ar^+ ions is higher than N^+ and N_2^+ ions [9].

The crystalline structure and the preferred orientation of AlN films were characterized by X-ray diffraction (XRD) performed in $\theta - 2\theta$ scanning mode. The preferential orientation is a result of the competitive growth on (1 0 0) and (0 0 1) planes [9]. When the growth on (0 0 1) plane prevails the film is (0 0 2) oriented, whereas when the growth on (1 0 0) plane predominates, other preferred orientations may arise [9]. The deposition parameters of sputtered AlN films affect directly the crystallographic orientation of the film. The main parameters that determine the preferred orientation are: (i) the nitrogen concentration in the gas mixture; (ii) the distance from the substrate to the target; (iii) the energy and concentration of the sputtering ions [1,9]. Fig. 2 shows the *XRD* patterns of AlN samples prepared on Si substrates at target powers of 500 W and 1000 W, and different gas mixture ratios. The measured XRD patterns show prominent diffraction peaks at 35.9° and 37.8° corresponding to the (0 0 2) and (1 0 1) crystal planes of the hexagonal wurtzite phase of AlN, respectively. All the analyzed AlN samples showed both of these peaks either at powers of 500 W or at 1000 W, except the sample obtained at 1000 W with a N_2 gas mixture ratio of 0.27, where the peak corresponding to AlN (0 0 2) vanished completely. With regard to device applications it is desirable to develop AlN with a high degree of *c*-axis (0 0 2) orientation to obtain high values of electromechanical coupling factor k_t^2 [8]. When the power is increased not all sputtered material that reaches the substrate is AlN [10,11]. In addition, it is known that texturing in thin films is a function of their thickness. Thus, the decrease in preferred orientation as a consequence of the increase in sputtering power is not necessarily due to differences in energy delivered at the substrates but could also be due to differences in thin film thicknesses [1]. Despite good crystalline quality, some of the prepared AlN samples exhibited poor *c*-axis orientation, along with other crystal orientations that are not normal to the substrate plane. This characteristic is due to the non-

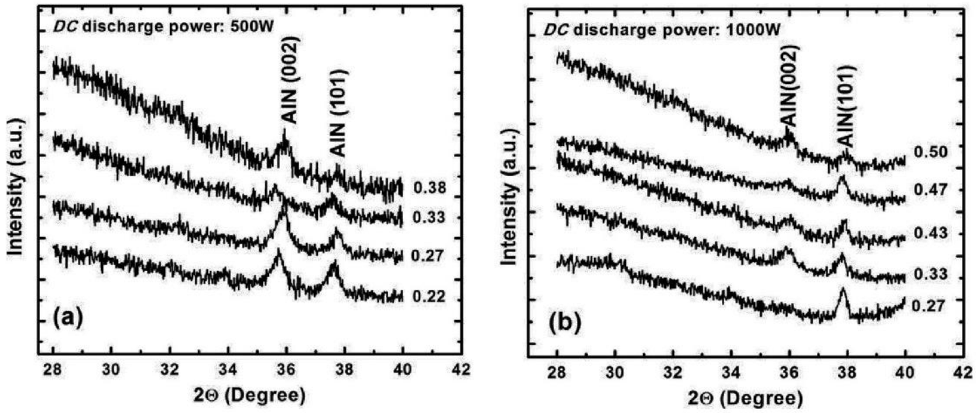

Fig. 2. X-ray diffraction patterns of AlN films deposited at different values of N_2 gas mixture ratios and discharge powers of (a) 500 W and (b) 1000 W.

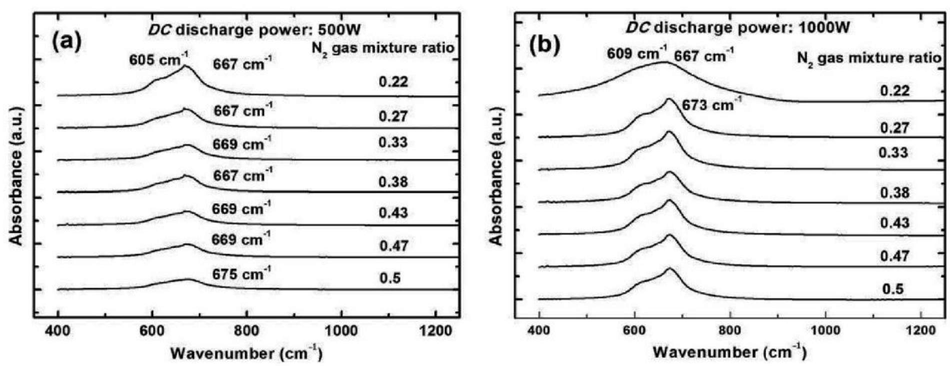

Fig. 3. FTIR spectra of the sputtered AlN films deposited at different N_2 gas mixture ratios and discharge powers of (a) 500 W and (b) 1000 W.

equilibrium conditions existing between the energy of the sputtered particles and the energy at the substrate surface. Further experiments addressed to optimize deposition parameters are being carried out, to improve the adatom mobility, therefore attempt to obtain AlN with a high degree of *c*-axis orientation.

The refractive index (η) of sputter-deposited AlN is dependent on the sputtering conditions since it is related to the composition and density of the films. For polycrystalline AlN films obtained by dc reactive sputtering, the refractive index varies from 1.9 to 2.1. Smaller values than this can be observed in the presence of impurities (such as oxygen) or nitrogen vacancies [3]. The refractive index of our dielectric AlN samples, determined from the measurements of the ellipsometric angles Δ and ψ, revealed that they are in the ranges of 2.0–2.2 and 2.1–2.7, for the AlN prepared with a sputtering power of 500 W and 1000 W, respectively. This wide range can be attributed to the variation in density and composition because of the differences in discharge power and N_2 concentration used in preparation of each sample.

The formation of aluminum nitride was also supported by FTIR spectrometry characterized in the range of 400–4000 cm^{-1}. The FTIR spectra of the sputtered AlN films exhibit characteristic modes at 611, 670, 890 and 912 cm^{-1}, corresponding to A1(TO), E1(TO), A1(LO) and E1(LO) vibration modes, respectively [12,13]. Fig. 3 shows the FTIR spectra of the films deposited at 500 W and 1000 W as discharge power and different nitrogen concentrations in the gas mixture. The spectra were obtained by subtraction of the Si substrate absorption. The displayed spectra exhibit a main band around 670 cm^{-1} and 673 cm^{-1}, and a side band around 605 cm^{-1} and 609 cm^{-1}, in samples obtained at a sputter power of 500 W and 1000 W, respectively. They correspond to the E1(TO) and A1(TO) modes of wurtzite AlN, respectively. The samples prepared at lower nitrogen ratios showed a more intense E1(TO) absorption peaks in relation to A1(TO), indicating a presence of more numbers of wurtzite modes at lower nitrogen ratio. The FTIR peaks may be shifted from their characteristic position due to the residual stress in the AlN film caused by the sputtering process [12], and the predominance of TO modes in the AlN films indicates existence of large nanocrystals in the structure [14].

The surface topography of the films was examined using AFM in semi-contact mode taken on 5×5 μm^2 surface areas at room temperature. Fig. 4 shows AFM images of the AlN samples deposited with a discharge power of 500 W and 1000 W, at N_2 gas ratio of 0.11 (images 4a and 4c) and of 0.47 (images 4b and 4d), respectively. The surface topography (morphology) of the studied films is influenced by both discharge power and N_2 gas ratio. The rounded grain shape changes from small to large with the increase

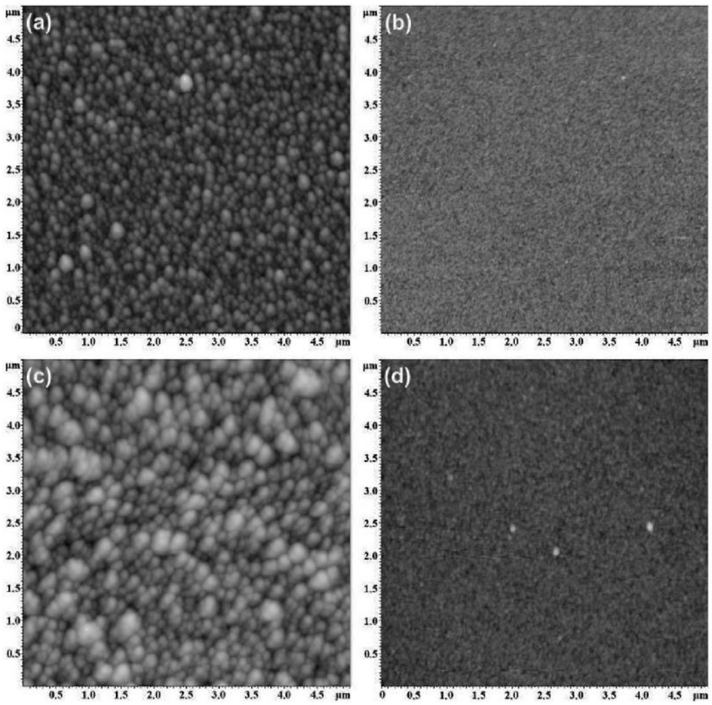

Fig. 4. AFM images of AlN films deposited at: (a) 500 W and 0.11 gas ratio, (b) 500 W and 0.47 gas ratio, (c) 1000 W and 0.11 gas ratio, and (d) 1000 W and 0.47 gas ratio.

in discharge power from 500 W to 1000 W, at the same N_2 gas ratio of 0.11. Increasing the N_2 gas ratio to 0.47 and the discharge power to 1000 W, the films form a texture-like structure. The grain size also increases with the increase in the discharge power. The estimated surface roughness (RMS) of the films was 7.88 and 20.60 nm at a N_2 gas ratio of 0.11, 500 W and 1000 W; and 0.73 and 0.91 nm at a N_2 gas ratio of 0.47, 500 W and 1000 W, respectively. Therefore, the results indicate a rougher surface with the increase of discharge power and a smoother surface with the increase of the N_2 gas ratio. The rough surface formed at low nitrogen concentrations is due to the reduced number of collisions of the sputtered atoms [10,15]. As mentioned above, very smooth AlN films were obtained at a discharge power of 500 W and N_2 gas ratio of 0.47. Low values of roughness are associated with low acoustic loss in AlN films, which is interesting for applications in electro-acoustic devices, such as SAW.

The electrical resistivity of the samples was obtained from the sheet resistances measured by a four-point probe method and the thickness was measured by a surface profiler. When the N_2 gas ratio is lower than 0.22, the film still shows a metallic behavior, whereas when R is higher than 0.22, the conducting property of the film changes to a dielectric behavior.

Four sets of MIS capacitors were fabricated using sputtered AlN films as the insulating layers. The dielectric properties were studied as a function of insulator thickness, nitrogen concentration in the gas mixture and heat treatment of the capacitors. The thickness and the N_2 flow rate used to obtain the AlN insulator layer are the following: (i) MIS_1: 25 nm AlN, 80 sccm N_2; (ii) MIS_2: 20 nm AlN/10 nm SiO_2, 80 sccm N_2; (iii) MIS_3: 18 nm AlN, 30 sccm N_2; and (iv) MIS_4: 31 nm AlN/10 nm SiO_2, 30 sccm N_2. The discharge power and the Ar flow rate in the process were 1000 W and 80 sccm, respectively. In order to analyze the hysteresis behavior, a thin SiO_2 film was stacked to the AlN layer in MIS_2 and MIS_4.

Many properties of electronic materials, such as electrical and optical properties, are influenced by the dielectric constant ε. This parameter can be determined from C–V measurements of MIS capacitors, performed at room temperature, 1 MHz frequency, using the well-known formula $C = \varepsilon\varepsilon_0 A/d$. The calculated dielectric constant obtained from the MIS capacitors for the AlN layers was approximately 9.5, which is compatible with the expected value for this material [16,17].

The SiO_2/AlN structures (MIS_2 and MIS_4) have insulator layers thicker than MIS_1 and MIS_3 capacitors, hence, lower capacitance values than these structures. Fig. 5 shows the C–V characteristics of the MIS_1 and MIS_2 capacitors measured prior to and after heat treatment for 10 min at 430 °C in hydrogen environment. Since the structures fabricated using AlN at different N_2 ratios showed no significant differences in their behavior, only the results of MIS_1 and MIS_2 capacitors are discussed here. The improvement in electrical characteristics was observed only for heat treatments of 5 and 10 min, showing saturation for longer process. The heat treatment does not affect the parameters that determine the capacitance (ε, ε_0, A and d), however, this process considerably influences the flat band voltage. As we can clearly observe in Fig. 5, the flat band voltage exhibits a negative shift on both structures without the heat treatment. This behavior indicates existence of positive charges trapped in the dielectric-silicon interface [16]. With heat treatment it is clear that a passivation of charge traps occurs, which reduces the flat band voltage.

The hysteresis occurs due to mobile charges in the AlN-semiconductor interface (strongly influenced by the Al). This phenomenon is less evident in structures with a thin SiO_2, which inhibits the

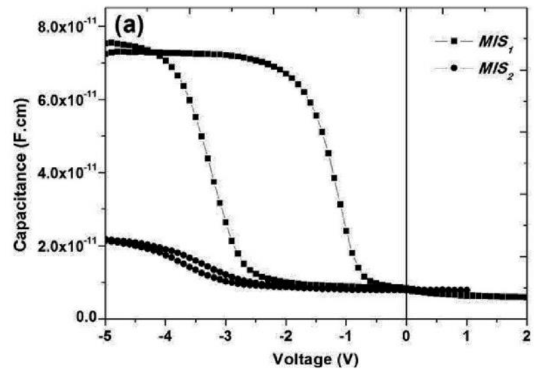

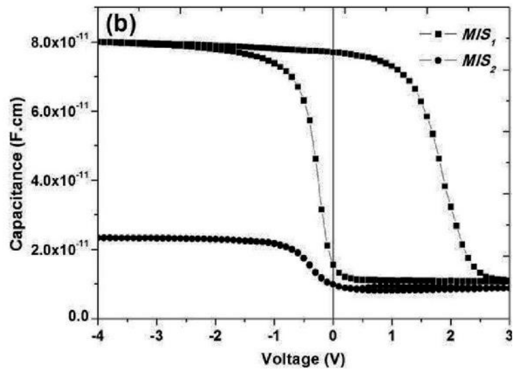

Fig. 5. C-V curves of MIS capacitors with AlN and SiO_2/AlN as insulating layer (a) before the heat treatment and (b) with 10 min of heat treatment.

movement of the mobile charges in the dielectric-semiconductor interface. Opposite to what is observed for the flat band voltage, the heat treatment does not have considerable effects in the hysteresis. This behavior indicates that AlN film hinders the diffusion paths, delaying the hydrogen progress through the AlN-silicon interface [16,17]. The physical thicknesses of the insulator layers varied in the range 18–25 nm in the structures without oxide, and 27–38 nm in the capacitors with SiO_2 layer. The calculated EOT for the capacitors varied in the range 10–15.2 nm and 44.5–64.4 nm, respectively. In both types of structures the EOT is not affected by the heat treatments. Similar behavior has been observed by other authors [16] for MIS structures when only an AlN film is used as insulator and EOT is smaller than the physical thickness of the material. Therefore, the reported results indicate a reasonable quality of the obtained AlN films, and that they are suitable for applications in fabrication of some specific electronic devices.

4. Conclusions

The paper reports the results of AlN thin films prepared by dc reactive magnetron sputtering with different sputtering powers and N_2 concentrations. The influence of these parameters on structural and morphological properties was investigated. MIS structures were also fabricated to analyze electrical characteristics of AlN applied as insulating material.

The characterization of fabricated samples revealed that dielectric AlN films with deposition rate as high as 70 nm/min can be attained by the control of either target power or N_2 flow in the gas mixture. The measured XRD patterns showed prominent peaks at 35.9° and 37.8°, corresponding to the (0 0 2) and (1 0 1) crystal planes, respectively, or wurtzite AlN. The values of refractive index were in the range of 2.0–2.2, for the samples prepared at 500 W as the discharge power, thus showing formation of the polycrystalline AlN films. The FTIR analysis exhibited the E1(TO) and A1(TO) modes of wurtzite AlN, supporting also the formation of AlN films in our samples. Moreover, the surface topography analyses by AFM indicated relatively smooth AlN films, and a tendency to become rougher with the increase in dc discharge power and smoother with the increase of N_2 gas ratio. The electrical resistivity of the samples showed a metallic behavior when the N_2 gas ratio is lower than 0.22. For higher values, the conducting property of the film changes to dielectric behavior.

The MIS structures fabricated using AlN at different N_2 ratios showed no significant differences in their behavior. The improvement in some electrical characteristics was observed only in heat treatments of 5–10 min, showing saturation with a longer process. The calculated dielectric constant of the AlN layers obtained from the MIS capacitors was approximately 9.5. This result is compatible with the expected value for sputtered AlN films and it was not influenced by the heat treatment. The calculated EOT was considerably higher than the physical thicknesses in the structures with the thin oxide layer. The hysteresis phenomenon was less evident in the MIS structures with a thin oxide film, and it exhibited no significant changes after the heat treatment. However, this process reduces the flat band voltage due to the passivation of charge traps. The obtained results are consistent with those reported in the literature and indicate formation of AlN films with reasonably good quality, suitable for applications in specific electronic devices.

Acknowledgements

The authors would like to thank the CCS staff for technical assistance in processing and characterizations of the samples, Prof. Dr. Lisandro P. Cardoso of IFGW/UNICAMP for the XRD measurements, and the Brazilian agencies CNPq, CAPES, and FAPESP for the financial support.

References

[1] A. Khanna, D.G. Bhat, J. Vac. Sci. Technol., A 25 (3) (2007) 557–565.
[2] J.A. Ruffner, P.G. Clem, B.A. Tuttle, et al., Thin Solid Films 354 (1999) 256–261.
[3] V. Dimitrova, D. Manova, E. Valcheva, Mat. Sci. Eng. B68 (1999) 1–4.
[4] T.P. Drusedau, J. Blasing, Thin Solid Films 377–378 (2000) 27–31.
[5] M. Benetti, D. Cannatà, F. Di Pietrantonio, et al., Appl. Phys. Lett. 87 (2005) 1735041–1735043.
[6] G. Wingqvist, J. Bjurstrom, L. Liljeholm, et al., Sensors Actuators, B 123 (2007) 466–473.
[7] K. Kusaka, D. Taniguchi, T. Hanabusa, et al., Vacuum 66 (2002) 441–446.
[8] L. Vergara, M. Clement, E. Iborra, et al., Diam. Relat. Mater. 13 (2004) 839–842.
[9] M. Clement, E. Iborra, J. Sangrador, et al., J. Appl. Phys. 94 (3) (2003) 1495–1500.
[10] K. Jagannadham, A.K. Sharma, Q. Wei, et al., J. Vac. Sci. Technol., A 16 (5) (1998) 2804–2815.
[11] X.-H. Xu, H.-S. Wu, C.-J. Zhang, et al., Thin Solid Films 388 (2001) 62–67.
[12] J.X. Zhang, H. Cheng, Y.Z. Chen, et al., Surf. Coat. Technol. 198 (2005) 68–73.
[13] A.S. Hervas, E. Iborra, M. Clement, et al., Diam. Relat. Mater. 12 (2003) 1186–1189.
[14] H. Hobert, H.H. Dunken, J. Meinschien, et al., Vib. Spectrosc. 19 (1999) 205–211.
[15] M.B. Assouar, M. El Hakiki, O. Elmazria, et al., Diam. Relat. Mater. 13 (2004) 1111–1115.
[16] F. Engelmark, J. Westlinder, G.F. Iriarte, et al., IEEE Electron Devices 50 (5) (2003) 1214–1219.
[17] T. Adam, J. Kolodzey, C.P. Swann, et al., Appl. Surf. Sci. 175–176 (2001) 428–435.